ANALYTICAL MODELING OF REINFORCED CONCRETE BEAM-TO-COLUMN CONNECTIONS

A THESIS SUBMITTED TO
THE GRADUATE SCHOOL OF NATURAL AND APPLIED SCIENCES
OF
MIDDLE EAST TECHNICAL UNIVERSITY

BY

MEHMET ÜNAL

IN PARTIAL FULFILLMENT OF THE REQUIREMENTS
FOR
THE DEGREE OF MASTER OF SCIENCE
IN
CIVIL ENGINEERING

JULY 2010

Approval of the thesis:

ANALYTICAL MODELING OF REINFORCED CONCRETE BEAM-TO-COLUMN CONNECTIONS

submitted by **MEHMET ÜNAL** in partial fulfillment of the requirements for the degree of **Master of Science in Civil Engineering Department, Middle East Technical University** by,

Prof. Dr. Canan Özgen _____
Dean, Graduate School of **Natural and Applied Sciences**

Prof. Dr. Güney Özcebe _____
Head of Department, **Civil Engineering**

Assist. Prof. Dr. Burcu Burak _____
Supervisor, **Civil Engineering Dept., METU**

Examining Committee Members:

Prof. Dr. Tuğrul Tankut _____
Civil Engineering Dept., METU

Assist. Prof. Dr. Burcu Burak _____
Civil Engineering Dept., METU

Assoc. Prof. Dr. Erdem Canbay _____
Civil Engineering Dept., METU

Assist. Prof. Dr. Afşin Sarıtaş _____
Civil Engineering Dept., METU

Assist. Prof. Dr. Eray Baran _____
Civil Engineering Dept., Atılım University

Date: _____

I hereby declare that all information in this document has been obtained and presented in accordance with academic rules and ethical conduct. I also declare that, as required by these rules and conduct, I have fully cited and referenced all material and results that are not original to this work.

Name, Last name: Mehmet Ünal

Signature:

ABSTRACT

ANALYTICAL MODELING OF REINFORCED CONCRETE BEAM-TO-COLUMN CONNECTIONS

Ünal, Mehmet

M.Sc., Department of Civil Engineering

Supervisor: Assist. Prof. Dr. Burcu Burak

July 2010, 129 Pages

Prior studies indicated that beam-to-column connections of reinforced concrete (RC) moment resisting frame structures experience considerable deformations under earthquake loading and these deformations have a major contribution to story drift of the building. In current analysis and design applications, however, the connection regions are generally modeled as rigid zones and the inelastic behavior of the joint is not taken into account. This assumption gives rise to an underestimation of the story drifts and hence to an improper assessment of the seismic performance of the structure. In order to implement the effect of these regions into the seismic design and analysis of buildings, a model that properly represents the seismic behavior of connection regions needs to be developed. In this study, a parametric model which predicts the joint shear strength versus strain relationship is generated by investigating the several prior experimental studies on RC beam-to-column connections subjected to cyclic loading and establishing an extensive database. Considering previous experimental research and employing statistical correlation method, parameters that significantly influence the joint behavior

are determined and these parameters are combined together to form a joint model. This model is then verified by comparing the results obtained from the dynamic earthquake analysis by Perform 3D with the experimental ones. The main contribution of the developed model is taking into account parameters like the effect of eccentricity, column axial load, slab, wide beams and transverse beams on the seismic behavior of the connection region, besides the key parameters such as concrete compressive strength, reinforcement yield strength, joint width and joint transverse reinforcement ratio.

Keywords: Beam-to-column Connections, Seismic Loading, Joint Model, Joint Shear, Joint Deformation,

ÖZ

BETONARME KOLON-KİRİŞ BİRLEŞİM BÖLGELERİNİN ANALİTİK MODELLENMESİ

Ünal, Mehmet

Yüksek Lisans, İnşaat Mühendisliği Bölümü

Tez Yöneticisi: Yrd. Doç. Dr. Burcu Burak

Temmuz 2010, 129 Sayfa

Daha önceden yapılan çalışmalar, betonarme kolon-kiriş birleşim bölgelerinin deprem kuvvetleri altında ihmal edilemeyecek kadar fazla deforme olduklarını ve bu deformasyonların kat yatay ötelenmesinde büyük katkılarının olduğunu göstermiştir. Ancak, mevcut analiz ve tasarım uygulamalarında bu bölgeler genelde rijit modellenir ve elastik olmayan davranış gözardı edilir. Bu varsayım, kat yatay ötelenmesinin gerçek değerinden az tahmin edilmesine sebep olduğu için yapının deprem yükü altındaki performansı doğru değerlendirilememiş olur. Birleşim bölgelerinin etkisini binaların tasarımına ve analizine katmak için kolon-kiriş birleşim bölgesi davranışını gerçekçi bir şekilde tanımlayabilecek bir model oluşturulmalıdır. Bu çalışmada, birleşim bölgesi için kesme dayanımı ile deformasyonu arasındaki ilişkiyi olabildiğince yakın bir şekilde tahmin eden parametrik bir model, geçmiş deneysel çalışmaların incelenmesi ve geniş bir veritabanına aktarılması ile oluşturulmuştur. Daha önceden yapılmış deneysel çalışmaların sonuçlarını gözönünde bulundurarak ve istatistiksel korelasyon yöntemiyle, birleşim davranışında en etkili faktörler belirlenmiş ve bu faktörler birleştirilerek bir model oluşturulmuştur. Bu model daha sonra Perform 3D bilgisayar programında

dinamik deprem analizleri yapılarak ve analiz sonuçları deneysel sonuçlarla kıyaslanarak doğrulanmıştır. Geliştirilen bu modelin en büyük katkısı; beton basınç dayanımı, donatı akma dayanımı ve birleşim yatay donatı oranı gibi ana parametrelerin yanı sıra dışmerkezliğin, kolona uygulanan eksenel yük miktarının, döşemenin, geniş kirişlerin ve enlemesine kirişlerin etkilerini de hesaba katan parametreler içermesidir.

Anahtar Kelimeler: Kolon-Kiriş Birleşim Bölgesi, Deprem Kuvvetleri, Birleşim Modeli, Birleşim Bölgesi Kesme Dayanımı, Birleşim Bölgesi Kesme Deformasyonu

To My Family

ACKNOWLEDGEMENTS

I would like to express my sincere gratitudes to my supervisor Assist. Prof. Dr. Burcu Burak for her guidance, advice, criticism and encouragements throughout the research. Without her support and patience, this study would not have been completed.

I also owe my gratitudes to my father, Ibrahim Ünal and my mother, Munise Ünal for their support and love and my brother, Gökhan Ünal and my sister, Neslihan Ünal for providing a trustworthy and enjoyable environment.

TABLE OF CONTENTS

LIST OF TABLES

TABLES

LIST OF FIGURES

FIGURES

LIST OF SYMBOLS

A_o : cross-sectional area of the transverse reinforcement

A_c: core area of column section measured from outside edge to outside edge of hoop reinforcement

A_g: gross area of column section

A_{sh}: total cross-sectional area of all legs of hoop reinforcement, including crossties, crossing a section having core dimension b_c''

b_b: beam width

b_c: column width

b_c'': core dimension of tied column, outside to outside edge of transverse reinforcing bars, perpendicular to the transverse reinforcement area A_{sh} being designed

b_e: effective beam flange width

b_j: effective joint width

d_b: nominal diameter of reinforcing bar

d": depth of the beam between top and bottom reinforcement

e: eccentricity between beam and column centerlines

E: modulus of elasticity

f_c: concrete compressive strength

f_y: yield strength of reinforcing bars

G: shear modulus

h_b: beam depth

h_c: column depth

I: moment of inertia

l_{eff}: effective length of the lateral reinforcement in the loading direction

l_{dh}: development length of a hooked longitudinal bar

L_p: plastic hinge length

m: slope to define the effective width of joint transverse to the direction of shear

M_r: moment strength ratio

M_u: ultimate moment capacity

N: column axial load

n: number of layers of transverse reinforcement in the effective confined area

s_h: center-center spacing of hoops

t: slab thickness

V_u: design shear force in joint

V_j: joint shear force

v_j: joint shear stress

x: perpendicular distance from longitudinal axis of beam to column side

α: stress multiplier for longitudinal reinforcement at joint-member interface

ε: strain of the reinforcement

γ: shear strength factor reflecting confinement of joint by lateral members

ρ_s: volumetric transverse reinforcement ratio of hoop

ρ_{core}: volumetric reinforcement confinement ratio determined considering the effective confined area as the joint core area

ρ_{gross}: volumetric reinforcement confinement ratio determined considering the effective confined area as the gross connection area

$\rho_{onelayer}$: volumetric reinforcement confinement ratio determined considering the effective area that contains one layer of joint transverse reinforcement

θ: beam rotation, rad.

ν: poisson ratio

CHAPTER 1

INTRODUCTION

1.1 OVERVIEW

ACI-ASCE Committee 352 Recommendations (2002) [2] defines a beam-to-column joint as the region of the column within the depth of the deepest beam framing into that column. Beam-to-column connection region, on the other hand, represents the joint plus the columns, beams and slab adjacent to the joint. Beam-to-column connections play an important role in the seismic behavior of reinforced concrete structures, since they undergo considerable deformations under earthquake loading. If these regions are not properly designed and detailed, they fail prematurely under strong earthquake ground motions. For more than 40 years, many experimental studies have been carried out focusing on beam-to-column connections. Several prior studies indicated that joint deformations have a major contribution to story drift. Therefore, the seismic behavior of beam-to-column connections significantly influences the earthquake response of reinforced concrete frame structures. When the connections can resist the lateral forces transferred from the beams and columns without significant decrease in the joint strength and stiffness, the drift values will not be magnified.

In the design of reinforced concrete moment resisting frame structures; the “strong column - weak beam” philosophy is recommended to ensure the generation of beam plastic hinging at large displacements, rather than column hinging. Beam-to-column connections, therefore, are expected to behave in the elastic range. However,

experimental studies showed that they undergo large inelastic shear deformations even when the strong column - weak beam design philosophy is followed. It was also observed that the inelastic behavior of connections subjected to cyclic loading significantly affects the overall behavior of the test specimen and should not be neglected. However, in current analysis and design applications, the connection regions are generally modeled as rigid zones and the inelastic behavior of the joint is not taken into account. This assumption gives rise to an underestimation of the story drifts and hence to an improper assessment of the seismic performance of the structure. Therefore, a model needs to be developed to properly represent the inelastic seismic behavior of beam-to-column connections.

In order to define the inelastic behavior, the influential factors should be considered. The key parameters affecting the connection performance are column-to-beam moment strength ratio, confinement provided by the lateral reinforcement and beams surrounding the connection region, anchorage of the beam longitudinal reinforcement and shear stress level in the joint. In addition, material properties, section dimensions, eccentricity between the centerlines of beam and column, axial load acting on the column and presence of wide beams or slab also affect the connection behavior.

1.2 RESEARCH OBJECTIVES AND SCOPE

In this analytical study, an extensive database was formed based on prior experimental data to observe the effect of different parameters on the seismic performance of beam-to-column connections. During the selection process, special attention was given so that the chosen specimens include dependable joint shear strength and distortion data. By using statistical correlation methods, most influential parameters on the joint shear strength and deformation are determined and a parametric model to predict the joint inelastic behavior is proposed. The main contribution of the proposed model is to take into account several key parameters such as axial load level, eccentricity of the joint,

wide beam effect, effective joint width, joint geometry, confinement due to transverse reinforcement and adjoining members. While considering the key parameters, ACI 318 (2008) and 352 (2002) Guidelines were followed and special attention was given to keep the model simple and practical to use in design applications. After establishing the parametric model that predicted the joint behavior, it was verified by setting the physical model in Perform 3D and analyzing with the original load cases. A commercially available program Perform 3D was used in the nonlinear analysis of the specimens. Although it has some limitations, such as not being able to define pinching, the use of this program will enable the practicing engineers to apply the proposed model into their analyses. The analysis results showed that the proposed model was acceptable and can easily be integrated into design applications.

1.3 THESIS OUTLINE

In this thesis study, an analytical model for reinforced concrete beam-to-column connections is developed by using an extensive experimental database. The model is then verified through the dynamic earthquake analysis. There are six chapters in this thesis study focusing on the modeling and verification steps:

Chapter 1 provides brief information on RC beam-to-column connections and their behavior under earthquake loading. The scope and the objective of the thesis study are presented in this chapter.

Chapter 2 presents the literature survey on RC beam-to-column connections. The prior experimental and analytical studies carried out on different types of connections and the code recommendations are investigated and summarized.

Chapter 3 introduces the constructed database. The data selection procedure and details of each chosen experiment are described in this chapter.

Chapter 4 explains the modeling of the joint shear stress - strain behavior. First, the key parameters affecting the joint behavior are identified. Second, the method to develop a parametric prediction of joint shear strength and strain are presented separately. Third, all parameters belonging to each experiment are tabulated. Finally, the predicted joint shear stress vs. strain relationship is compared with the experimental values.

Chapter 5 presents the verification of the analytical joint model by using commercial computer software. First, the physical modeling of beams, columns and joint region are explained and the loading cases are illustrated. Then, the analysis results are presented and compared with the experimental results.

Chapter 6 gives the summary and the conclusions of the present study. The procedure followed throughout the study is summarized and conclusions are drawn. Moreover, the future recommendations are made regarding the improvement of this analytical model.

CHAPTER 2

LITERATURE REVIEW

2.1 OVERVIEW:

In order to understand the behavior of beam-to-column connections in more detail, several experimental and analytical studies have been carried out for more than 40 years. Many researchers have investigated the parameters influencing joint behavior by constructing and testing connection subassemblies. Joint shear strength, reinforcement detailing, connection geometry and axial loading are the most frequently examined parameters in these experiments. Since different connection types such as interior, exterior and corner (knee) connections behave differently, they are examined separately. Besides the experimental studies, the seismic behavior of the connections is assessed analytically. By changing the parameters in the analytical models, the influence of the aforementioned parameters are examined. Consequently, researchers came up with analytical models that take into account the connection behavior under earthquake loading.

Several researchers who have carried out studies on beam-to-column connections came together in 1985 and published a report of recommendations for design of beam-to-column connections. The final version of this report is ACI-ASCE Committee 352 Recommendations (ACI 352R-02) [2] which was published in 2002. In ACI 352R-02, recommendations on significant subjects in connection design such as beam and column proportions, confinement of the joint core, limitation of the joint shear stress, ratio of

column-to-beam flexural strengths, detailing of columns and beams near the joint region and development length of longitudinal beam and column bars are given. The recommendations in this state-of-the-art report are based on laboratory tests and field studies and also some areas in which further research is needed is identified.

In addition, Chapter 21 (Special Provisions for Seismic Design) of ACI 318-08 (Building Code Requirements for Structural Concrete) [1] provides design requirements of beam-to-column connections. However, there are some restrictions in application of these recommendations as far as the material strengths and connection geometry is concerned. The structures having concrete compressive strength above 15000 psi (100 MPa) is out of scope. Furthermore, these recommendations do not apply when the design beam width b_b is more than the smaller of 3 b_c and (b_c + 1.5 h_c), where b_c and h_c are the column width and depth, respectively.

According to ACI 352R-02, beam-to-column connections are classified as interior, exterior and corner connections depending on the number of members framing into the joint. In **Figure 2.1**, connection types given in this report are summarized. Beam-to-column connections are also classified in two categories with respect to the loading conditions and expected deformations. Type 1 connections are composed of members designed to satisfy ACI 318-02 strength requirements, but excluding Chapter 21, which do not need high energy dissipation capacity. Type 2 connections, on the other hand, are designed on the basis of seismic considerations in which energy dissipation through reversals of deformation into the elastic range is required.

Turkish Earthquake Code (TEC 2007) [35] classifies beam-to-column joints of high ductility level frame systems into two categories based on their confinement level due to adjoining beams. When beams frame into the all faces of joint region and in case the width of each beam is not smaller than the 3/4 of the adjacent column width, then the connection is defined as a confined connection. On the other hand, the connection is defined as an unconfined connection when one of these conditions is not satisfied.

ACI 352R-02 states the design forces in the connection region which may be axial, flexural, shear or torsional. The free body diagrams of the joint region due to gravity loading and lateral loading are shown in Error! Reference source not found.**.2** as they are defined in ACI 352R-02. In this figure, the compression forces and the tensile forces applied by the beams and columns are denoted as C and T respectively. The joint shear forces, on the other hand, are represented by V. The subscripts b is used for beam, subscript c is for column and subscript s used to represent slab.

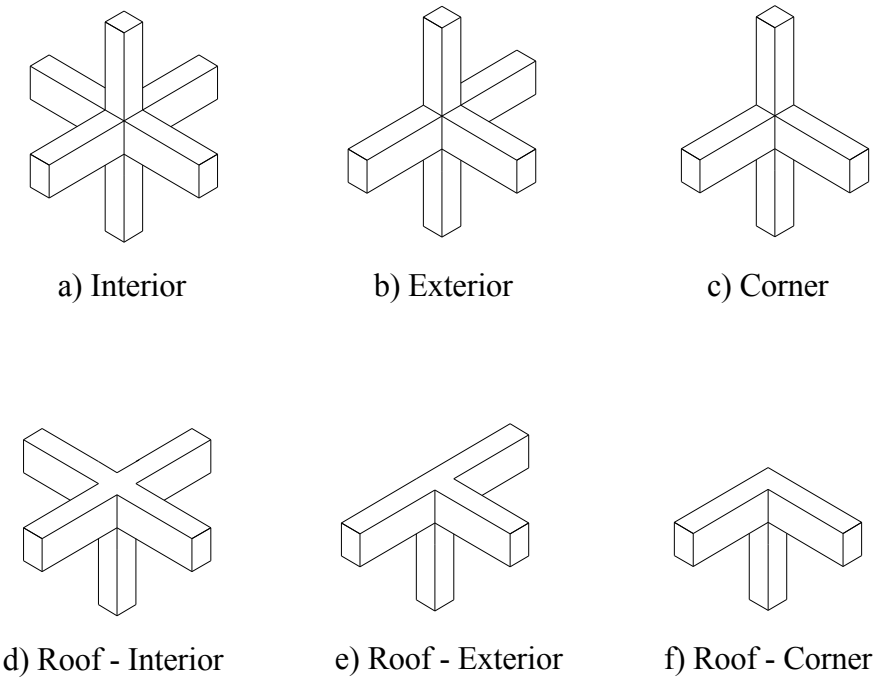

Figure 2.1: Types of Beam-to-Column Connections

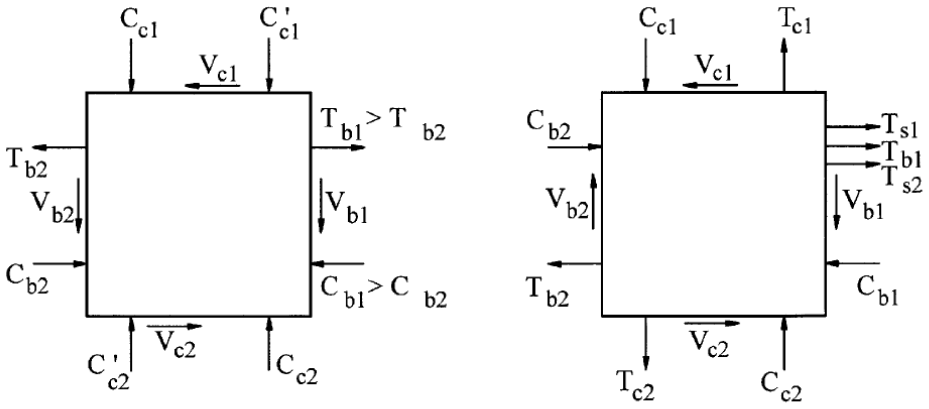

Figure 2.2: Joint Forces at Critical Sections (ACI 352R-02)

2.2 MAIN PARAMETERS AFFECTING BEAM-TO-COLUMN CONNECTION BEHAVIOR:

There are several factors which are influential on the behavior of reinforced concrete beam-to-column connections. These factors are examined in various experimental studies worldwide. In this section, most significant parameters are presented and studies concerning these parameters are introduced.

2.2.1 Moment Strength Ratio

The ratio of the sum of the nominal flexural strength of columns above and below the joint to the sum of the nominal flexural strength of beam sections framing in to the joint is called the moment (flexural) strength ratio, "M_r". According to ACI 352R-02, M_r should not be less than 1.2 for Type 2 connections in order to satisfy "strong column-weak beam" philosophy. As long as this requirement is satisfied under seismic lateral loading, the plastic hinging will be ensured to develop in the beam ends rather than in the columns. It should be noted that beam flexural strength under positive bending is determined taking into account the effective slab reinforcement participation.

Turkish Earthquake Code (TEC 2007) also requires that the sum of the ultimate moment capacities of columns framing into a connection should be at least 20 % more than the sum of the ultimate moment capacities of beams framing into the same connection as given in **Equation 2.1.** In this equation, M_{ra} and M_{ru} represent the ultimate moment capacities of the top and bottom columns, and M_{ri} and M_{rj} denote the ultimate moment capacities of the right and left beams in the direction of earthquake loading.

$$(M_{ra} + M_{ru}) \geq 1.2\,(M_{ri} + M_{rj}) \qquad \textbf{(2.1)}$$

When slabs are present in the floor system, effective beam width (b_e) should be computed and used in the calculation of the beam flexural capacity. ACI 318-08 describes the computation of effective beam width (b_e) in Chapter 8.12. According to this definition, when slab is present on each side of the beam, the beam should be regarded as a T-beam. The effective flange width should not exceed one-quarter of the span length of the beam and the effective overhanging flange width on each side of the web must be smaller than eight times the flange thickness and one half the clear distance to the next web. In case there is slab on one side only, the effective overhanging flange width should not exceed one-twelfth the span length of the beam, six times the slab thickness and one-half the clear distance to the next web.

The studies that aim to investigate the effect of Moment Flexural Strength Ratio include the experimental study by Ehsani and Wight [11] on the behavior of exterior reinforced concrete beam-to-column connections subjected to earthquake loading. Six specimens were tested in this study and the effects of different parameters influencing connection behavior are investigated. One of the main parameters that was investigated is the moment strength ratio (M_r) and it was found that when M_r is greater than 1.4, formation of plastic hinges in the joint is prevented or prolonged.

2.2.2 Joint Shear

Horizontal or vertical shear stresses in the joint region arise from flexural tension, flexural compression and shear forces applied by the beams and columns framing into the joint. Beam-to-column connections should be designed to resist these shear stresses

in two perpendicular directions. Transverse reinforcement plays an important role in resisting the horizontal shear. Longitudinal reinforcement of the column, on the other hand, helps to resist vertical shear. Under earthquake loading, horizontal shear is more vital than the vertical one, therefore, ACI-ASCE Committee 352 Recommendations mainly focus on horizontal shear. According to these recommendations, the ultimate horizontal shear force on an effective joint region is computed at the mid-height of the joint as seen in **Figure 2.3**. The ultimate horizontal joint shear force (V_u) is calculated as;

$$
\begin{aligned}
&V_u = T_{b1} + T_{s1} + T_{s2} + C_{b2} - V_{col,1} \\
&\text{where:} \\
&T_{b1} = \alpha f_y(A_{s1}); \quad T_{s1} = \alpha f_y(A_{s,s1}) \; ; \quad T_{s2} = \alpha f_y(A_{s,s2}) \\
&C_{b2} = T_{b2} = A_{s2}\alpha f_y
\end{aligned}
\qquad \textbf{(2.2)}
$$

In this equation, α is a stress multiplier to take into account the effect of strain hardening and the possibility of having higher than nominal yield stress for the reinforcing bars. It may change between 1.10 and 1.25, but generally taken as 1.25. In addition to this, f_y is the nominal yield strength of the reinforcing steel, A_{s1} and A_{s2} are the areas of top and bottom reinforcement, $A_{s,s1}$ and $A_{s,s2}$ are the areas of the slab reinforcement within the effective beam width. T and C represent the tensile and the compressive forces acting on the joint.

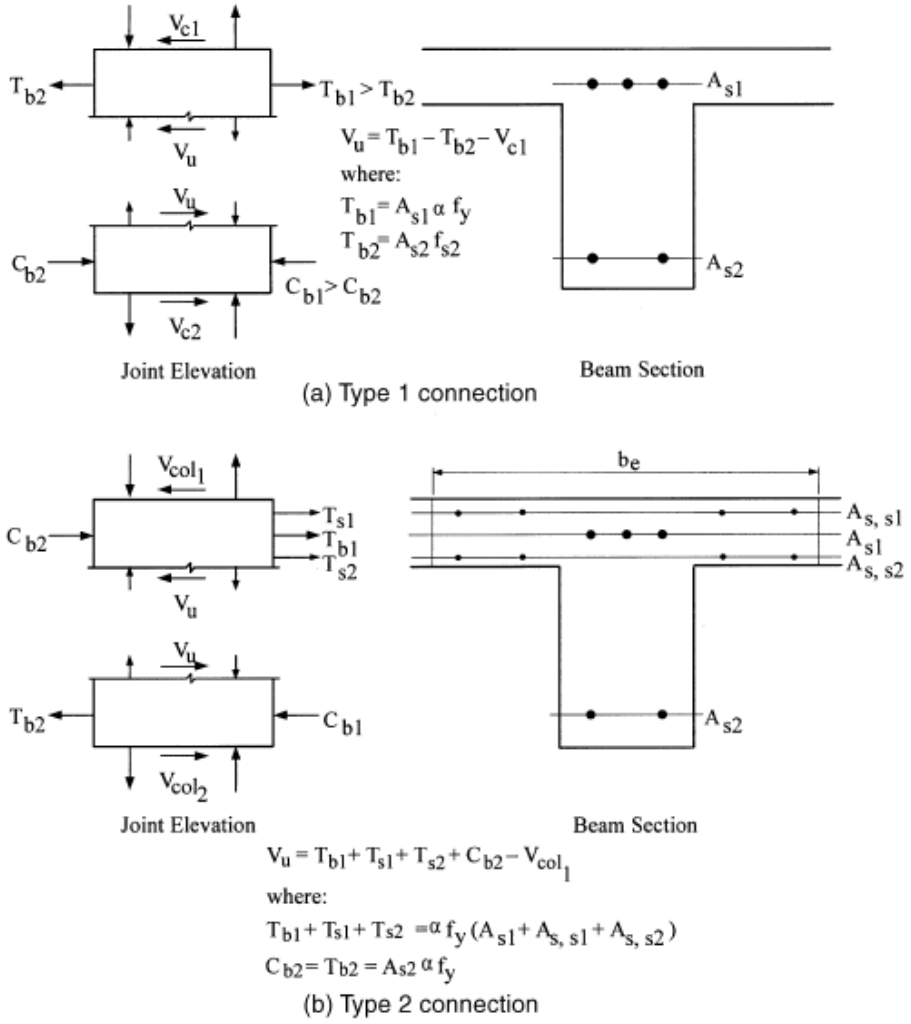

Figure 2.3: Computation of Joint Shear (ACI 352R-02)

ACI 352R-02 recommends the following design equation;

$$\phi V_n \geq V_u \qquad \textbf{(2.3)}$$

where $\phi = 0.85$ and V_n is the nominal shear strength which is defined as;

$$V_n = \gamma\sqrt{f_c'}\, b_j h_c \text{ (psi)}$$
$$V_n = 0.083\gamma\sqrt{f_c'}\, b_j h_c \text{ (MPa)} \quad \textbf{(2.4)}$$

where b_j is the effective joint width transverse to the direction of shear, h_c is the depth of column in the direction of loading, f_c' is the compressive strength of the concrete in the joint region and γ is the shear strength factor (**Table 2.1**) varying based on the continuity of column and the number of confining elements. The effective joint width is defined as the smallest of;

$$\frac{b_b + b_c}{2},$$
$$b_b + \sum \frac{mh_c}{2} \quad \text{and} \quad \textbf{(2.5)}$$
$$b_c$$

where, b_b = width of the longitudinal beam,

b_c = width of the column transverse to the direction of shear,

m = slope for defining effective joint width (**Figure 2.4**). For joints whose eccentricity between the beam centerline and the column centroid exceeds $b_c/8$, m should be taken as 0.3, for all other cases, m is taken as 0.5.

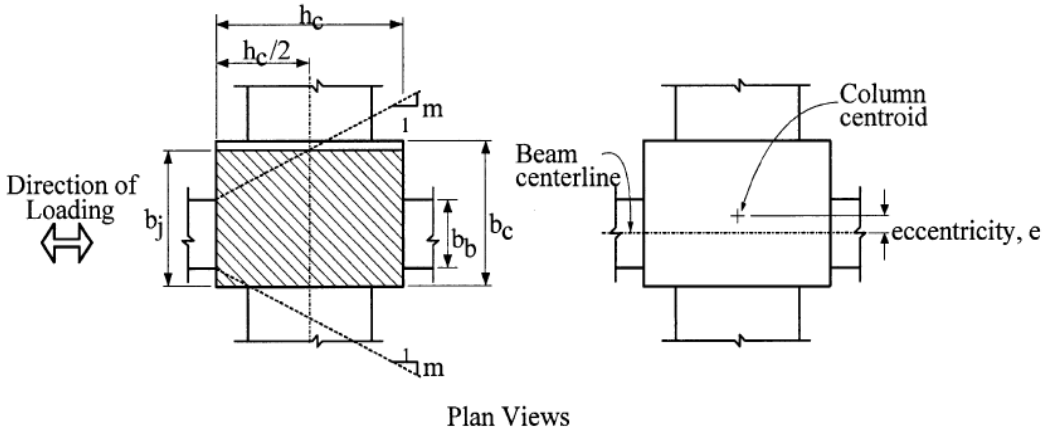

Figure 2.4: Effective joint width (ACI 352R-02)

Table 2.1: Values of Joint Shear Strength Factor (γ)

Classification	Type 1		Type 2	
	psi	MPa	psi	MPa
A. Joints with a continuous column				
A.1 Joints effectively confined on all four vertical faces	24	2.00	20	1.67
A.2 Joints effectively confined on three vertical faces or on two opposite vertical faces	20	1.67	15	1.25
A.3 Other Cases	15	1.25	12	1.00
B. Joints with a discontinuous column				
B.1 Joints effectively confined on all four vertical faces	20	1.67	15	1.25
B.2 Joints effectively confined on three vertical faces or on two opposite vertical faces	15	1.25	12	1.00
B.3 Other Cases	12	1.00	8	0.67

ACI 318-08 also recommends the same shear strength factors as ACI 352R-02. However, the effective joint width definition is different in ACI 318-08; b_j should not exceed the smaller of beam width (b_b) plus column depth (h_c) and twice the smaller perpendicular distance from longitudinal axis of beam to column side (x) plus the beam width (b_b). (**Figure 2.5)**

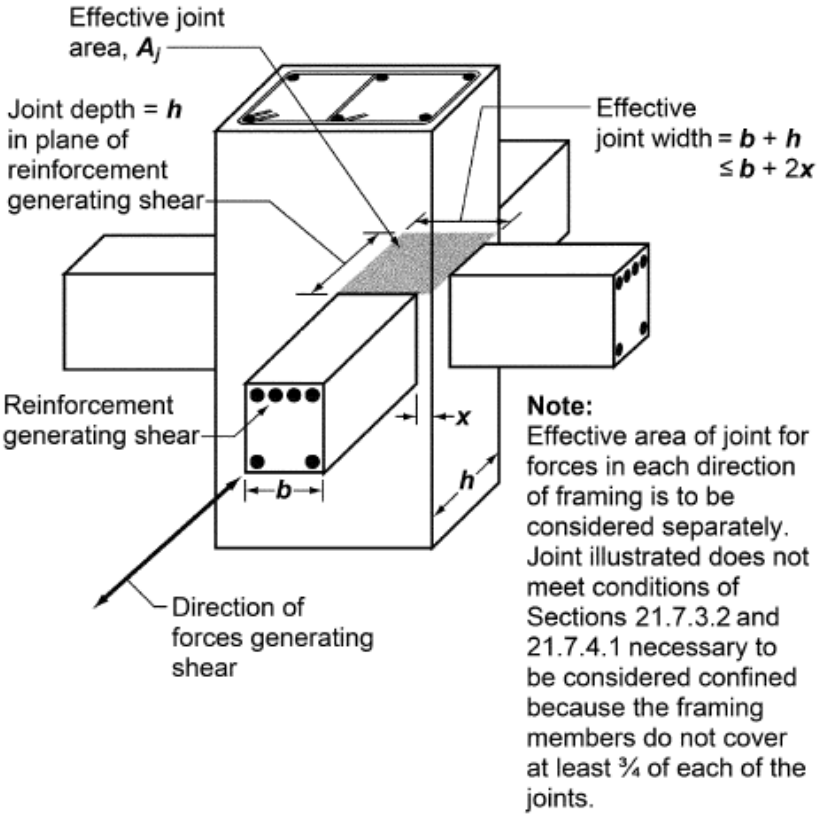

Figure 2.5 : Effective Joint Width and Effective Joint Area (ACI 352R-02)

TEC 2007 focuses mainly on the shear capacity of beam-to-column joints. In order to check the safety of connections, the shear force along the direction of earthquake loading is calculated by **Equation (2.5)**. In this equation, f_{yk} is the characteristic strength of beam longitudinal reinforcement, A_{s1} and A_{s2} are the total area of top and bottom beam longitudinal reinforcement and V_{col} is the lateral force acting on the column. When only one beam frames into the column, A_{s2} is taken as zero.

$$V_e = 1.25 f_{yk} (A_{s1} + A_{s2}) - V_{col} \qquad \textbf{(2.6)}$$

The shear capacity computed by **Equation (2.5)** is then compared with the limitations given in **Equation (2.6)**. In case these limitations are not satisfied, TEC 2007 recommends increasing the cross-sectional dimensions of beams and/or columns.

(a) In confined connections: $V_e \le 0.60\, b_j \cdot h \cdot f_{cd}$

(b) In unconfined connections: $V_e \le 0.45\, b_j \cdot h \cdot f_{cd}$ **(2.7)**

where; b_j is the effective joint width computed as illustrated in **Figure 2.6**

h is the column depth

f_{cd} is the design concrete compressive strength, obtained by dividing f_{ck} by a material factor which is taken as 1.5 for cast in place concrete.

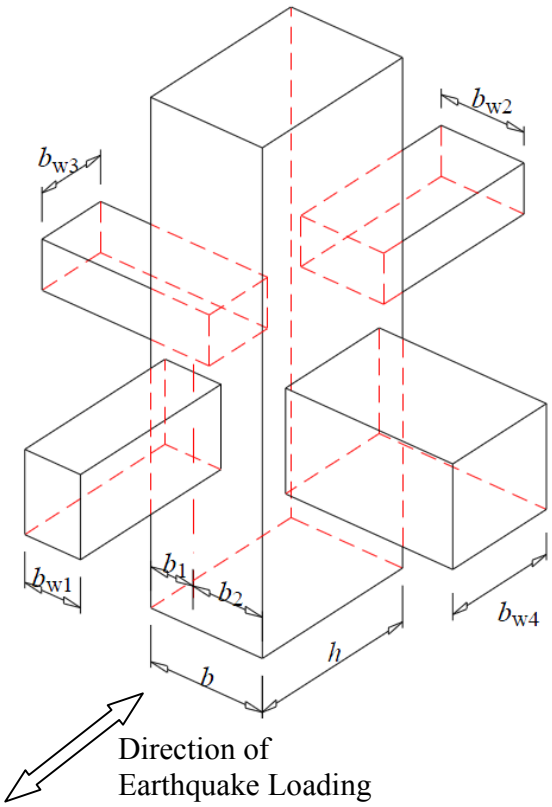

If b_{w1} and $b_{w2} \ge b$, then $b_j = b$

If b_{w1} and $b_{w2} < b$, then

$b_j = 2 \min(b_1, b_2)$

$b_j \le (b_{w1} + h)$ (for $b_{w1} < b_{w2}$)

Figure 2.6: Definition of Joint Dimensions According to Turkish Earthquake Code (TEC 2007)

In recent years, there are several studies about the effect of joint shear on the behavior of reinforced concrete connections. Durrani and Wight [10] investigated interior beam-to-column connections under earthquake loading and concluded that joint shear stress has a significant influence on seismic performance of connections. In other words, strength

degradation, stiffness loss, crack development and drift are affected by the level of joint shear stress. When Fujii and Morita [14] compared the joint behavior of interior and exterior reinforced concrete connections, the exterior joints had 80 % to 90 % of shear strength of interior joint subassemblies. Moreover, the ultimate shear strength was reached at a joint shear strain of 2.8 % for the interior joints and 1.5 % for the exterior joints. This indicates that the displacement ductility of interior frames is higher than that of exterior frames.

2.2.3 Bond Resistance

Bond resistance of the beam and column longitudinal reinforcement anchored in or passing through the joint is essential during intense seismic loading. When there is weak bonding between the reinforcing bars and the concrete, moment reversals cause strength deterioration in the member and give rise to the slippage of the reinforcement. ACI 352R-02 states that hooked or headed longitudinal beam reinforcement should be used in order to prevent slippage and the critical section for development of reinforcement should be taken at the face of the column for Type 1 connections and at the outside edge of the column core for Type 2 connections considering the spalling off of cover concrete under seismic loading.

Bond resistance in the connection region is related to the development length of the bar, the level of shear stress and the degree of confinement in the joint core. If these factors do not ensure full bond, then slippage takes place. Slippage gives rise to a loss of energy dissipation capacity and loss of stiffness. This can be observed as pinching in the lateral load versus displacement hysteresis curves obtained from tests on the seismic behavior of connections. Since the bond resistance is an important criterion and slippage or in other words “anchorage failure” is an undesirable failure type for the reinforced concrete beam-to-column connections, some experimental studies have been carried out on this issue.

In their experimental study Joh, Goto and Shibata [17] found out that using higher joint transverse reinforcement ratio reduced bond deterioration of longitudinal beam bars in

the joint. Kaku and Asakusa [18] outlined the bond behavior in reinforced concrete beam-to-column connections by investigating experimental studies carried out in the United States, New Zealand and Japan in the last ten years. Based on this research outputs, the factors affecting the bond behavior are column axial load, transverse reinforcement in the connection region and ratio of bottom beam reinforcement amount to top bar amount. The anchorage length of beam bars is also found to be significant.

For a sufficient bond resistance, ACI 352R-02 has requirements only for Type 2 connections that states all straight beam and column bars passing through the joint should satisfy:

$$\frac{h_c(\text{column})}{d_b(\text{beam bars})} \geq 20\frac{f_y}{60000} \geq 20 \text{ (psi)} \qquad \text{and} \qquad \frac{h_b(\text{beam})}{d_b(\text{column bars})} \geq 20\frac{f_y}{60000} \geq 20 \text{ (psi)}$$
$$\frac{h_c(\text{column})}{d_b(\text{beam bars})} \geq 20\frac{f_y}{420} \geq 20 \text{ (MPa)} \qquad \text{and} \qquad \frac{h_b(\text{beam})}{d_b(\text{column bars})} \geq 20\frac{f_y}{420} \geq 20 \text{ (MPa)} \qquad \textbf{(2.8)}$$

where h_c and h_b are the column and beam depth, d_b (beam bars) and d_b (column bars) are the diameter of beam and column longitudinal reinforcement, and f_y is the yield strength of reinforcement.

On the other hand, ACI 352R-02 states that the minimum required development length of beam bars measured from the critical section should be computed as;

$$l_{dh} = \frac{\alpha f_y d_b \text{ (psi)}}{75\sqrt{f_c'} \text{ (psi)}} \qquad \text{and} \qquad l_{dh} = \frac{\alpha f_y d_b \text{ (MPa)}}{6.2\sqrt{f_c'} \text{ (MPa)}} \qquad \textbf{(2.9)}$$

In this equation; l_{dh} is the development length of the bar, α is a stress multiplier taken as 1.25, d_b is the diameter of reinforcing bar and f_c' is the concrete compressive strength

2.2.4 Confinement of the Joint Core

Confinement of the joint core should be ensured for proper transfer of the column axial load and shear forces through the connection region and for sufficient anchorage of beam reinforcement. Confinement of the joint core can be achieved by the help of joint

transverse reinforcement, longitudinal column bars and transverse beams and slabs. ACI 352R-02 specifically focuses on joint transverse reinforcement since it also plays important role in joint shear resistance. Therefore, some recommendations regarding the minimum amount and maximum spacing of horizontal joint reinforcement are given in ACI 352R-02. When spiral reinforcement is used, the volumetric ratio (ρ_s) should be taken as the larger of the following equations:

$$\rho_S = 0.45\left(\frac{A_g}{A_c}-1\right)\frac{f_c'}{f_{yh}} \quad \text{for Type 1 and Type 2 Connections}$$
$$\rho_S = 0.12\frac{f_c'}{f_{yh}} \quad \text{for Type 2 Connections} \qquad \textbf{(2.10)}$$

where, f_{yh} is the yield strength of the spiral reinforcement; A_g and A_c are the gross and core area of the concrete column cross-section. If rectangular hoops and cross-ties are used as transverse reinforcement in the joint core, the cross-sectional area of a single hoop in each direction should be at least equal to:

$$A_{sh} = 0.3\frac{s_h b_c'' f_c'}{f_{yh}}\left(\frac{A_g}{A_c}-1\right) \quad \text{and} \quad A_{sh} = 0.09\frac{s_h b_c'' f_c'}{f_{yh}} \qquad \textbf{(2.11)}$$

Spacing limitations for the joint transverse reinforcement are also given in the codes. ACI 352R-02 recommends that the lateral center-to-center spacing between layers of horizontal transverse reinforcement (s_h) should not exceed the smallest of one-quarter of the minimum column dimension, six times the diameter of longitudinal column bars and 6 inches (150 mm). For confined connections, Turkish Earthquake Code (TEC 2007) requires that at least 40 % of the transverse reinforcement in the confined region of the bottom column should be used along the depth of the joint. On the other hand, diameter of the transverse reinforcement should not be less than 8 mm and spacing of transverse reinforcement should not exceed 150 mm. For unconfined connections, at least 60% of the transverse reinforcement in the confined region of the bottom column should be used along the depth of the joint. The diameter of the transverse reinforcement should not be

less than 8 mm as for the confined connections and spacing of transverse reinforcement should not exceed 100 mm.

Durrani and Wight [10] investigated the effect of joint hoop reinforcement in an experimental study and came up with a result that joint transverse reinforcement is one of the most important parameters for maintaining a desired ductility level in reinforced concrete beam-to-column connections. Ehsani and Wight [11] also claimed that providing more hoops with lower yield strength give better seismic performance in the joint region. In addition, Kaku and Asakusa [19] tested 18 exterior beam-to-column subassemblages with a varying amount of joint hoop reinforcement (0.12 % - 0.49 %) and observed that ductility of the specimens increased with increasing joint hoop reinforcement.

According to ACI 352R-02, for a joint to be considered as effectively confined on one of its sides, the horizontal transverse and normal members on that side should cover at least 3/4 of the width of the column, and the total depth of any of the confining members should not be less than 3/4 of the deepest member framing into the joint.

Kitayama, Otani, Aoyama [23] tested interior beam-to-column joint specimens with and without transverse beams whose other components were identical. It was determined that transverse beam may enhance the joint shear strength at least 1.2 times more than that of connections without transverse beams.

2.2.5 Axial Load Level

The effect of axial load level on the behavior of reinforced concrete beam-to-column connections was another parameter chosen to be studied. Although there is still no clear consensus on how much impact the axial load level provides, the general view on this issue is that column compression is a contributing factor in improving the joint shear strength.

Kaku and Asakusa [19] examined the ductility of exterior beam-column subassemblies when varying amount of axial load between 0 – 17 % of the column axial load capacity

was applied. It is observed that joint shear strength was higher when higher axial loads were applied to the column. Furthermore, ductility of subassemblages was higher when the applied axial compressive load increased.

Fujii and Morita [14] also investigated the effect of axial load level on the shear strength of exterior and interior connections. It is concluded that the increase of axial load from $f_c'/12$ to $f_c'/4$ did not affect the shear strength of interior joints. However, for the exterior joints, the same amount of axial load increase resulted in strength gain of about 11 %.

Clyde et al. [8] tested four specimens, two of which was under axial load of $0.1f_c'A_c$ and other two under $0.25f_c'A_c$. According to the test results, the joint shear strength capacities of specimens with higher axial load were approximately 8 % higher than those with lower applied axial load. Furthermore, it was observed that the specimens with axial load of $0.1f_c'A_c$ dissipated about 20 % higher energy than the specimens with $0.25f_c'A_c$ axial load.

2.2.6 Concrete Strength

Concrete compressive strength is influential on both joint shear strength and bond resistance. Therefore, it is one of the most significant factors on the seismic performance of connections. There are many studies on high-strength and varying strength reinforced concrete connection specimens. Ehsani and Alameddine [12] carried out experiments on high-strength reinforced concrete connections with compressive strength between 55 and 97 MPa. The researchers found out that high concrete compressive strength results in high shear capacity but lower ductility.

Guimaraes, Kreger and Jirsa [16] tested two interior beam-column-slab connection subassemblies having concrete compressive strength of 4000 and 12000 psi respectively. When the joint shear strengths of the connections were measured, it was inferred from the test results that joint shear strength is a function of approximately square root of concrete compressive strength.

2.2.7 Presence of Slab

Numerous studies have shown that presence of a slab makes a significant effect on the performance of Type 2 connections (ACI 352R-02). Laboratory experiments on beam-column-slab specimens have indicated that when the connection subassemblies are subjected to large displacement histories, reinforcement across the entire slab width may be effective as beam tension reinforcement. As described in Section 2.1 effective beam width should be computed when there is confinement from the slab.

In order to examine the influence of slab on connection behavior; Kitayama, Otani, Aoyama [23] conducted an experimental study. In this study, identical connections with and without floor slabs were cyclically loaded and the average joint shear stresses was computed. The researchers concluded that joint shear strength increases at least 1.1 times with the presence of floor slabs (**Figure 2.7**).

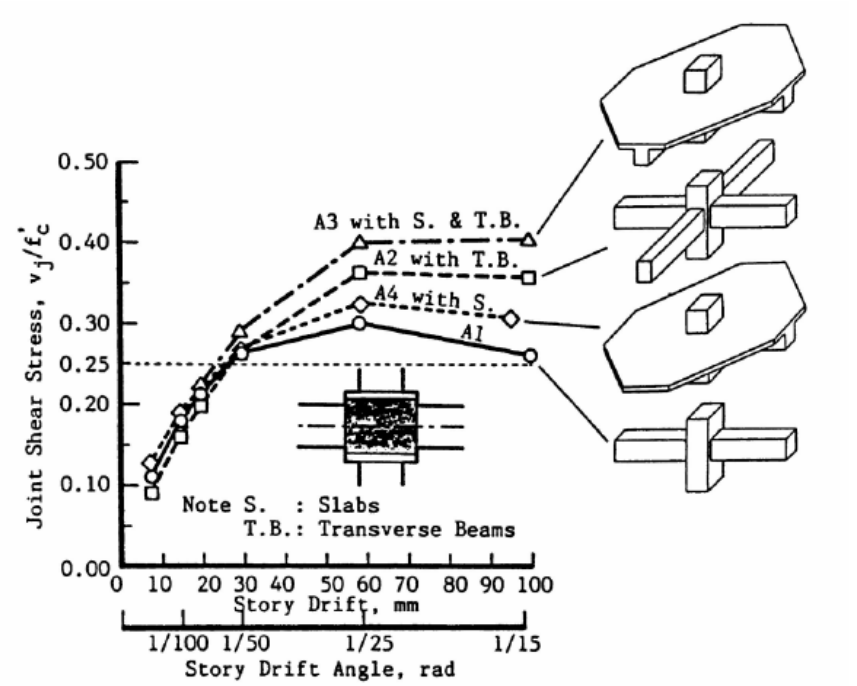

Figure 2.7: Story Drift – Joint Shear Stress Relationship (Kitayama, Otani, Aoyama 1991)

French and Moehle [13] stated that the main contribution of slab results from its participation as a tensile element that improves the flexural resistance of the longitudinal beams when the beam top is in tension. The researchers also claimed that the slab effect depends on several parameters such as connection type (interior or exterior) and stiffness of the transverse beam.

LaFave and Wight [24] tested 4 RC exterior wide-beam-column-slab connections. In this experimental study, slab participation was one of the investigated parameters and it was concluded that presence of slab resulted in an increase in the torsional stresses on the beams. Because of this reason, the shear stress increased in the joint region.

In addition, Burak and Wight [3] investigated the eccentric beam-to-column connection subassemblies that includes floor slab. It was observed that the floor slab provided extra confinement to subassemblies and therefore, the degradation of joint shear stiffness and strength were delayed. Moreover, the expected severe damage level of the eccentric connections without a floor system was not observed and the damage in general significantly decreased when slab was included in the test setup.

2.3 ECCENTRIC BEAM-TO-COLUMN CONNECTIONS:

In cases where the beam centerline does not coincide with the column centerline, eccentricity is present. These types of connections are named as “eccentric connections” and generally observed in the exterior frames of buildings. Raffaelle and Wight [32] define the forces induced in an eccentric connection as in **Figure 2.8**. Since bending in the beam produces compression and tension forces and these forces are concentrated toward one side of the connection due to eccentricity, there will be torsional stresses. When torsion is present, eccentric connections experience additional shear forces. Based on the results of this study, the cracks due to these shear forces start to form first in the exterior (flush) side of the connection and therefore the damage will be more extensive on the exterior face of the joint comparing to the interior face.

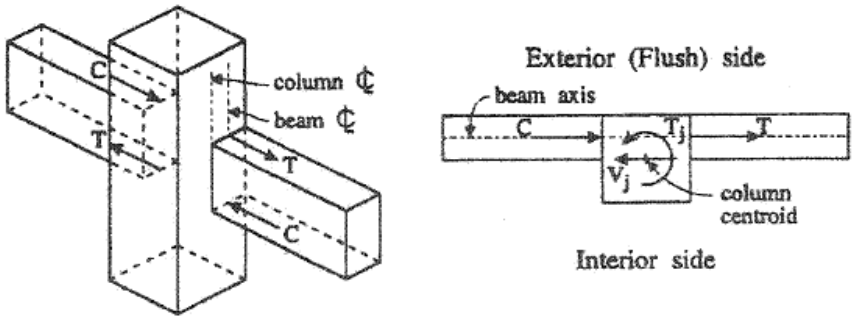

Figure 2.8: Forces Acting on Eccentric Beam-to-Column Connections (Raffaelle and Wight 1995)

Recent experimental studies on eccentric beam-to-column connections indicated that eccentricity between beam and column centerlines generally tends to reduce the strength of structures. Raffaelle and Wight [32] examined the effect of eccentricity on the performance of beam-to-column connections and observed that eccentric beam-to-column connections have a reduced joint strength. In addition, cracking patterns of the connection is observed and found that most damage is concentrated in the beams near the column and in the joint region. Moreover, strains in the joint transverse reinforcement on the exterior side are larger than those of the interior side. Therefore, a new definition was proposed for the effective joint width since the eccentricity prevented the specimens from reaching their predicted story shear strength. As a result, the following formula was suggested as the effective joint width of eccentric connections:

$$b_j = \frac{b_c}{1+\frac{3e}{x_c}} \quad \text{where} \quad x_c \text{ is the smaller of } b_c \text{ and } h_c \qquad \textbf{(2.12)}$$

Chen and Chen [6] tested six beam-to-column connection specimens one specimen was concentric, one of them was eccentric with same properties of the concentric one and the rest of the specimens were eccentric connections having spread-ended beams, which

have enlarged beam width. Based on the test results, the researchers concluded that the subassemblies with eccentricity had lower stiffness and energy dissipation capacities. The eccentricity gave rise to more severe crack damage on the flush side of the joint when compared to that on the interior side. It was also concluded that eccentric connections with spread-ended beams show better seismic performance compared to the eccentric connections with normal beams.

Teng and Zhou [34] tested six beam-to-column connections. Four of the subassemblies were eccentric and the rest were concentric. The researchers stated that joint eccentricity slightly reduces the story shear strength and lateral stiffness of the connections. Therefore, it is suggested that eccentric reinforced concrete connections shall be treated as concentric joints with a slight reduction in lateral stiffness while carrying out structural analysis.

Shin and LaFave [31] investigated eccentric connections with floor slabs and found out that the strength reduction due to eccentricity significantly decreases due to the confinement of floor slabs. Burak and Wight (2005) also investigated the effect of floor system on the behavior of eccentric connections and observed that if the transverse beams and the slab are included in the test set up, the joint shear strength was increased and the differences between the seismic performance of eccentric and concentric connections were diminished. It was seen that damage and the cracking patterns were not critical when the floor system was present in the eccentric connections. Nevertheless, as the eccentricity gets higher, wider cracks were seen.

Finally, Lee and Ko [26] conducted one of the recent experiments on eccentric reinforced concrete beam-to-column connections subjected to cyclic loading in principal directions. One of the most significant conclusions drawn was that the influence on the connection was slight when the joint eccentricity was equal to 1/8 of the width of the column. As the eccentricity increase to 1/4 of the column width, then significant strength and ductility reduction were observed.

2.4 WIDE BEAM-TO-COLUMN CONNECTIONS:

Connection regions for which the framing beam has a width larger than the column width are classified as wide beam-to-column connections. In a structure with wide beams, some of the beam longitudinal reinforcement is anchored in the column core while the rest is anchored to the transverse beam. The most significant parameters for the behavior of wide beam-to-column connections are the amount of reinforcement anchored to the column core and the beam width to column width ratio. According to ACI 352R-02, effective wide beam width is more closely related to the column depth than it is to the wide beam depth.

Since the depth of the wide beam is smaller than its width, the moment of inertia with respect to the flexural axis will also be smaller than that of the conventional beams. As a result, wide beam connections have lower stiffness which leads to higher lateral drifts during earthquake loading. In order to take this effect into account, Burak and Wight [3] defined the effective joint width for the wide beam-to-column connections as;

$$b_j = b_c + \frac{1}{4} \cdot (b_b - b_c) \qquad \textbf{(2.13)}$$

Burak and Wight [3] tested one eccentric specimen with a floor system having a wide beam. The total depth of the wide beam was less than 3/4 of the depth of the spandrel beam which is a limiting factor for effective confinement given in ACI 352R-02. The test results showed that the confinement from the wide beam was not sufficient for the joint and thus shear strength capacity of the connection region reduced significantly

Gentry and Wight [15], in accord with the results of their experimental study on exterior wide beam-to-column connections, concluded that the large width of the beams results in lower shear stress in the beam flexural plastic hinge locations. Thus, the amount of transverse confining reinforcement at the wide beam ends next to the beam-to-column connections may be reduced.

LaFave and Wight [24] tested three exterior wide beam-column-slab subassemblies under quasistatic cyclic loading and concluded that wide beams influenced the joint behavior positively by providing extra confinement. It was observed that performance of wide beam connections were better when b_w/b_c ratio was greater than three and when more than two-thirds of the wide beam longitudinal reinforcement was anchored to the transverse beam outside the column core.

Quintero-Febres and Wight [36] tested three interior wide beam-column-slab connections under cyclic loading. All of the specimens reached their expected capacities at 2 % drift and kept those capacities till the end of the test without failure or significant strength loss. Therefore, it is concluded that wide beam interior connections can withstand large drifts without significant strength and stiffness degradation.

Climent [7] also carried out studies on reinforced concrete wide beam-to-column connections. Different from other researchers, shaking table is used in order to test one exterior and one interior connection having the same beam and column dimensions and detailing. The researchers concluded that wide beam-to-column connections possess low ultimate energy-dissipation capacity and high lateral flexibility.

2.5 ANALYTICAL MODELING OF BEAM-TO-COLUMN CONNECTIONS

Based on experimental results, numerous analytical studies have been conducted to investigate the effect of different parameters on the seismic behavior of connection region and predict the load–deformation relationships. Consequently, analytical models representing the joint shear stress and strain have been proposed.

Parra-Montesinos and Wight [29] proposed an analytical model for estimating shear strength and strain of reinforced concrete beam-to-column connections. Experimental results of cyclic connection tests were utilized to develop a factor for defining principle tensile and compression strains versus shear distortion response. The development of

this model was based on the state of plane strains in the joint. The researchers also included the effect of eccentricity by adding a coefficient to the analytical model.

Lowes and Altoontash [27] developed a joint model that includes a four-node 12 degree-of-freedom finite element representing hysteretic beam-column elements which take into account material, geometric and design parameters such as ductility and reinforcement detailing. The researchers compared the simulated and observed response of some joint subassemblies and concluded that the developed joint model is suitable for use in predicting the response of reinforced concrete beam-to-column connections subjected to earthquake loading (**Figure 2.9**).

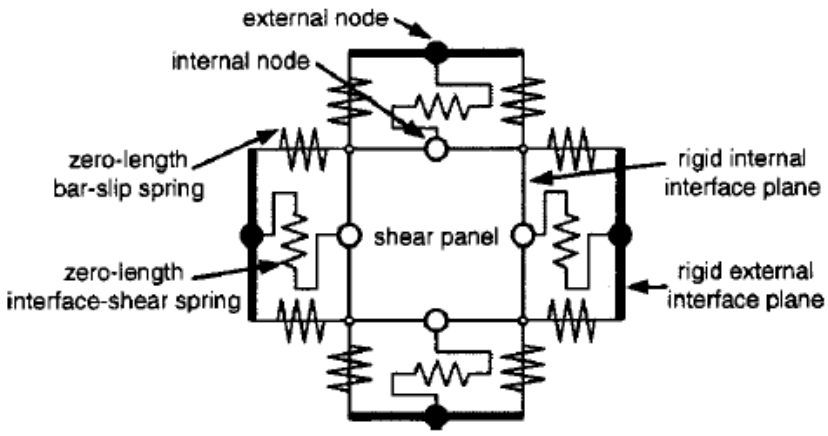

Figure 2.9: Finite Element Definition of RC Beam-to-Column Connection Region (Lowes and Altoontash 2003)

Shin and LaFave [31] investigated the effects of some key parameters such as concrete compressive strength, joint reinforcement and axial load effect from numerous beam-to-column connection tests. Afterwards, an analytical method was proposed to estimate the hysteretic joint shear stress versus strain behavior by employing modified compression field theory. This model was presented by rigid elements located along the joint edges and nonlinear rotational springs placed in one of the four hinges linking the rigid elements (**Figure 2.10**). When the model was applied to the analysis of some specimens tested previously, it adequately predicted the overall load-displacement response.

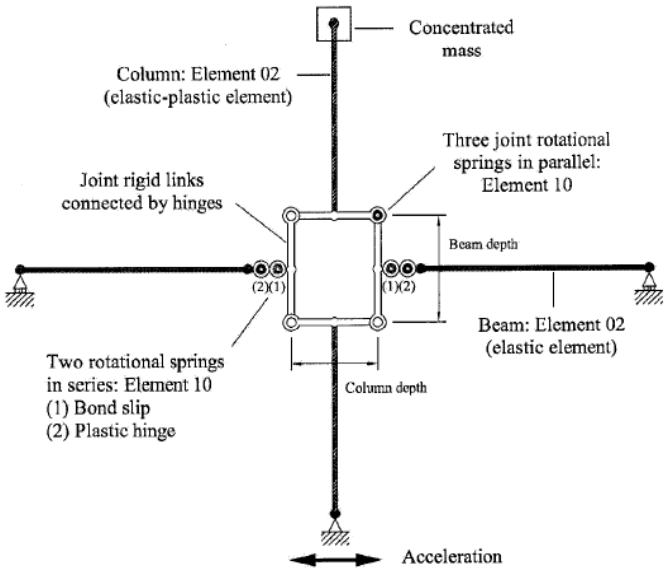

Figure 2.10: Model of Beam-to-Column Connection Subassembly (Shin and LaFave 2004)

Mitra and Lowes [28] improved previously developed model of Altoontash and Lowes by changing the element definition. A numerical simulation of the parameters in conjunction with finite element analysis to predict the joint shear strength was utilized in this study. For the simulation of the joint core, a compression-strut model was used and for the simulation of joint stiffness, bond-slip response was also considered besides nonlinear joint core response. An extensive experimental database of beam-to-column subassemblies was used in order to evaluate the accuracy of the model. The results showed that the model predicts the actual behavior with about 80 – 90 % accuracy.

Burak and Wight [3] used experimental results and developed a joint model that takes into account the joint shear strain and predicts the joint shear behavior. The model presents an optimized equation including concrete compressive strength, geometry and eccentricity parameters. The subassemblies were analyzed using the joint model and consistent results were obtained. Besides, a five story building was analyzed by using both rigid connections and connections with the developed joint model. It was concluded

that if the joint model was not included in the analysis the roof drifts could be underestimated up to 25 %.

Canbolat [4] developed a parametric joint model that takes into account the material properties, geometric properties and confinement provided by the joint hoop reinforcement. The model was used in the dynamic time history analysis of a five-story RC building. The results showed that the roof drifts differed up to 25 % when the analytical joint model was utilized.

More recently, Kim and LaFave [21] used statistical methods to evaluate the effect of key parameters such as concrete compressive strength, panel geometry, confinement due to joint reinforcement, column axial compression and bond demand level of the longitudinal reinforcement on the joint behavior. It was concluded that joint shear capacity mostly depends on concrete compressive strength; however, joint panel geometry has only a slight effect on seismic performance. After having determined the most influential parameters on joint shear stress-strain behavior, an equation representing joint shear strength was developed by using Bayesian parameter estimation approach.

CHAPTER 3

DATABASE COLLECTION

A database of experimental results was generated in order to be used in the prediction of the joint shear strength vs. deformation behavior of reinforced concrete beam-to-column connections under earthquake loading. Therefore, numerous prior experiments on reinforced concrete beam-to-column connections were examined and the ones that include the parameters considered in this study were selected. The tests which do not provide detailed data on joint shear strength and deformation were not considered. In this chapter, selection criteria of the experiments, properties of the specimens and experimental results are described and the resulting database is presented.

3.1 SELECTION CRITERIA AND GENERAL PROPERTIES OF SPECIMENS

Experimental studies involving both interior and exterior connections tested under cyclic loading are investigated and included in the database. Roof connections, on the other hand, are not considered since there are few studies on this type of connections in the literature to construct a reliable model. All of the joint subassemblies included in the database were tested under cyclic lateral loading. Tests on precast beam-to-column connections are out of scope of this study. Moreover, subassemblies including fiber reinforced cementitious composites are not included in the database.

The specimens used in the database involve conventional beam, column and connection design in which ACI Building Code guidelines are followed. The database contains specimens with wide beams, slabs and/or transverse beams. Moreover, in order to investigate the effect of eccentricity on the joint shear strength, specimens that have eccentricity between the centerlines of the longitudinal beams and the column are included in the database.

While constructing database, general layout of specimens, that is the length of top and bottom columns and right and left beams were tabularized first. Then, geometric and material properties of beams, columns and joint regions were entered in to the table. As for the geometric properties; height and width of members, longitudinal and transverse reinforcement amount and their detailing were considered. The number and spacing of stirrups in the joint region, the height and width of the joint core and the area of the joint reinforcement were also considered. For the material properties; the compressive strength of concrete at the test date and the yield strengths of all reinforcement used were included in the database. Furthermore, when there is eccentricity or axial load applied to the column, these properties were also incorporated into the database. At the presence of a slab, the effective beam width was computed and given in the table. Finally, cyclic test results such as lateral load versus displacement or drift, joint shear stress versus joint shear strain responses were examined and incorporated into the resulting database.

3.2 SELECTED EXPERIMENTS

After investigating numerous experimental studies carried out worldwide, 17 of them containing 100 specimens were selected and a database was formed. As mentioned before, besides the key parameters such as material and geometric characteristics of the connection subassemblies, special attention was also given to parameters such as eccentricity, wide beams and slabs. In this section, the specimens used in the database are introduced and described based on aforementioned properties.

3.2.1 Specimens with Conventional Members and Characteristics

One of the studies included in the database is the one in which Durrani and Wight [10] tested three interior beam-to-column connections (X1, X2 and X3) under earthquake-type loading. The specimens are representative models of interior connections isolated at the inflection points of the beams and columns. Beams have a rectangular cross-section whereas the columns are square.

Another set of specimens belongs to the experimental study of Ehsani and Wight [11]. Six exterior reinforced concrete beam-to-column connections (1B, 2B, 3B, 4B, 5B, 6B) were tested and the behavior under cyclic loading was examined. Column and beam dimensions and the lateral reinforcement ratio of the joint region are the variables investigated in this study.

Fujii and Morita [14] made a comparison between the behavior of interior and exterior RC beam-to-column connections. There are four interior (A1, A2, A3, A4) and four exterior (B1, B2, B3, B4) subassemblies. Test variables were beam bar strength, column axial load and the amount of joint hoop reinforcement. These experiment subassemblies were also incorporated into the database.

Finally, 18 specimens of Kaku and Asakusa [19] were included in the database. The specimens were all designed as about one third of full scale structures. Column axial load (N), amount of joint hoop reinforcement (ρ_w) and moment flexural ratio (M_r) were the experimental variables whose effects on the seismic behavior of connections were investigated.

3.2.2 Specimens Constructed with High-Strength Material

In order to define a parameter that accounts for the effect of concrete compressive strength or reinforcement yield strength, the studies involving connections constructed with varying strength of materials were investigated.

One of the studies selected for the database to account for material strength was carried out by Ehsani and Alameddine [12]. The researchers tested four groups of specimens

(LLs, LHs, HLs, HHs). There are three specimens in each group, thus total of twelve specimens were tested. The first letter indicates low or high joint shear whereas the second letter shows a low or high confinement level. Three specimens in each group are named with a numeral which indicates concrete compressive strength in ksi units.

Another selected research on varying-strength material is the experiment conducted by Oka and Shiohara [33]. Nine specimens (J-1, J-2, J-4, J-5, J-6, J-7, J-8, J-10, J-11) were tested in this study. The specimens had a scale of approximately 1/2.5. The main variables of the specimens were the concrete compressive strength, the reinforcement yield strength and the amount of beam longitudinal reinforcement.

Finally, four specimens of Guimaraes, Kreger and Jirsa [16] were incorporated into the database since the specimens (J2, J4, J5, J6) were constructed with normal and high-strength concrete, longitudinal and transverse reinforcement. In this experiment joint-shear provisions were assessed for interior beam-column-slab connections constructed using high-strength materials.

3.2.3 Specimens with Eccentricity

In the database, studies involving eccentric connections were also included. In the study by Raffaelle and Wight [32], four reinforced concrete eccentric beam-to-column specimens were tested. Besides the eccentricity, the main parameters varied in the specimens were the beam width, beam depth, and the amount of beam flexural reinforcement.

Chen and Chen [6] also investigated the cyclic behavior of RC eccentric beam-to-column connections. This research included six beam-to-column subassemblies one of which is concentric (JC), another one is eccentric (JE) and the rest are the eccentric connections with spread-ended beams (JS1, JS2, JS3 and JS4). For the database, however, only JC and JE specimens were selected to be used since these two specimens are nearly identical except for the eccentricities. On the other hand, JS series were not included because spread end in the beams affects the joint behavior significantly and the

data to propose a parameter reflecting spread-end behavior is limited in the database of this study.

Teng and Zhou [34] tested five interior reinforced concrete beam-to-column connection subassemblies (S1, S2, S3, S5, and S6). S1 was concentric, the rest were eccentric. However, the eccentricities of specimens S3 and S6 were twice as high as that of S2 and S5. In addition, S1, S2 and S3 have different member geometry and detailing than S5 and S6.

Burak and Wight [3] tested 3/4-scale eccentric reinforced concrete beam-column-slab subassemblies under cyclic lateral loading. The significance in this study is that the lateral load was applied to the subassemblies in two principal directions. Thus, the behavior in the direction parallel to the spandrel and normal beams were investigated separately. The spandrel beams had eccentricity between the centerline of the beam and the centroidal axis of the column. As a result, five specimens from this study (1-S, 2-S, 3-S, 2-N, and 3-N) were selected to investigate the effect of the floor system on the behavior of eccentric beam-to-column connections. Specimens 2-S and 3-S are eccentric interior connections, 2-N and 3-N are concentric exterior ones.

Another set of experiments on eccentric connections included in the database is from the study of Lee and Ko [26]. There were five specimens in this experiment set with varying eccentricities. Column width, column depth, moment strength ratio, and embedment length of beam reinforcement are the key variables of these specimens. The researchers also aimed to see the effect of loading in the strong or weak directions on joint shear capacity by changing the loading direction.

3.2.4 Specimens with Wide Beams

Gentry and Wight [15] tested four exterior 3/4-scale reinforced concrete beam-to-column connection specimens including transverse beams. The variables investigated in these experiments are the beam width-to-column width ratio, the percentage of the total flexural reinforcement anchored in the column core, the column moment strength to beam moment strength ratio and the shear stress applied to the joint.

Another selected study on wide beam-to-column connections was the experiments of LaFave and Wight [24]. The researchers tested four reinforced concrete exterior beam-to-column connections. Three of the specimens included wide beam (EWB 1, EWB 2, and EWB 3) whereas the fourth specimen (ENB 1) had a conventional beam in order to make a comparison. On the other hand, floor slab was present in order to see its effect on wide beam-to-column connections. All of the test specimens were about three-quarter-scale of real exterior beam-to-column connections. The width of the beam and the reinforcement fraction anchored in the column core vary in these experiments.

Experiment of Quintero-Febres and Wight [36] was selected for the database. In this experiment, three interior wide beam-column-slab connections (IWB 1, IWB 2, IWB 3) were tested under lateral loading. Beam and column dimensions are the control variables in this study. Hence, the effect of geometry on joint shear strength behavior was examined.

Burak and Wight [3] also investigated the effect of wide beams in their study. One of their above-mentioned specimens (3-N) has wide beam in the loading direction. Therefore, this specimen was utilized in the database to assess the wide beam effect besides the influence of eccentricity and presence of slab.

3.2.5 Specimens with Slab

The experiments of Kitayama, Otani and Aoyama [23] were selected for the database. Four interior beam-to-column joint specimens (A1-without slab, A2-with slab, A3-with slab and transverse beam, and A4-without slab but with transverse beams) were tested under cyclic loading and the effect of slab and transverse beams on the joint behavior were investigated in this study.

Shin and LaFave [31] investigated the effect of floor slabs on the seismic performance of reinforced concrete exterior beam-column-slab connections. The specimens (SL1, SL2, SL3, SL4) tested in this study were incorporated into the database since they involve the parameters such as eccentricity, floor slabs and transverse beams.

3.3 RESULTING DATABASE

As a result, the experimental database consists of 100 specimens from 17 different research projects. **Table 3.1** summarizes the type of the specimens that are considered in this analytical study in terms of number of interior and exterior specimens and the number of specimens having wide beams, slabs and eccentricity.

Table 3.1: Connection Types in the Database

	Interior	**Exterior**	**TOTAL:**
Connections with Conventional Beam	40	49	*89*
Connections with Wide Beam	3	8	*11*
Connections with Slab	16	6	*22*
Connections without Slab	27	51	*78*
Connections with Eccentricity	9	4	*13*
Connections without Eccentricity	34	53	*87*
TOTAL:	***43***	***57***	***100***

Table 3.2 shows the main properties of the specimens including geometric properties such as column width (b_c), column depth (h_c), beam width (b_b) and beam depth (h_b). Moreover, when the connection has a slab; slab thickness (t) and effective beam width (b_e) are also given. Material strengths, f_c and f_y represent the concrete compressive strength and yield strength of the longitudinal reinforcement respectively. The eccentricity between the centerlines of column and beam (e) are also provided in this table.

Table 3.3 presents the properties of the joint region and the amount of axial load applied to the column (N). For the joint lateral reinforcement, yield strength (f_y), number of layers and spacing of the reinforcement in the joint core, number of legs in a layer and reinforcement area for one bar are shown in this table. In addition, configurations of the hoops are shown with the letters by which S denotes square stirrup, D denotes diamond configuration and C denotes cross-ties.

Table 3.2: Experimental Database - Properties of Beams, Columns and Slab

Research Team	Specimen	Type	Column Properties				Beam Properties					e (mm)	t (mm)
			f_c (MPa)	f_y (MPa)	b_c (mm)	h_c (mm)	f_c (MPa)	f_y (MPa)	b_b (mm)	b_e (mm)	h_b (mm)		
Burak & Wight	1-S	Interior	39	441	356	356	29	448	203	611	381	76	102
	2-S	Interior	40	441	534	356	39	448	254	662	457	140	102
	3-S	Interior	32	441	534	356	29	448	254	662	457	140	102
	2-N	Exterior	40	441	356	534	39	448	305	1225	457	0	102
	3-N	Exterior	32	441	356	534	29	448	762	1225	305	0	102
Chen & Chen	JC	Exterior	20	457	500	500	20	457	300	-	500	0	-
	JE	Exterior	20	457	500	500	20	457	300	-	500	100	-
Durrani & Wight	X1	Interior	31	414	362	362	34	331	279	-	419	0	-
	X2	Interior	33	414	362	362	34	331	279	-	419	0	-
	X3	Interior	30	331	362	362	31	331	279	-	419	0	-
Ehsani & Alameddine	LL8	Exterior	55	457	356	356	55	457	311	-	508	0	-
	LH8	Exterior	55	457	356	356	55	457	311	-	508	0	-
	HL8	Exterior	55	457	356	356	55	457	311	-	508	0	-
	HH8	Exterior	55	457	356	356	55	457	311	-	508	0	-
	LL11	Exterior	76	457	356	356	76	457	311	-	508	0	-
	LH11	Exterior	76	457	356	356	76	457	311	-	508	0	-
	HL11	Exterior	76	457	356	356	76	457	311	-	508	0	-
	HH11	Exterior	76	457	356	356	76	457	311	-	508	0	-
	LL14	Exterior	96	457	356	356	96	457	311	-	508	0	-
	LH14	Exterior	96	457	356	356	96	457	311	-	508	0	-
	HL14	Exterior	96	457	356	356	96	457	311	-	508	0	-
	HH14	Exterior	96	457	356	356	96	457	311	-	508	0	-
Ehsani & Wight	1B	Exterior	34	414	300	300	34	331	259	-	480	0	-
	2B	Exterior	35	414	300	300	35	331	259	-	439	0	-
	3B	Exterior	41	414	300	300	41	331	259	-	480	0	-
	4B	Exterior	45	414	300	300	45	331	259	-	439	0	-
	5B	Exterior	24	414	340	340	24	331	300	-	480	0	-
	6B	Exterior	40	414	340	340	40	331	300	-	480	0	-
Fujii & Morita	A1	Interior	40	656	220	220	40	1090	160	-	250	0	-
	A2	Interior	40	395	220	220	40	417	160	-	250	0	-
	A3	Interior	40	656	220	220	40	1090	160	-	250	0	-
	A4	Interior	40	656	220	220	40	1090	160	-	250	0	-
	B1	Exterior	30	395	220	220	30	1090	160	-	250	0	-
	B2	Exterior	30	395	220	220	30	417	160	-	250	0	-
	B3	Exterior	30	395	220	220	30	1090	160	-	250	0	-
	B4	Exterior	30	395	220	220	30	1090	160	-	250	0	-
Gentry & Wight	1	Exterior	28	441	356	356	28	469	864	-	305	0	-
	2	Exterior	28	441	356	356	28	469	762	-	305	0	-
	3	Exterior	28	441	356	356	28	469	864	-	305	0	-
	4	Exterior	28	441	356	356	28	469	864	-	305	0	-
Guimaraes, Kreger & Jirsa	J2	Interior	26	414	508	508	28	463	406	1295	508	0	127
	J4	Interior	29	517	508	508	32	463	406	1295	508	0	127
	J5	Interior	95	414	508	508	78	543	406	1295	508	0	127
	J6	Interior	70	517	508	508	92	459	406	1295	508	0	127

Table 3.2 (Continued)

Research Team	Specimen	Type	Column Properties				Beam Properties					e (mm)	t (mm)
			f_c (MPa)	f_y (MPa)	b_c (mm)	h_c (mm)	f_c (MPa)	f_y (MPa)	b_b (mm)	b_e (mm)	h_b (mm)		
Kaku & Asakusa	Specimen 1	Exterior	31	360	220	220	31	391	160	-	220	0	-
	Specimen 2	Exterior	42	360	220	220	42	391	160	-	220	0	-
	Specimen 3	Exterior	42	360	220	220	42	391	160	-	220	0	-
	Specimen 4	Exterior	45	360	220	220	45	391	160	-	220	0	-
	Specimen 5	Exterior	37	360	220	220	37	391	160	-	220	0	-
	Specimen 6	Exterior	40	360	220	220	40	391	160	-	220	0	-
	Specimen 7	Exterior	32	395	220	220	32	391	160	-	220	0	-
	Specimen 8	Exterior	41	395	220	220	41	391	160	-	220	0	-
	Specimen 9	Exterior	41	395	220	220	41	391	160	-	220	0	-
	Specimen 10	Exterior	44	395	220	220	44	391	160	-	220	0	-
	Specimen 11	Exterior	42	395	220	220	42	391	160	-	220	0	-
	Specimen 12	Exterior	35	395	220	220	35	391	160	-	220	0	-
	Specimen 13	Exterior	46	395	220	220	46	391	160	-	220	0	-
	Specimen 14	Exterior	41	395	220	220	41	391	160	-	220	0	-
	Specimen 15	Exterior	40	395	220	220	40	391	160	-	220	0	-
	Specimen 16	Exterior	37	395	220	220	37	391	160	-	220	0	-
	Specimen 17	Exterior	40	395	220	220	40	391	160	-	220	0	-
	Specimen 18	Exterior	41	395	220	220	41	391	160	-	220	0	-
Kitayama, Otani & Aoyama	A1	Interior	31	550	300	300	31	795	200	-	300	0	-
	A2	Interior	31	550	300	300	31	795	200	-	300	0	-
	A3	Interior	31	550	300	300	31	795	200	675	300	0	70
	A4	Interior	31	550	300	300	31	795	200	675	300	0	70
LaFave & Wight	EWB 1	Exterior	43	462	356	356	29	483	864	1226	305	0	102
	EWB 2	Exterior	39	462	356	356	30	462	864	1226	305	0	102
	EWB 3	Exterior	35	434	305	508	34	434	940	1226	305	0	102
	ENB 1	Exterior	27	434	305	508	25	434	305	1226	559	0	102
Lee & Ko	S0	Exterior	33	455	400	600	33	455	300	-	450	0	-
	S50	Exterior	34	455	400	600	34	455	300	-	450	50	-
	W0	Exterior	29	455	600	400	29	455	300	-	450	0	-
	W75	Exterior	30	455	600	400	30	455	300	-	450	75	-
	W150	Exterior	29	455	600	400	29	455	300	-	450	150	-
Oka & Shiohara	J-1	Interior	81	638	300	300	81	638	240	-	300	0	-
	J-2	Interior	81	1456	300	300	81	1456	240	-	300	0	-
	J-4	Interior	73	515	300	300	73	515	240	-	300	0	-
	J-5	Interior	79	839	300	300	79	839	240	-	300	0	-
	J-6	Interior	79	676	300	300	79	676	240	-	300	0	-
	J-7	Interior	79	676	300	300	79	676	240	-	300	0	-
	J-8	Interior	79	370	300	300	79	370	240	-	300	0	-
	J-10	Interior	39	700	300	300	39	700	240	-	300	0	-
	J-11	Interior	39	372	300	300	39	372	240	-	300	0	-
Quintero-Febres & Wight	IWB1	Interior	28	414	356	356	28	414	889	1226	305	0	102
	IWB2	Interior	28	414	356	356	28	414	660	1226	305	0	102
	IWB3	Interior	28	414	330	508	28	414	838	1226	305	0	102

Table 3.2 (Continued)

Research Team	Specimen	Type	Column Properties				Beam Properties					e (mm)	t (mm)
			f_c (MPa)	f_y (MPa)	b_c (mm)	h_c (mm)	f_c (MPa)	f_y (MPa)	b_b (mm)	b_e (mm)	h_b (mm)		
Raffaelle & Wight	1	Interior	29	414	356	356	29	476	254	-	381	51	-
	2	Interior	27	414	356	356	27	476	178	-	381	89	-
	3	Interior	38	414	356	356	38	476	191	-	381	83	-
	4	Interior	19	414	356	356	19	476	191	-	559	83	-
Shin & LaFave	SL 1	Interior	36	538	457	330	30	503	279	694	406	89	102
	SL 2	Interior	41	538	457	330	36	503	178	593	406	140	102
	SL 3	Interior	45	503	457	330	47	510	279	694	406	0	102
	SL 4	Interior	31	503	279	368	31	510	279	694	406	0	102
Teng & Zhou	S1	Interior	33	530	400	300	33	510	200	-	400	0	-
	S2	Interior	34	530	400	300	34	510	200	-	400	50	-
	S3	Interior	35	530	400	300	35	510	200	-	400	100	-
	S5	Interior	39	530	400	200	39	425	200	-	400	50	-
	S6	Interior	38	530	400	200	38	425	200	-	400	100	-

Table 3.3: Experimental Database - Joint Properties and Axial Load Level

Research Team	Specimen	Joint	Joint Reinforcement						Axial load, N (kN)	$N/A_g.f_c$
		f_c (MPa)	f_y (MPa)	spacing (mm)	# of layers	Area (mm2)	Config.	# of legs		
Burak & Wight	1-S	29.0	441	95	4	127	S+D	4	196	0.053
	2-S	39.0	441	95	4	127	S+D	4	289	0.039
	3-S	29.0	441	95	4	127	S+D	4	234	0.042
	2-N	39.0	441	95	4	127	S+D	4	231	0.031
	3-N	29.0	441	95	4	127	S+D	4	169	0.031
Chen & Chen	JC	19.9	399	75	5	133	S+C	3	0	0.000
	JE	19.9	399	75	5	133	S+C	3	0	0.000
Durrani & Wight	X1	34.3	352	152	2	127	S+D	4	245	0.054
	X2	33.6	352	102	3	127	S+D	4	245	0.056
	X3	31.0	352	152	2	127	S+D	4	214	0.053
Ehsani & Alameddine	LL8	55.1	446	102	4	127	S+C	3	294	0.042
	LH8	55.1	446	61	6	127	S+C	3	294	0.042
	HL8	55.1	446	102	4	127	S+C	3	507	0.073
	HH8	55.1	446	61	6	127	S+C	3	507	0.073
	LL11	75.8	446	102	4	127	S+C	3	285	0.030
	LH11	75.8	446	61	6	127	S+C	3	276	0.029
	HL11	75.8	446	102	4	127	S+C	3	587	0.061
	HH11	75.8	446	61	6	127	S+C	3	605	0.063
	LL14	96.5	446	102	4	127	S+C	3	236	0.019
	LH14	96.5	446	61	6	127	S+C	3	222	0.018
	HL14	96.5	446	102	4	127	S+C	3	489	0.040
	HH14	96.5	446	61	6	127	S+C	3	476	0.039

Table 3.3 (Continued)

Research Team	Specimen	Joint	Joint Reinforcement						Axial load, N (kN)	$N/A_g.f_c$
		f_c (MPa)	f_y (MPa)	spacing (mm)	# of layers	Area (mm2)	Config.	# of legs		
Ehsani & Wight	1B	33.6	437	112	2	127	S+D	4	178	0.059
	2B	34.9	437	99	2	127	S+D	4	222	0.071
	3B	40.9	437	84	3	127	S+D	4	222	0.060
	4B	44.6	437	76	3	127	S+D	4	222	0.055
	5B	24.3	437	109	2	127	S+D	4	356	0.126
	6B	39.8	437	117	2	127	S+D	4	303	0.066
Fujii & Morita	A1	40.2	297	50	3	28	S	2	147	0.076
	A2	40.2	297	50	3	28	S	2	147	0.076
	A3	40.2	297	50	3	28	S	2	441	0.227
	A4	40.2	297	35	4	28	S+S	4	441	0.227
	B1	30.0	297	50	3	28	S	2	98	0.068
	B2	30.0	297	50	3	28	S	2	98	0.068
	B3	30.0	297	50	3	28	S	2	343	0.236
	B4	30.0	297	35	4	28	S+S	4	343	0.236
Gentry & Wight	1	27.6	441	102	2	71	S+D	4	89	0.026
	2	27.6	441	102	2	71	S+D	4	89	0.026
	3	27.6	441	102	2	71	S+D	4	89	0.026
	4	27.6	441	102	2	71	S+D	4	89	0.026
Guimaraes, Kreger & Jirsa	J2	27.6	549	102	3	127	S+C	3	0	0.000
	J4	31.6	549	102	4	127	S+C	3	0	0.000
	J5	77.9	511	102	3	285	S+C+C	4	0	0.000
	J6	92.1	511	102	3	285	S+C+C	4	0	0.000
Kaku & Asakusa	Specimen 1	31.1	250	52	4	28	S	2	258	0.171
	Specimen 2	41.7	250	52	4	28	S	2	199	0.099
	Specimen 3	41.7	250	52	4	28	S	2	0	0.000
	Specimen 4	44.7	281	52	4	7	S	2	360	0.166
	Specimen 5	36.7	281	52	4	7	S	2	160	0.090
	Specimen 6	40.4	281	52	4	7	S	2	0	0.000
	Specimen 7	32.2	250	52	4	28	S	2	194	0.124
	Specimen 8	41.2	250	52	4	28	S	2	160	0.080
	Specimen 9	40.6	250	52	4	28	S	2	0	0.000
	Specimen 10	44.4	281	52	4	7	S	2	360	0.168
	Specimen 11	41.9	281	52	4	7	S	2	160	0.079
	Specimen 12	35.1	281	52	4	7	S	2	0	0.000
	Specimen 13	46.4	250	52	4	28	S	2	-100	-0.045
	Specimen 14	41.0	281	52	4	7	S	2	160	0.081
	Specimen 15	39.7	281	52	4	7	S	2	160	0.083
	Specimen 16	37.4	250	52	4	28	S	2	0	0.000
	Specimen 17	39.7	250	52	4	28	S	2	0	0.000
	Specimen 18	40.7	250	52	4	28	S	2	0	0.000
Kitayama, Otani & Aoyama	A1	30.6	326	45	3	28	S+C	3	177	0.064
	A2	30.6	326	45	3	28	S+C	3	177	0.064
	A3	30.6	326	45	3	28	S+C	3	177	0.064
	A4	30.6	326	45	3	28	S+C	3	177	0.064

Table 3.3 (Continued)

Research Team	Specimen	Joint	Joint Reinforcement						Axial load, N (kN)	$N/A_g.f_c$
		f_c (MPa)	f_y (MPa)	spacing (mm)	# of layers	Area (mm2)	Config.	# of legs		
LaFave & Wight	EWB 1	28.9	482	89	3	71	S+D	4	0	0.000
	EWB 2	30.3	482	89	3	71	S+D	4	0	0.000
	EWB 3	34.5	482	76	4	71	S+C	3	0	0.000
	ENB 1	24.8	482	76	5	71	S+C	3	0	0.000
Lee & Ko	S0	32.6	471	100	3	79	S+C	3	700	0.089
	S50	34.2	471	100	3	79	S+C	3	700	0.085
	W0	28.9	471	100	3	79	S+C+C+C	5	700	0.101
	W75	30.4	471	100	3	79	S+C+C+C	5	700	0.096
	W150	29.1	471	100	3	79	S+C+C+C	5	700	0.100
Oka & Shiohara	J-1	81.2	1374	50	5	28	S	2	834	0.114
	J-2	81.2	1374	50	5	28	S	2	834	0.114
	J-4	72.8	1374	50	5	28	S	2	834	0.127
	J-5	79.2	1374	50	5	28	S	2	834	0.117
	J-6	79.2	775	100	3	28	S	2	834	0.117
	J-7	79.2	857	50	5	28	S	2	834	0.117
	J-8	79.2	775	50	5	28	S	2	834	0.117
	J-10	39.2	598	50	5	28	S	2	834	0.236
	J-11	39.2	401	50	5	28	S	2	834	0.236
Quintero-Febres & Wight	IWB1	27.6	503	83	3	71	S+S	4	0	0.000
	IWB2	27.6	503	83	3	71	S+S	4	0	0.000
	IWB3	27.6	503	83	3	71	S+C	3	0	0.000
Raffaelle & Wight	1	28.6	441	89	3	71	S+D	4	89	0.025
	2	26.8	441	89	3	71	S+D	4	89	0.026
	3	37.7	441	89	3	71	S+D	4	89	0.019
	4	19.3	441	89	5	71	S+D	4	89	0.036
Shin & LaFave	SL 1	29.9	468	83	3	71	S+C	3	0	0.000
	SL 2	36.1	468	83	3	71	S+C	3	0	0.000
	SL 3	47.4	551	83	3	71	S+C	3	0	0.000
	SL 4	31.1	579	83	3	71	S+C	3	0	0.000
Teng & Zhou	S1	33.0	440	75	3	79	S+C	3	441	0.111
	S2	34.0	440	75	3	79	S+C	3	441	0.108
	S3	35.0	440	75	3	79	S+C	3	441	0.105
	S5	39.0	440	50	3	79	S+C	3	343	0.110
	S6	38.0	440	50	3	79	S+C	3	343	0.113

CHAPTER 4

ANALYTICAL JOINT MODEL DEFINITION:

From several experimental studies on seismic behavior of reinforced concrete beam-to-column connections, it was observed that if a deformable joint model is not defined in frame modeling, lateral drift of the structure was underestimated [3]. Therefore, a joint model representing the inelastic activity in the connection region should be developed to be used in the analytical modeling of a reinforced concrete building subjected to earthquake loading. Since this inelastic activity in the joint region is based on the deterioration of shear strength and stiffness, the shear stress versus strain behavior of the joint region should be predicted to construct the joint model.

In order to predict the shear strength and strain behavior, prior experimental data on joint shear strength versus distortion of beam-to-column connections which provides accurate joint shear strength and strain measurements were utilized. The parameters which were believed to be influential on the behavior of joints were listed in a database. By using statistical correlation methods, the most effective parameters were determined whereas the ones which have a negligible effect on the shear strength behavior were disregarded. Consequently, an equation to accurately predict the maximum joint shear strength of reinforced concrete beam-to-column connections subjected to earthquake loading was generated. Final parameters in the equation are defined in terms of ratios and powers of some of the key individual parameters to accurately represent their effect on the capacity and obtain the minimum average error and the highest correlation with the experimental values. While carrying out these steps, the guidelines given in ACI Committee 318

(2008), Building Code Requirements for Structural Concrete and ACI-ASCE Committee 352 (2002), Recommendations for Design of Beam-Column Connections in Monolithic Reinforced Concrete Structures were followed. After obtaining an equation for predicting the maximum joint shear strength, two more critical points in the joint shear strength versus shear strain curve were determined by using the statistical data. The points where initial cracking and accumulation of inelastic activity are observed were selected as the two critical points. Then, a formula was developed to obtain the shear distortion at these critical points. In this chapter, the procedure followed to develop the shear strength and shear strain will be explained and the details on selecting the key parameters will be given.

4.1 JOINT SHEAR STRENGTH DEFINITION

4.1.1 Selection of Key Parameters Affecting Joint Shear Strength

As mentioned in Chapter 2, there are several factors affecting the maximum joint shear strength of reinforced concrete beam-to-column connections. Impact of these parameters on the seismic behavior was mostly determined through the individual experimental studies. However, each study presents different results and ideas on the rate of influence of the parameters. An approach is outlined to integrate these results and develop a parametric equation representing the joint shear strength.

Prior experimental studies indicated that material strength of both concrete and reinforcing steel play an important role in joint shear strength capacity. Moreover, confinement is an important factor affecting the joint behavior. Confinement is either provided by the transverse reinforcement in the joint or by the transverse beams and slab framing into the connection region. To take in to account the effect of confinement, volumetric confinement ratio is determined in three different ways considering the effective confined area as the gross connection area, joint core area and the effective area that contains one layer of joint transverse reinforcement as given in the following equation:

$$\rho_{gross} = \frac{n \times A_o \times l_{eff}}{h_c \times b_c \times h_b}$$

$$\rho_{core} = \frac{n \times A_o \times l_{eff}}{h_{c,core} \times b_{c,core} \times h_{b,core}} \quad \textbf{(4.1)}$$

$$\rho_{onelayer} = \frac{A_o \times l_{eff}}{h_{c,core} \times b_{c,core} \times s}$$

where, n is the number of layers of transverse reinforcement in the effective confined area, A_o is the cross-sectional area of the transverse reinforcement, l_{eff} denotes the effective length of the lateral reinforcement in the loading direction, b_c is the column width, h_c and h_b represent the depth of the column and beam respectively and s is the spacing of the transverse reinforcement.

In addition to these parameters, column and beam dimensions, axial load acting on the column, and the eccentricity between the longitudinal axes of the column and the beam are some other factors affecting the joint shear strength. Prior studies proved that the effective joint width is an important parameter that defines the joint shear strength. Thus, effective joint width of all specimens is calculated following the guidelines of ACI-ASCE Committee 352 Recommendations (2002). Moreover, the effective joint width recommended by LaFave et.al. [25] was also considered in the development of the proposed formula. For wide beams, the effective joint width recommended by Burak and Wight [5] was used in the computations. These effective joint width definitions are presented below:

1) ACI-352 Recommendations define the effective joint width as the smallest of:

$$b_j = \frac{b_b + b_c}{2} \quad ; \qquad b_j = b_b + \sum \frac{m \cdot h_c}{2} \quad ; \qquad b_c \quad \textbf{(4.2)}$$

2) LaFave, Bonacci, Burak, & Shin define the effective joint width as:

$$b_j = \frac{b_b + b_c}{2} \quad \textbf{(4.3)}$$

3) Burak and Wight define the effective joint width of connections with wide beams as:

$$b_j = b_c + \frac{1}{4} \times (b_b - b_c) \quad \textbf{(4. 4)}$$

where, b_b is the width of the longitudinal beam,

b_c is the column width perpendicular to the direction of loading,

h_c is the full depth of column,

m is the slope to define effective width of joint perpendicular to the direction of shear. For joints where the eccentricity between the beam centerline and the column centroid exceeds $b_c/8$, m = 0.3; for all other cases, m = 0.5.

In the database, $v_{j,max}$ is computed by dividing maximum joint shear force observed in the test to the effective joint area, which is the multiplication of the effective joint width and the column depth. When the experimental results did not include maximum shear forces or stresses, strain gage data for top and bottom longitudinal beam reinforcement was utilized to compute maximum joint shear force. By using tensile forces on the longitudinal bars, maximum joint shear stresses are calculated as shown in **Figure 4.1**. In this figure, tensile forces (T_1 and T_2) are obtained by using **Equation (4.5**). In this equation the stress multiplier 1.25 of ACI 352R-2002 takes into account the fact that the actual yield stress of a typical reinforcing bar is 10 to 25 % higher than the nominal value, and there could be strain hardening.

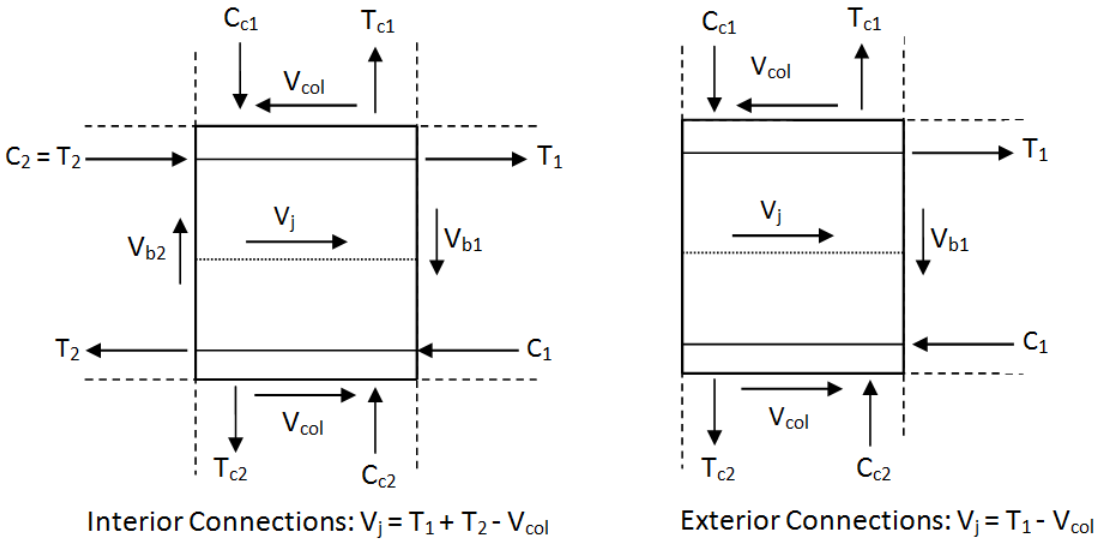

Figure 4.1: Computation of the horizontal joint shear in interior and exterior connections

$$T = (1.25) \cdot A_s \cdot f_y \quad \text{if} \quad \varepsilon_s \geq \varepsilon_y$$
$$T = A_s \cdot \varepsilon \cdot E \quad \text{if} \quad \varepsilon_s < \varepsilon_y \qquad \textbf{(4.5)}$$

In order to evaluate the influence of different parameters on joint shear strength, a correlation coefficient defined in **Equation (4.6)** is used. In this statistical approach, y is the joint shear strength and x is taken as the selected independent variable. The variables and their linear correlations with maximum joint shear strength are presented in **Table 4.1**. Although these correlation values are rough estimates for the effect of parameters on the shear strength since the relationships are expected to be nonlinear, a simple comparative relationship between the shear strength and each variable is obtained. As it can be seen from **Table 4.1**, concrete compressive strength has the highest correlation with the joint shear strength as also concluded by other studies [24]. In addition, reinforcement ratio and axial load has high correlation coefficients, whereas the joint geometry has only a minor effect.

In this table, some parameters have negative correlations with the experimental joint shear strength. This negative sign indicates that the parameter is inversely proportional

to the dependent variable. Moreover, for some parameters such as f_y and b_c, this coefficient is negative for exterior specimens while positive for interior ones. This deviation in the key parameters is believed to be resulting from the use of a single parameter, which cannot be directly correlated to the shear strength. Therefore, in the resulting model the combination of these parameters with each other are utilized since it is seen that the parameters obtained by the combination of key factors give better correlations.

$$\text{Correlation(X,Y)}=\frac{\sum(x-\bar{x})\cdot(y-\bar{y})}{\sqrt{\sum(x-\bar{x})^2\cdot\sum(y-\bar{y})^2}} \quad \textbf{(4.6)}$$

Table 4.1: Correlation of key parameters with the experimental joint shear strength

$V_{j,max}$ (b_j, Eq. 4.3 & 4.4)	f_c	f_y	ρ_{core}	ρ_{gross}	$\rho_{onelayer}$	b_c	h_c	b_b	h_b	N	e
Exterior	0.6598	-0.063	0.4559	0.3299	0.5197	-0.298	-0.415	-0.415	0.1781	0.3726	-0.229
Interior	0.6858	0.1002	0.2473	0.2821	0.5542	0.0275	0.1285	-0.173	0.0101	0.2159	-0.425

$V_{j,max}$ ($b_{j,352}$)	f_c	f_y	ρ_{core}	ρ_{gross}	$\rho_{onelayer}$	b_c	h_c	b_b	h_b	N	e
Exterior	0.6386	0.0522	0.5214	0.3906	0.5671	-0.236	-0.379	-0.198	0.1654	0.3760	-0.198
Interior	0.6898	0.1298	0.2927	0.3304	0.5779	0.0475	0.1669	-0.080	-0.008	0.1906	-0.425

4.1.2 Maximum Joint Shear Strength Prediction

After determining the influence rate of the parameters on maximum joint shear strength using the correlation coefficient, the key parameters were selected to develop a formula for the prediction of maximum joint shear strength. The correlation ratios of parameters were compared with each other and it is seen that ratios of some parameters is highly related to the shear strength capacity. Therefore, the ratio which gives higher correlations with the experimental results is taken as a contributing factor for the determination of the joint shear strength.

As mentioned before, the most influential parameters are concrete compressive strength and volumetric joint reinforcement ratio. **Table 4.1** indicates that $\rho_{onelayer}$ has higher correlation value when compared to ρ_{core} and ρ_{gross}, therefore, $\rho_{onelayer}$ is selected to be used in the formula. On the other hand, when joint geometry is considered, it is observed that depth of the column has the highest correlation coefficient than other geometric properties. Furthermore, it is determined that axial load and eccentricity effects should be included in the proposed formula. In order to make an accurate prediction for the maximum joint shear stress, first, effect of the joint type (interior or exterior) and number of transverse beams confining the connection region were taken into consideration. In the final formula, contributing parameters are selected as concrete compressive strength (f_c) in the connection region, joint transverse reinforcement yield strength (f_y), joint volumetric ratio for one layer of transverse reinforcement ($\rho_{onelayer}$), effective joint width (b_j), column depth (h_c), eccentricity (e), axial load (N), the presence of slab and wide or conventional transverse beams.

Interior and exterior connection behavior is different under seismic loading due to the confinement of the connection region by the transverse beams. In order to take this into account, a parameter, defined as JT (Joint Type Index), is included in the equation. For different joint types, ACI-ASCE Committee 352 recommendations are followed while determining the values of the joint type indices. Connection subassemblies investigated in this study are divided into five categories from A to E, and joint types and corresponding joint type index values are given in **Figure 4.2**.

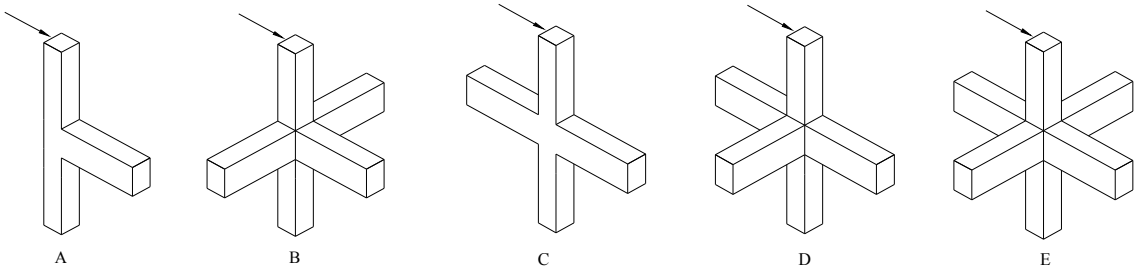

A=1.0	B=1.25	C=1.25	D=1.25	E=1.67

Figure 4.2: Joint types and joint type index (JT) value in MPa

Afterwards, the joint type index (JT) was multiplied with both concrete compressive strength and transverse reinforcement yield strength in the connection region. In order to have a close prediction on the shear strength, different powers of f_c and f_y were evaluated. Eventually, the closest prediction was obtained for the power "1/6" for both f_c and f_y. The predicted shear strength at the end of this step was JT $(f_c.f_y)^{1/6}$. After this step, the prediction was improved by including the effects of other key parameters.

As mentioned before, one of the most effective parameters on the joint shear strength is volumetric reinforcement ratio for one layer of transverse joint reinforcement. Thus, all the variables are multiplied with $\rho_{onelayer}$ and a better prediction is obtained. From the database, it is observed that when $\rho_{onelayer}$ is less than 1.0, its effect on the shear strength is negligible. Moreover, it is seen that there is not a linearly proportional relationship between shear strength and volumetric joint reinforcement ratio. Therefore, the square root of $\rho_{onelayer}$ is used when $\rho_{onelayer}$ is greater than 1.0. As a result, the following equation defines the effect of volumetric joint reinforcement ratio:

$$\rho_{onelayer}\ (\%) = 1.0 \quad \text{if} \quad \rho_{onelayer} < 1.0$$
$$\rho_{onelayer}\ (\%) = (\rho_{onelayer})^{0.5} \quad \text{if} \quad \rho_{onelayer} \geq 1.0 \qquad \textbf{(4.7)}$$

Eccentric beam-to-column connections were observed to have a reduced capacity when compared to concentric ones. In the established experimental database, it is seen that the maximum joint shear strength of eccentric connections are about 10 – 15% lower than that of concentric ones. To account for the effect of eccentricity, some geometrical properties are investigated and e/b_c ratio is considered to be the most critical parameter. This parameter was incorporated into the shear strength equation such that as eccentricity increases the strength decreases and it has no effect on the capacity of concentric connections. Since the relationship between eccentricity and shear strength is not linear, the square root of the variable is then taken and **Equation (4.8)** is used to define the parameter that accounts for the effect of eccentricity**.**

$$\text{Eccentricity Effect (EE)} = \sqrt{\frac{1}{1+e/b_c}} \qquad \textbf{(4.8)}$$

Another parameter considered in the prediction of the joint shear capacity is the axial load applied to the column. Axial load provides confinement and a stiffness increase in the joint region, if it is not too high to prematurely cause crushing. The parameter given in **Equation (4.9)** increases correlation and decreases error by taking into account the effect of axial load. It should be noted that the gross area of the column is used within the parameter because the load is applied before crushing occurs.

$$\text{Axial Load Effect (NE)} = 1+\frac{N}{A_g \cdot f_c} \qquad \textbf{(4.9)}$$

Because the column dimension in the loading direction, the column depth, is one of the most influential parameters for the performance of beam-to-column connections in moment resisting frame structures subjected to seismic loading, its effect on the proposed equation of joint shear strength was investigated. The ratio of the column width to column depth is known to influence the shear resistance of the connection

region (Raffaelle and Wight [32]). Therefore, a parameter is developed and named as column index (CI), given in **Equation (4.10)**. The factor is limited to 1.0 to be used as a penalty factor when the column is loaded along its weak axis.

$$\text{Column Index (CI)} = \begin{cases} \sqrt{\dfrac{b_c}{h_c}} & \text{when} \quad \dfrac{b_c}{h_c} < 1.0 \\ 1.0 & \text{when} \quad \dfrac{b_c}{h_c} \geq 1.0 \end{cases} \qquad \textbf{(4.10)}$$

Slab is another effective means of confinement for the connection region. Some prior studies [13], [23] showed that presence of slab in the floor system provides extra shear strength for the joint region. In order to take the presence of slab into account the effective beam width and the reinforcement ratio in the flange can be considered. Therefore, flexural capacity for the T-shaped beam cross section is calculated and divided to that of the rectangular beam section having same depth and web width. The resulting parameter defines the contribution of the slab. This parameter is named as slab index (SI) and formulized as below:

$$\begin{aligned} SI &= \frac{M_u \text{ (Flanged Section)}}{M_u \text{ (Rectangular Section)}} && \text{;when there is slab} \\ SI &= 1 && \text{;when there is no slab} \end{aligned} \qquad \textbf{(4.11)}$$

Finally, the effect of wide beams was considered, because as the beams get wider and shallower, the confinement provided to the connection region and therefore, the shear strength of the joint decreases. The geometric properties of the wide beam are taken into account by multiplying the ratio of beam depth to beam width, which indicates the aspect ratio of the section for the beams, with the ratio of joint width to beam width that gives an idea on the confined region of the joint. The resulting parameter that defines the wide beam effect proposed in the model is shown in **Equation (4.12).**

$$\text{Wide Beam Effect (WB)} = \begin{cases} WB = 1 - \frac{h_b}{b_b} \times \frac{b_j}{b_b} & \text{; when wide beams are present in the loading direction} \\ WB = 1 & \text{; when there are no wide beams in the loading direction} \end{cases} \quad \textbf{(4.12)}$$

The correlation of each selected parameter with the experimental joint shear strength is shown in **Table 4.2**. As compared to the correlations of individual key factors, higher correlations are obtained for the resulting parameters. Since the correlations of parameters are assessed for all specimens, some parameters such as Joint Type (JT) and Slab Index (SI) give negative correlations for exterior specimens while positive for interior specimens. This is believed to result from the limited data containing the JT and SI parameters for the exterior subassemblies.

Table 4.2: Correlation of Parameters with the Experimental Maximum Joint Shear Strength

Experimental vj-max (MPa)	JT	$(fc.fy)^{1/6}$	ρ_{joint}	Ecc. Effect (EE)	Column Index (CI)	Axial Load Effect (NE)	Slab Index (SI)	Wide Beam Effect (WB)	Predicted vj-max (MPa)
Interior	0.410	0.507	0.663	0.377	0.189	0.193	0.278	0.248	0.868
Exterior	-0.330	0.610	0.655	0.272	0.455	0.265	-0.341	0.324	0.815
All	0.518	0.471	0.442	0.072	0.298	0.188	0.332	0.262	0.882

The resulting formula for maximum joint shear strength prediction is given in **Equation (4.13)**, first in terms of indices, then in terms of individual parameters.

$$V_j(MPa) = JT \cdot (f_c \cdot f_y)^{1/6} \cdot \rho_{onelayer} \cdot EE \cdot CI \cdot NE \cdot WB \cdot SI$$

$$V_j(MPa) = JT \cdot (f_c \cdot f_y)^{1/6} \cdot \rho_{onelayer} \sqrt{\frac{1}{1+e/b_c}} \cdot \sqrt{\frac{b_c}{h_c}} \cdot (1+\frac{N}{A_g \cdot f_c}) \cdot (1-\frac{h_b}{b_b} \cdot \frac{b_j}{b_b}) \cdot SI \quad \textbf{(4.13)}$$

Predicted joint shear strength values obtained from **Equation (4.13)** and their comparison with the experimental ones are presented in **Table 4.3**. In order to make a comparison with the currently used code values, joint shear strength computed by the nominal shear strength definition given in ACI 352R-02 recommendations (**Equation 4.14)** are also presented in the table. The error between the predicted and experimental values, predicted and code-recommended values and finally code-recommended and experimental values are also provided. The error formula which is given by Equation 4.15 to 4.17 can be utilized to test the accuracy of the model. The average error between predicted and experimental values of joint shear strength is -4.2 % whereas the absolute average error is 14.4 %. This error can be regarded as acceptable, because bar slippage was not taken into account and the experimental maximum joint shear strength might include some error when it was computed from the strain gage data, which might sometimes be affected by the noise in the environment. It is also observed that ACI 352R-02 values for the maximum joint shear strength are significantly higher than the experimental ones for some specimens such as Specimens 2-N and 3-N of Burak & Wight, since ACI 352R-02 does not take column and beam aspect ratios into account, whereas the proposed formula results in a better prediction. For Specimen 18 of Kaku & Asakusa and Specimen ENB1 of LaFave & Wight the joint shear strength was highly overestimated by both the proposed formula and by ACI 352R-02 recommendations. This overprediction of joint shear strength capacity is believed to be the result of premature failure due to column bar fracture in Specimen 18 and bond failure in Specimen ENB1, which are not taken into account in the development of the proposed formula.

$$v_j(MPa) = 0.083 \cdot \gamma \cdot \sqrt{f_c'} \quad \textbf{(4.14)}$$

$$\%\ \text{error between predicted and experimental } v_j : \frac{(v_j\text{-predicted}) - (v_j\text{-exp.})}{(v_j\text{-exp.})} \quad \textbf{(4.15)}$$

$$\%\ \text{error between predicted and code-recommended } v_j : \frac{(v_j\text{-predicted}) - (v_j\text{-ACI})}{(v_j\text{-ACI})} \quad \textbf{(4.16)}$$

$$\%\ \text{error between code-recommended and experimental } v_j : \frac{(v_j\text{-ACI}) - (v_j\text{-exp.})}{(v_j\text{-exp.})} \quad \textbf{(4.17)}$$

where, v_j-exp. is the experimental joint shear strength

v_j-predicted is the joint shear strength computed by Equation 4.13

v_j-ACI is the joint shear strength computed by Equation 4.14.

In order to compare the predicted values to the experimental ones, linear correlation coefficient is utilized. In the resulting model, a correlation of 88 % is obtained between the predicted and experimental values of joint shear strength. As compared to correlations of individual parameters with the experimental joint shear strength, the resulting formula, which is the combination of these parameters, gives a much higher correlation. This proves the validation of the method utilized in this study. Experimental versus predicted values of joint shear strength for all specimens are shown in **Figure 4.3**. For lower joint shear strength levels, the predicted values are closer to experimental ones. However, as the strength values get larger, the error increases. The overall trend of the graphical comparison shows a slight underestimation of strength which is conservative. In Figure 4.4, the comparison of the shear strength values computed by ACI equation and the experimental joint shear strength are presented. As it can be observed from this figure, the proposed formula gives more conservative results with less scatter when compared to the equation recommended by ACI 352 R-02.

Table 4.3: Maximum Joint Shear Strength Prediction

Research Team	Specimen	vj - experimental (MPa)	vj - predicted (MPa)	vj - ACI (MPa)	% error between vj-predicted and vj - experimental	% error between vj-ACI and vj-experimental	% error between vj-predicted and vj-ACI
Burak & Wight	1-S	8.51	7.17	6.70	-15.72	-21.24	7.01
	2-S	7.88	6.70	7.78	-14.97	-1.29	-13.86
	3-S	7.56	6.52	6.70	-13.75	-11.28	-2.78
	2-N	4.88	5.45	7.78	11.66	59.17	-29.85
	3-N	3.38	3.84	6.70	13.30	98.08	-42.80
Chen & Chen	JC	3.63	4.77	4.45	31.48	22.48	7.35
	JE	3.77	4.36	4.44	15.61	17.91	-1.95
Durrani & Wight	X1	6.17	6.31	7.29	2.32	18.19	-13.43
	X2	6.83	7.10	7.22	3.95	5.71	-1.67
	X3	6.09	6.20	6.93	1.71	13.77	-10.60
Ehsani & Alameddine	LL8	7.26	6.20	7.39	-14.57	1.90	-16.16
	LH8	7.07	8.20	7.39	16.01	4.60	10.91
	HL8	8.32	6.54	7.39	-21.42	-11.15	-11.56
	HH8	8.31	8.44	7.39	1.53	-11.07	14.17
	LL11	6.49	6.62	8.67	2.03	33.65	-23.66
	LH11	7.88	8.54	8.67	8.35	10.04	-1.54
	HL11	8.16	6.82	8.67	-16.41	6.25	-21.32
	HH11	8.61	8.82	8.67	2.45	0.69	1.75
	LL14	7.40	6.82	9.78	-7.86	32.13	-30.27
	LH14	7.51	8.80	9.78	17.10	30.22	-10.07
	HL14	NA	6.96	9.78	NA	NA	-28.85
	HH14	8.71	8.98	9.78	3.07	12.32	-8.24
Ehsani & Wight	1B	7.33	6.02	5.77	-17.89	-21.28	4.31
	2B	7.48	6.51	5.89	-13.00	-21.28	10.52
	3B	7.29	7.19	6.37	-1.37	-12.67	12.94
	4B	7.44	7.62	6.65	2.41	-10.58	14.52
	5B	6.62	5.70	4.91	-13.86	-25.82	16.13
	6B	4.90	5.66	6.28	15.56	28.12	-9.81
Fujii & Morita	A1	9.86	6.43	6.31	-34.79	-35.93	1.78
	A2	9.08	6.43	6.31	-29.23	-30.47	1.78
	A3	9.86	7.33	6.31	-25.63	-35.93	16.08
	A4	10.07	9.53	6.31	-5.35	-37.28	50.91
	B1	5.89	4.86	6.82	-17.48	15.76	-28.72
	B2	5.12	4.86	6.82	-4.99	33.28	-28.72
	B3	6.52	5.63	6.82	-13.73	4.52	-17.46
	B4	6.88	7.32	6.82	6.41	-0.83	7.31
Gentry & Wight	1	4.36	4.93	6.54	13.24	50.00	-24.51
	2	4.49	4.67	6.54	3.98	45.48	-28.53
	3	4.95	4.93	6.54	-0.23	32.16	-24.51
	4	5.60	4.93	6.54	-11.92	16.67	-24.51
Guimaraes, Kreger & Jirsa	J2	10.58	9.24	8.73	-12.72	-17.54	5.85
	J4	9.73	9.53	9.34	-2.02	-4.03	2.10
	J5	18.19	17.15	14.65	-5.72	-19.46	17.06
	J6	16.58	17.54	15.93	5.80	-3.95	10.16

Table 4.3 (Continued)

Research Team	Specimen	vj - experimental (MPa)	vj - predicted (MPa)	vj - ACI (MPa)	% error between vj-predicted and vj - experimental	% error between vj-ACI and vj-experimental	% error between vj-predicted and vj-ACI
Kaku & Asakusa	Specimen 1	6.20	5.21	5.55	-15.91	-10.41	-6.13
	Specimen 2	6.20	5.13	6.43	-17.18	3.74	-20.17
	Specimen 3	5.30	4.67	6.43	-11.81	21.35	-27.33
	Specimen 4	6.00	5.62	6.66	-6.27	10.98	-15.55
	Specimen 5	5.20	5.09	6.03	-2.20	16.04	-15.71
	Specimen 6	5.10	4.74	6.33	-7.04	24.13	-25.11
	Specimen 7	6.30	5.03	5.65	-20.09	-10.29	-10.93
	Specimen 8	6.10	5.04	6.39	-17.40	4.80	-21.18
	Specimen 9	6.00	4.65	6.35	-22.45	5.77	-26.68
	Specimen 10	6.05	5.62	6.64	-7.06	9.70	-15.28
	Specimen 11	6.00	5.15	6.45	-14.23	7.45	-20.18
	Specimen 12	5.00	4.63	5.90	-7.38	18.02	-21.52
	Specimen 13	5.30	4.55	6.78	-14.23	28.01	-32.99
	Specimen 14	5.90	5.14	6.38	-12.96	8.09	-19.47
	Specimen 15	6.00	5.12	6.28	-14.66	4.59	-18.40
	Specimen 16	6.10	4.59	6.09	-24.76	-0.15	-24.65
	Specimen 17	4.40	4.64	6.28	5.36	42.63	-26.13
	Specimen 18	3.00	4.66	6.35	55.17	111.80	-26.74
Kitayama, Otani & Aoyama	A1	9.18	6.17	6.89	-32.79	-24.99	-10.40
	A2	11.02	8.23	9.18	-25.32	-16.65	-10.40
	A3	12.24	8.96	6.89	-26.79	-43.74	30.14
	A4	9.49	6.72	9.18	-29.15	-3.21	-26.80
LaFave & Wight	EWB 1	5.34	5.16	6.70	-3.50	25.33	-23.00
	EWB 2	4.94	5.16	6.85	4.60	38.85	-24.67
	EWB 3	4.75	4.49	7.31	-5.50	53.92	-38.61
	ENB 1	2.96	5.11	6.20	72.65	109.49	-17.58
Lee & Ko	S0	3.94	4.44	5.69	12.49	44.23	-22.01
	S50	3.76	4.20	5.82	11.76	55.03	-27.91
	W0	4.84	5.73	5.35	18.26	10.54	6.98
	W75	4.88	5.42	5.49	11.22	12.65	-1.27
	W150	4.93	5.13	5.37	3.97	8.97	-4.59
Oka & Shiohara	J-1	NA	9.66	11.22	NA	NA	-13.87
	J-2	NA	9.66	11.22	NA	NA	-13.87
	J-4	NA	9.60	10.62	NA	NA	-9.62
	J-5	NA	9.65	11.08	NA	NA	-12.93
	J-6	NA	8.77	11.08	NA	NA	-20.85
	J-7	10.49	8.92	11.08	-15.02	5.58	-19.51
	J-8	NA	8.77	11.08	NA	NA	-20.85
	J-10	12.35	8.27	7.79	-33.03	-36.86	6.07
	J-11	NA	7.74	7.79	NA	NA	-0.77
Quintero-Febres & Wight	IWB1	5.39	7.11	8.71	31.96	61.64	-18.36
	IWB2	6.82	6.49	8.71	-4.95	27.72	-25.58
	IWB3	5.35	5.50	8.71	2.75	62.77	-36.88
Raffaelle & Wight	1	6.00	5.78	6.66	-3.74	10.88	-13.18
	2	5.12	5.55	6.45	8.37	25.96	-13.97
	3	5.42	5.79	7.64	6.97	41.09	-24.18
	4	4.76	5.27	5.47	10.89	14.99	-3.56

Table 4.3 (Continued)

Research Team	Specimen	vj - experimental (MPa)	vj - predicted (MPa)	vj - ACI (MPa)	% error between vj-predicted and vj - experimental	% error between vj-ACI and vj-experimental	% error between vj-predicted and vj-ACI
Shin & LaFave	SL 1	5.94	6.06	6.81	2.13	14.64	-10.92
	SL 2	8.65	6.40	7.48	-26.01	-13.54	-14.43
	SL 3	5.58	7.25	8.57	29.79	53.54	-15.47
	SL 4	7.56	6.56	6.95	-13.22	-8.16	-5.51
Teng & Zhou	S1	8.60	6.86	7.15	-20.21	-16.84	-4.06
	S2	8.60	6.48	7.26	-24.62	-15.59	-10.71
	S3	8.30	6.16	7.37	-25.76	-11.26	-16.34
	S5	7.50	7.54	7.78	0.49	3.67	-3.07
	S6	7.30	7.14	7.67	-2.23	5.13	-7.00

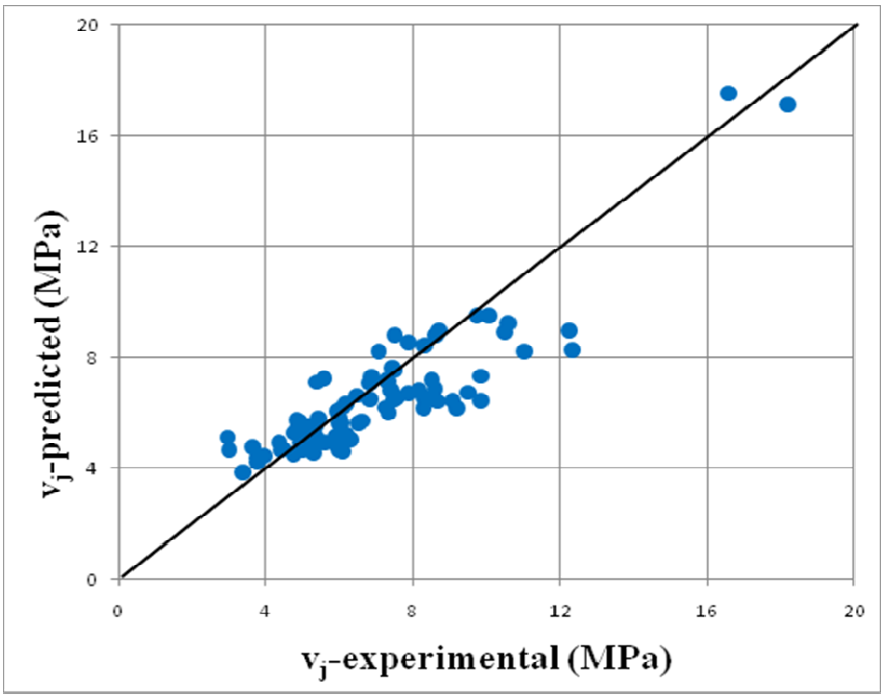

Figure 4.3: Predicted versus Experimental Joint Shear Strength

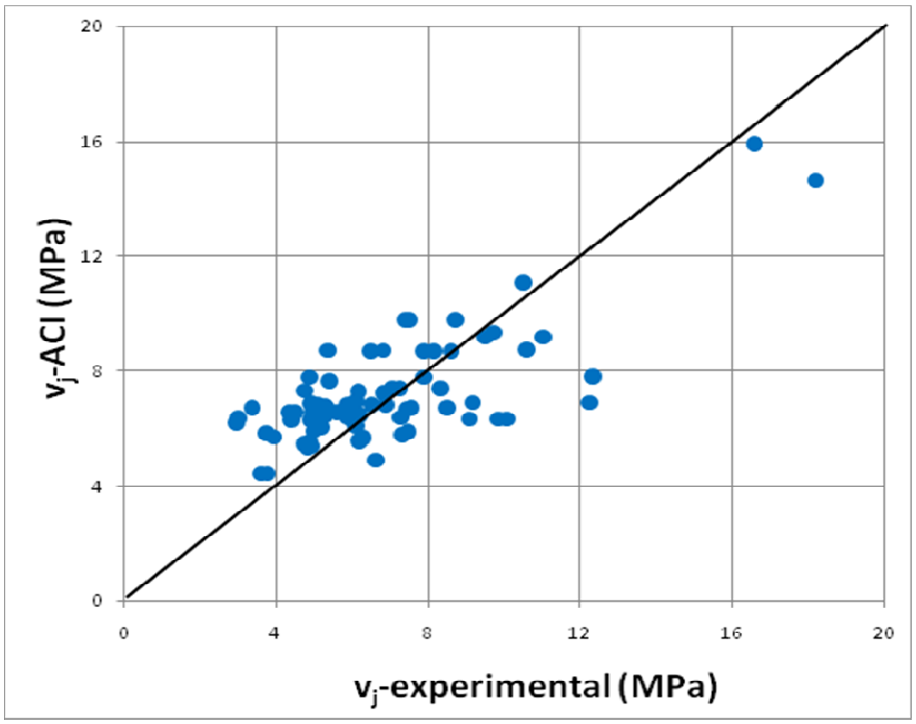

Figure 4.4: ACI Recommended versus Experimental Joint Shear Strength

In Turkish Earthquake Code, the limitations for the maximum joint shear strength differ for confined and unconfined connections. For unconfined connections:

$$V_e \le 0.60 \cdot b_j \cdot h \cdot f_{cd} \quad \textbf{(4.18)}$$

and for confined connections:

$$V_e \le 0.45 \cdot b_j \cdot h \cdot f_{cd} \quad \textbf{(4.19)}$$

where, V_e is the shear force in the direction of earthquake loading,

b_j is the effective joint width according to TEC 2007,

h is the column depth,

f_{cd} is the design compressive strength of concrete.

The shear strength limitations based on TEC 2007 are also computed and compared with the predicted joint shear strength values and the ones given in ACI 352

Recommendations (**Equation 4.14**) in **Table 4.4**. It can be seen from the table that joint shear predictions made by both the proposed formula and the ACI 352 recommended formula are conservative compared to the maximum joint shear strength limitations given in TEC 2007. The deviations are generally large which indicates that the guidelines of TEC 2007 on the seismic behavior of beam-to-column connections should be revised.

Table 4.4: Turkish Earthquake Code (TEC 2007) Limitations for Maximum Joint Shear Strength

Research Team	Specimen	Confinement due to beams	vj - TEC'07 (MPa)	vj - predicted (MPa)	vj - ACI (MPa)	% deviation between vj - TEC'07 and vj - predicted	% deviation between vj - TEC'07 and vj - ACI
Burak & Wight	1-S	Unconfined	8.7	7.17	6.70	21.27	29.76
	2-S	Unconfined	11.7	6.70	7.78	74.69	50.48
	3-S	Unconfined	8.7	6.52	6.70	33.48	29.76
	2-N	Unconfined	11.7	5.45	7.78	114.52	50.48
	3-N	Unconfined	8.7	3.84	6.70	126.85	29.76
Chen & Chen	JC	Unconfined	6.0	4.77	4.45	25.23	34.43
	JE	Unconfined	6.0	4.36	4.44	37.01	34.33
Durrani & Wight	X1	Unconfined	10.3	6.31	7.29	63.05	41.15
	X2	Unconfined	10.1	7.10	7.22	42.09	39.72
	X3	Unconfined	9.3	6.20	6.93	50.08	34.17
Ehsani & Alameddine	LL8	Unconfined	16.5	6.20	7.39	166.73	123.62
	LH8	Unconfined	16.5	8.20	7.39	101.63	123.62
	HL8	Unconfined	16.5	6.54	7.39	152.87	123.62
	HH8	Unconfined	16.5	8.44	7.39	95.87	123.62
	LL11	Unconfined	22.7	6.62	8.67	243.50	162.22
	LH11	Unconfined	22.7	8.54	8.67	166.31	162.22
	HL11	Unconfined	22.7	6.82	8.67	233.29	162.22
	HH11	Unconfined	22.7	8.82	8.67	157.71	162.22
	LL14	Unconfined	28.9	6.82	9.78	324.23	195.83
	LH14	Unconfined	28.9	8.80	9.78	228.96	195.83
	HH14	Unconfined	28.9	8.98	9.78	222.38	195.83
Ehsani & Wight	1B	Unconfined	10.1	6.02	5.77	67.27	74.48
	2B	Unconfined	10.5	6.51	5.89	61.07	78.02
	3B	Unconfined	12.3	7.19	6.37	70.46	92.53
	4B	Unconfined	13.4	7.62	6.65	75.61	101.11
	5B	Unconfined	7.3	5.70	4.91	27.91	48.55
	6B	Unconfined	11.9	5.66	6.28	110.56	89.92

Table 4.4 (Continued)

Research Team	Specimen	Confinement due to beams	vj - TEC'07 (MPa)	vj - predicted (MPa)	vj - ACI (MPa)	% deviation between vj - TEC'07 and vj - predicted	% deviation between vj - TEC'07 and vj - ACI
Fujii & Morita	A1	Unconfined	12.1	6.43	6.31	87.63	90.97
	A2	Unconfined	12.1	6.43	6.31	87.63	90.97
	A3	Unconfined	12.1	7.33	6.31	64.52	90.97
	A4	Unconfined	12.1	9.53	6.31	26.55	90.97
	B1	Unconfined	9.0	4.86	6.82	85.16	31.98
	B2	Unconfined	9.0	4.86	6.82	85.16	31.98
	B3	Unconfined	9.0	5.63	6.82	59.89	31.98
	B4	Unconfined	9.0	7.32	6.82	22.99	31.98
Gentry & Wight	1	Unconfined	8.3	4.93	6.54	67.56	26.50
	2	Unconfined	8.3	4.67	6.54	76.99	26.50
	3	Unconfined	8.3	4.93	6.54	67.56	26.50
	4	Unconfined	8.3	4.93	6.54	67.56	26.50
Guimaraes, Kreger & Jirsa	J2	Confined	11.1	9.24	8.73	19.66	26.66
	J4	Confined	12.7	9.53	9.34	32.72	35.51
	J5	Confined	31.1	17.15	14.65	81.63	112.62
	J6	Confined	36.8	17.54	15.93	109.87	131.19
Kaku & Asakusa	Specimen 1	Unconfined	9.3	5.21	5.55	78.95	67.97
	Specimen 2	Unconfined	12.5	5.13	6.43	143.63	94.50
	Specimen 3	Unconfined	12.5	4.67	6.43	167.66	94.50
Kaku & Asakusa	Specimen 4	Unconfined	13.4	5.62	6.66	138.46	101.38
	Specimen 5	Unconfined	11.0	5.09	6.03	116.49	82.47
	Specimen 6	Unconfined	12.1	4.74	6.33	155.66	91.45
	Specimen 7	Unconfined	9.7	5.03	5.65	91.89	70.92
	Specimen 8	Unconfined	12.4	5.04	6.39	145.30	93.34
	Specimen 9	Unconfined	12.2	4.65	6.35	161.76	91.92
	Specimen 10	Unconfined	13.3	5.62	6.64	136.90	100.70
	Specimen 11	Unconfined	12.6	5.15	6.45	144.27	94.97
	Specimen 12	Unconfined	10.5	4.63	5.90	127.38	78.45
	Specimen 13	Unconfined	13.9	4.55	6.78	206.20	105.17
	Specimen 14	Unconfined	12.3	5.14	6.38	139.50	92.87
	Specimen 15	Unconfined	11.9	5.12	6.28	132.59	89.78
	Specimen 16	Unconfined	11.2	4.59	6.09	144.45	84.20
	Specimen 17	Unconfined	11.9	4.64	6.28	156.92	89.78
	Specimen 18	Unconfined	12.2	4.66	6.35	162.30	92.16
Kitayama, Otani & Aoyama	A1	Unconfined	9.2	6.17	6.89	48.78	33.31
	A2	Confined	12.2	8.23	9.18	48.78	33.31
	A3	Confined	12.2	8.96	6.89	36.58	77.75
	A4	Unconfined	9.2	6.72	9.18	36.58	-0.02
LaFave & Wight	EWB 1	Unconfined	8.7	5.16	6.70	68.35	29.62
	EWB 2	Unconfined	9.1	5.16	6.85	76.12	32.67
	EWB 3	Unconfined	10.3	4.49	7.31	130.37	41.43
	ENB 1	Unconfined	7.4	5.11	6.20	45.61	20.01

Table 4.4 (Continued)

Research Team	Specimen	Confinement due to beams	vj - TEC'07 (MPa)	vj - predicted (MPa)	vj - ACI (MPa)	% deviation between vj - TEC'07 and vj - predicted	% deviation between vj - TEC'07 and vj - ACI
Lee & Ko	S0	Unconfined	9.8	4.44	5.69	120.50	71.98
	S50	Unconfined	10.3	4.20	5.82	144.35	76.15
	W0	Unconfined	8.7	5.73	5.35	51.36	61.92
	W75	Unconfined	9.1	5.42	5.49	68.21	66.07
	W150	Unconfined	8.7	5.13	5.37	70.30	62.48
Oka & Shiohara	J-7	Unconfined	23.8	8.77	11.08	170.94	114.44
	J-10	Unconfined	11.8	7.74	7.79	52.03	50.87
Quintero-Febres & Wight	IWB1	Confined	11.0	7.11	8.71	54.96	26.50
	IWB2	Confined	11.0	6.49	8.71	69.98	26.50
	IWB3	Confined	11.0	5.50	8.71	100.40	26.50
Raffaelle & Wight	1	Unconfined	8.6	5.78	6.66	48.41	28.85
	2	Unconfined	8.0	5.55	6.45	45.00	24.75
	3	Unconfined	11.3	5.79	7.64	95.11	47.93
	4	Unconfined	5.8	5.27	5.47	9.75	5.84
Shin & LaFave	SL 1	Unconfined	9.0	6.06	6.81	47.91	31.77
	SL 2	Unconfined	10.8	6.40	7.48	69.20	44.79
	SL 3	Unconfined	14.2	7.25	8.57	96.27	65.90
	SL 4	Unconfined	9.3	6.56	6.95	42.32	34.47
Teng & Zhou	S1	Unconfined	9.9	6.86	7.15	44.28	38.42
	S2	Unconfined	10.2	6.48	7.26	57.35	40.50
	S3	Unconfined	10.5	6.16	7.37	70.39	42.56
	S5	Unconfined	11.7	7.54	7.78	55.24	50.48
	S6	Unconfined	11.4	7.14	7.67	59.72	48.54

4.1.3 Prediction of Critical Joint Shear Strength Points

In order to predict the joint inelastic behavior accurately, some critical points on the envelope of nonlinear hysteresis loops were generated. The first critical point is taken as the point of crack initiation and named as $v_{j,cr}$. This point may generally be regarded as the end of the initial elastic portion of the curve. The second critical point is selected as the sudden slope change in between the cracking and the maximum shear strength points where accumulation of inelastic activity is observed. This intermediate point is represented with $v_{j,i}$. An illustration of how the critical points are selected form the joint shear stress versus joint shear strain diagram of a specimen is shown in **Figure 4.5**. When the hysteresis curve is not symmetric in positive and negative loading directions,

the average value for two loading directions is used. The complete trilinear behavior utilized in the model definition is illustrated in **Figure 4.6.**

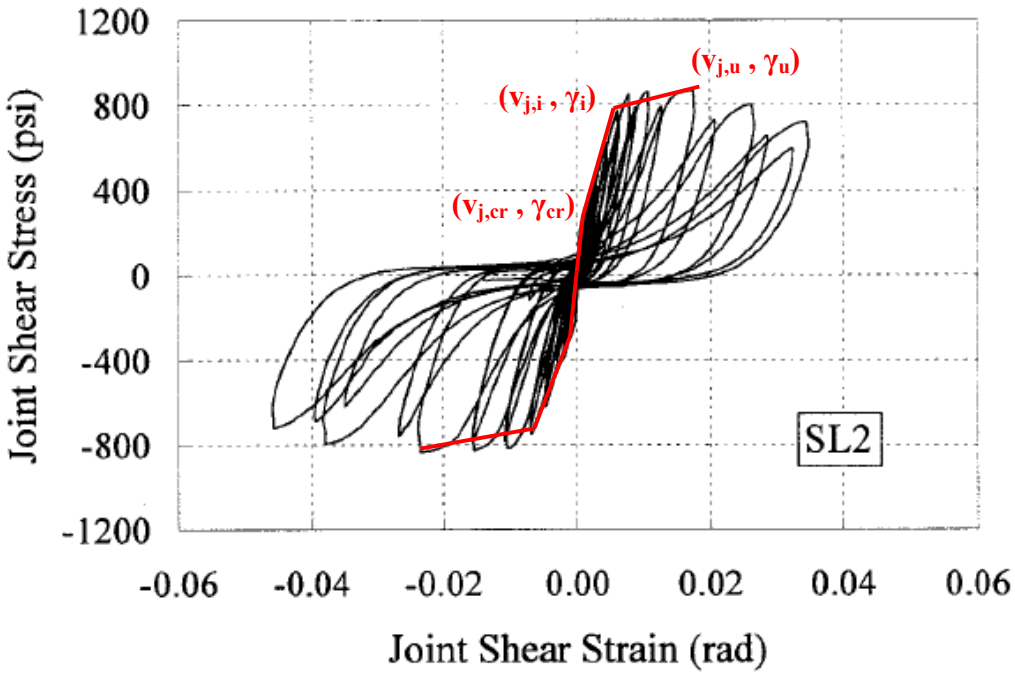

Figure 4.5: Critical Points for the Joint Shear Stress- Strain Diagram of Specimen SL2 – Shin and LaFave [31]

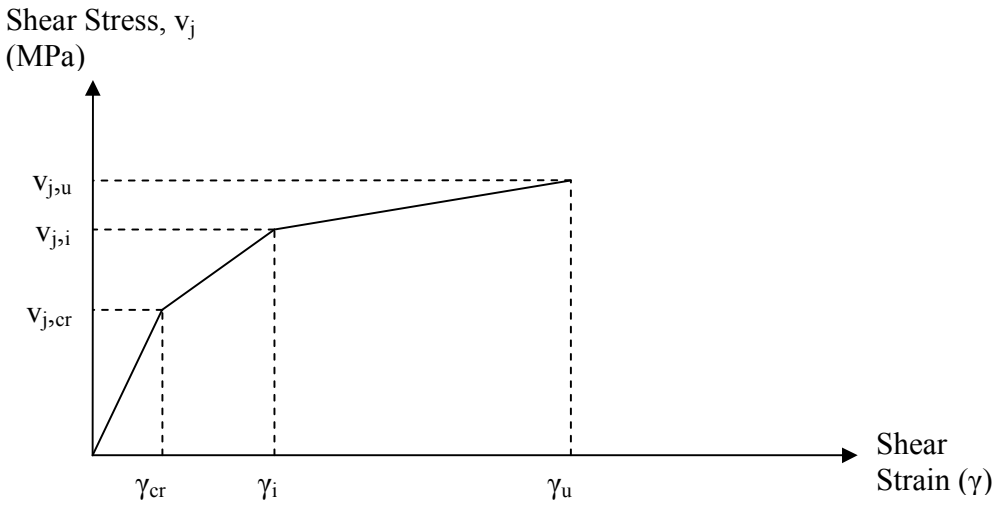

Figure 4.6: Trilinear Shear Stress – Strain Behavior

In order to propose a formula for the $v_{j,i}$ point, the experimental data was evaluated. Relationship between $v_{j,u}$ and $v_{j,i}$ was assessed for interior and exterior specimens separately. As a result of this assessment, the average of $v_{j,i}$ value was found about 0.91 $(v_{j,u})_{average}$ for exterior specimens and 0.89 $(v_{j,u})_{average}$ for interior specimens. Consequently, the $v_{j,i}$ is taken as 0.9 $v_{j,u}$ for all specimens.

For the $v_{j,cr}$ point, the same method was followed and the $v_{j,cr}$ value was estimated approximately. Based on the experimental results, it was found that $v_{j,cr}$ is equal to 0.47 $(v_{j,u})_{average}$ for exterior specimens and 0.37 $(v_{j,u})_{average}$ for interior specimens. Therefore, the $v_{j,cr}$ value was taken as 0.4 $v_{j,u}$ for the sake of simplicity.

4.2 JOINT SHEAR STRAIN DEFINITION

A parametric definition was also generated for the joint shear strain at the corresponding critical points. As shown in **Figure 4.5,** the shear strain values for three points (γ_{cr}, γ_i and γ_u) were selected and a prediction equation was developed.

4.2.1 Selection of Key Parameters Affecting Joint Shear Strain

The parameters such as concrete compressive strength, joint reinforcement yield strength, volumetric reinforcement ratio, column and beam dimensions, presence of slabs and transverse beams, axial load and eccentricity are considered as the influential parameters for the joint shear strain. The influence of these parameters was checked through correlation analysis as it was done for joint shear strength. Due to a higher uncertainty involved in the strain values some of which are due to measurement methods, the correlations are not higher than 30 %. This leads to a difficulty in predicting the joint shear strain. From the experimental results, it was seen that shear strength at the critical point, $v_{j,i}$ had a better correlation with the corresponding joint shear strain, γ_i. Therefore, an equation developed in which the joint shear stress is an independent variable of the joint shear strain.

Shear modulus (G) is defined as the ratio of shear stress to shear strain in the elastic range. Therefore, G is taken as a key parameter while developing the relationship between joint shear stress and joint shear strain. G is determined as below:

$$G=\frac{E}{2(1+\nu)} \quad \text{and} \quad E=4750\sqrt{f_c} \tag{4.20}$$

where E is the modulus of Elasticity in MPa, f_c is the concrete compressive strength in MPa and ν is the Poisson ratio. Since there is not a linear relationship between joint shear stress and strain. Some power forms of the ratio of $v_{j,i}$ to G were evaluated. The highest correlation and the minimum error were obtained when the power is 0.7. Then, in order to enhance the prediction, this equation was divided by joint type index (JT). Since JT represents the confinement level supplied by adjoining beams, it is inversely proportional to joint shear strain. So, the resulting equation was multiplied by 1/JT.

Finally, the ratio of the column depth to the effective joint width was determined as an influential parameter based on the statistical data of the experimental results. Therefore, the equation was multiplied by h_c/b_j. Many trials were also made with other parameters to improve the prediction further but a considerable change was not obtained. This is also an expected result, because the main parameter to limit joint deformations is the confinement of the connection region, which can be defined by the two parameters explained above. Moreover, including more parameters which did not have a significant improvement of the results, made the equation more complex, these parameters were not included in the resulting prediction of γ_i. As a result, the eventual equation is defined as:

$$\gamma_i=\left(\frac{v_{j,u}\text{-predicted}}{G}\right)^{0.7}\cdot\frac{1}{JT}\cdot\frac{h_c}{b_j} \tag{4.21}$$

4.2.2 Prediction of the Critical Joint Shear Strain Points

Having obtained the intermediate point for joint shear strain (γ_i), the shear strain points corresponding to the ultimate and the cracking shear stresses were also estimated by examining the experimantal data. The ratios of the experimantal values of cracking and

ultimate strains to the intermediate strains for all specimens were listed and the averages were found as in **Table 4.5**.

Table 4.5: Average and Standard Deviations for the Ratios of the Strains at Critical Points

	γ_{cr}/γ_i		γ_u/γ_i	
	Average	Standard Deviation	Average	Standard Deviation
Interior Specimens	0.183	0.0832	3.084	0.845
Exterior Specimens	0.165	0.0567	3.803	1.598

As it is seen from the above table, cracking value of joint shear strain is about 0.16 of the intermediate point and the standard deviation is not so high. This deviation might result from the uncertainties due to the difficulty in measurement of the strain at the first cracking point. The prediction equation is obtained as **Equation (4.22)**, where the coefficient is taken as 0.15 to be conservative.

$$\gamma_{cr} = 0.15 \cdot \gamma_i \quad \textbf{(4.22)}$$

Following the same procedure, maximum value is estimated as an equation including γ_i. From the table, it is seen that the joint shear strain capacity corresponding to the ultimate joint shear stress (γ_u) is about 3 times larger than γ_i. Since the standard deviation is higher in this case, the coefficient multiplied with γ_i is selected as 2.5 to make a better prediction. The resulting equation is as shown in **Equation (4.23).**

$$\gamma_u = 2.5 \cdot \gamma_i \quad \textbf{(4.23)}$$

4.3 RESULTING ANALYTICAL JOINT MODEL

After investigating the effects of several parameters on the joint behavior as mentioned above, a trilinear model of joint shear stress versus strain behavior was developed. For each critical point in the model, a parametric equation was developed which accurately predicts the experimental behavior. The resulting equations are summarized below:

$$
\begin{aligned}
v_{j,u}\ (\text{MPa}) &= JT \cdot (f_c \cdot f_y)^{1/6} \cdot \rho_{onelayer} \cdot EE \cdot CI \cdot NE \cdot WB \cdot SI \\
v_{j,cr}\ (\text{MPa}) &= 0.4 \cdot V_{j,u} \\
v_{j,i}\ (\text{MPa}) &= 0.9 \cdot V_{j,u} \\
\gamma_i &= \left(\frac{v_{j,u}}{G} \right)^{0.7} \cdot \frac{1}{JT} \cdot \frac{h_c}{b_j} \\
\gamma_{cr} &= 0.15 \cdot \gamma_i \\
\gamma_u &= 2.5 \cdot \gamma_i
\end{aligned}
\qquad \textbf{(4.24)}
$$

The parameters used in the shear strength and shear strain definition are shown in **Table 4.6**. In this table; JT represents the joint type index, $b_{j,ACI}$ accounts for the effective joint width defined in ACI-352R-02 Recommendations, given by **Equation (4.2)**, E represents modulus of elasticity, G is the shear modulus, and the other terms are the parameters used in **Equation (4.24).**

Table 4.6: Parameters Used in the Model

Research Team	Specimen	JT		bj - mm	$(fc.fy)^{1/6}$	$\rho_{onelayer}$ (4.5)	EE (4.8)	Column Index (CI) (4.10)	Axial Load Effect (4.9)	SI (4.11)	WB (4.12)	E - MPa	G - MPa
Burak & Wight	1-S	D	1.25	256	4.84	1.12	0.91	1.00	1.05	1.11	1.00	25580	10931
	2-S	D	1.25	307	5.08	1.00	0.89	1.00	1.04	1.14	1.00	29664	12677
	3-S	D	1.25	307	4.84	1.00	0.89	1.00	1.04	1.16	1.00	25580	10931
	2-N	A	1	331	5.08	1.15	1.00	0.82	1.03	1.11	1.00	29664	12677
	3-N	A	1	458	4.84	1.15	1.00	0.82	1.03	1.08	0.76	25580	10931
Chen & Chen	JC	A	1	400	4.47	1.07	1.00	1.00	1.00	1.00	1.00	21200	9060
	JE	A	1	375	4.47	1.07	0.91	1.00	1.00	1.00	1.00	21184	9053
Durrani & Wight	X1	C	1.25	321	4.79	1.00	1.00	1.00	1.05	1.00	1.00	27824	11891
	X2	C	1.25	321	4.77	1.13	1.00	1.00	1.06	1.00	1.00	27543	11771
	X3	C	1.25	321	4.71	1.00	1.00	1.00	1.05	1.00	1.00	26449	11303

Table 4.6 (Continued)

Research Team	Specimen	JT		bj - mm	$(fc.fy)^{1/6}$	$\rho_{onelayer}$ (4.5)	EE (4.8)	Column Index (CI) (4.10)	Axial Load Effect (4.9)	SI (4.11)	WB (4.12)	E - MPa	G - MPa
Ehsani & Alameddine	LL8	A	1	333	5.39	1.10	1.00	1.00	1.04	1.00	1.00	35265	15071
	LH8	A	1	333	5.39	1.46	1.00	1.00	1.04	1.00	1.00	35265	15071
	HL8	A	1	333	5.39	1.13	1.00	1.00	1.07	1.00	1.00	35265	15071
	HH8	A	1	333	5.39	1.46	1.00	1.00	1.07	1.00	1.00	35265	15071
	LL11	A	1	333	5.69	1.13	1.00	1.00	1.03	1.00	1.00	41352	17672
	LH11	A	1	333	5.69	1.46	1.00	1.00	1.03	1.00	1.00	41352	17672
	HL11	A	1	333	5.69	1.13	1.00	1.00	1.06	1.00	1.00	41352	17672
	HH11	A	1	333	5.69	1.46	1.00	1.00	1.06	1.00	1.00	41352	17672
	LL14	A	1	333	5.92	1.13	1.00	1.00	1.02	1.00	1.00	46652	19937
	LH14	A	1	333	5.92	1.46	1.00	1.00	1.02	1.00	1.00	46652	19937
	HL14	A	1	333	5.92	1.13	1.00	1.00	1.04	1.00	1.00	46652	19937
	HH14	A	1	333	5.92	1.46	1.00	1.00	1.04	1.00	1.00	46652	19937
Ehsani & Wight	1B	A	1	279	4.95	1.15	1.00	1.00	1.06	1.00	1.00	27515	11758
	2B	A	1	279	4.98	1.22	1.00	1.00	1.07	1.00	1.00	28074	11998
	3B	A	1	279	5.11	1.33	1.00	1.00	1.06	1.00	1.00	30362	12975
	4B	A	1	279	5.19	1.39	1.00	1.00	1.06	1.00	1.00	31714	13553
	5B	A	1	320	4.69	1.08	1.00	1.00	1.13	1.00	1.00	23426	10011
	6B	A	1	320	5.09	1.04	1.00	1.00	1.07	1.00	1.00	29950	12799
Fujii & Morita	A1	C	1.25	190	4.78	1.00	1.00	1.00	1.08	1.00	1.00	30117	12870
	A2	C	1.25	190	4.78	1.00	1.00	1.00	1.08	1.00	1.00	30117	12870
	A3	C	1.25	190	4.78	1.00	1.00	1.00	1.23	1.00	1.00	30117	12870
	A4	C	1.25	190	4.78	1.30	1.00	1.00	1.23	1.00	1.00	30117	12870
	B1	A	1	190	4.55	1.00	1.00	1.00	1.07	1.00	1.00	26017	11118
	B2	A	1	190	4.55	1.00	1.00	1.00	1.07	1.00	1.00	26017	11118
	B3	A	1	190	4.55	1.00	1.00	1.00	1.24	1.00	1.00	26017	11118
	B4	A	1	190	4.55	1.30	1.00	1.00	1.24	1.00	1.00	26017	11118
Gentry & Wight	1	B	1.25	483	4.79	1.00	1.00	1.00	1.03	1.00	0.80	24936	10657
	2	B	1.25	457	4.79	1.00	1.00	1.00	1.03	1.00	0.76	24936	10657
	3	B	1.25	483	4.79	1.00	1.00	1.00	1.03	1.00	0.80	24936	10657
	4	B	1.25	483	4.79	1.00	1.00	1.00	1.03	1.00	0.80	24936	10657
Guimaraes, Kreger & Jirsa	J2	E	1.67	457	4.98	1.00	1.00	1.00	1.00	1.11	1.00	24968	10670
	J4	E	1.67	457	5.09	1.00	1.00	1.00	1.00	1.12	1.00	26712	11415
	J5	E	1.67	457	5.84	1.58	1.00	1.00	1.00	1.12	1.00	41912	17911
	J6	E	1.67	457	6.01	1.58	1.00	1.00	1.00	1.11	1.00	45573	19476

Table 4.6 (Continued)

Research Team	Specimen	JT		bj - mm	$(fc.fy)^{1/6}$	$\rho_{onelayer}$ (4.5)	EE (4.8)	Column Index (CI) (4.10)	Axial Load Effect (4.9)	SI (4.11)	WB (4.12)	E - MPa	G - MPa
Kaku & Asakusa	Specimen 1	A	1	190	4.45	1.00	1.00	1.00	1.17	1.00	1.00	26490	11320
	Specimen 2	A	1	190	4.67	1.00	1.00	1.00	1.10	1.00	1.00	30673	13108
	Specimen 3	A	1	190	4.67	1.00	1.00	1.00	1.00	1.00	1.00	30673	13108
	Specimen 4	A	1	190	4.82	1.00	1.00	1.00	1.17	1.00	1.00	31758	13572
	Specimen 5	A	1	190	4.67	1.00	1.00	1.00	1.09	1.00	1.00	28776	12297
	Specimen 6	A	1	190	4.74	1.00	1.00	1.00	1.00	1.00	1.00	30191	12902
	Specimen 7	A	1	190	4.48	1.00	1.00	1.00	1.12	1.00	1.00	26954	11519
	Specimen 8	A	1	190	4.66	1.00	1.00	1.00	1.08	1.00	1.00	30489	13029
	Specimen 9	A	1	190	4.65	1.00	1.00	1.00	1.00	1.00	1.00	30266	12934
	Specimen 10	A	1	190	4.82	1.00	1.00	1.00	1.17	1.00	1.00	31651	13526
	Specimen 11	A	1	190	4.77	1.00	1.00	1.00	1.08	1.00	1.00	30747	13140
	Specimen 12	A	1	190	4.63	1.00	1.00	1.00	1.00	1.00	1.00	28141	12026
	Specimen 13	A	1	190	4.76	1.00	1.00	1.00	0.96	1.00	1.00	32356	13827
	Specimen 14	A	1	190	4.75	1.00	1.00	1.00	1.08	1.00	1.00	30415	12998
	Specimen 15	A	1	190	4.73	1.00	1.00	1.00	1.08	1.00	1.00	29929	12790
	Specimen 16	A	1	190	4.59	1.00	1.00	1.00	1.00	1.00	1.00	29049	12414
	Specimen 17	A	1	190	4.64	1.00	1.00	1.00	1.00	1.00	1.00	29929	12790
	Specimen 18	A	1	190	4.66	1.00	1.00	1.00	1.00	1.00	1.00	30303	12950
Kitayama, Otani & Aoyama	A1	C	1.25	250	4.64	1.00	1.00	1.00	1.06	1.00	1.00	26279	11230
	A2	E	1.67	250	4.64	1.00	1.00	1.00	1.06	1.00	1.00	26279	11230
	A3	E	1.67	250	4.64	1.00	1.00	1.00	1.06	1.09	1.00	26279	11230
	A4	C	1.25	250	4.64	1.00	1.00	1.00	1.06	1.09	1.00	26279	11230
LaFave & Wight	EWB 1	B	1.25	483	4.91	1.00	1.00	1.00	1.00	1.05	0.80	25552	10920
	EWB 2	B	1.25	483	4.94	1.00	1.00	1.00	1.00	1.04	0.80	26153	11177
	EWB 3	B	1.25	464	5.05	1.04	1.00	0.77	1.00	1.05	0.84	27880	11914
	ENB 1	B	1.25	305	4.78	1.04	1.00	0.77	1.00	1.06	1.00	23657	10110
Lee & Ko	S0	A	1	350	4.99	1.00	1.00	0.82	1.09	1.00	1.00	27121	11590
	S50	A	1	350	5.03	1.00	0.94	0.82	1.09	1.00	1.00	27778	11871
	W0	A	1	400	4.89	1.06	1.00	1.00	1.10	1.00	1.00	25535	10913
	W75	A	1	400	4.93	1.06	0.94	1.00	1.10	1.00	1.00	26190	11192
	W150	A	1	360	4.89	1.06	0.89	1.00	1.10	1.00	1.00	25624	10950
Oka & Shiohara	J-1	C	1.25	270	6.94	1.00	1.00	1.00	1.11	1.00	1.00	42803	18292
	J-2	C	1.25	270	6.94	1.00	1.00	1.00	1.11	1.00	1.00	42803	18292
	J-4	C	1.25	270	6.81	1.00	1.00	1.00	1.13	1.00	1.00	40528	17320
	J-5	C	1.25	270	6.91	1.00	1.00	1.00	1.12	1.00	1.00	42272	18065
	J-6	C	1.25	270	6.28	1.00	1.00	1.00	1.12	1.00	1.00	42272	18065
	J-7	C	1.25	270	6.39	1.00	1.00	1.00	1.12	1.00	1.00	42272	18065
	J-8	C	1.25	270	6.28	1.00	1.00	1.00	1.12	1.00	1.00	42272	18065
	J-10	C	1.25	270	5.35	1.00	1.00	1.00	1.24	1.00	1.00	29740	12709
	J-11	C	1.25	270	5.01	1.00	1.00	1.00	1.24	1.00	1.00	29740	12709
Quintero-Febres & Wight	IWB1	E	1.67	489	4.90	1.05	1.00	1.00	1.00	1.02	0.81	24936	10657
	IWB2	E	1.67	432	4.90	1.05	1.00	1.00	1.00	1.09	0.70	24936	10657
	IWB3	E	1.67	457	4.90	1.00	1.00	0.81	1.00	1.04	0.80	24936	10657

Table 4.6 (Continued)

Research Team	Specimen	JT		bj - mm	$(fc.fy)^{1/6}$	$\rho_{onelayer}$ (4.5)	EE (4.8)	Column Index (CI) (4.10)	Axial Load Effect (4.9)	SI (4.11)	WB (4.12)	E - MPa	G - MPa
Raffaelle & Wight	1	C	1.25	305	4.82	1.00	0.94	1.00	1.02	1.00	1.00	25400	10855
	2	C	1.25	231	4.77	1.00	0.89	1.00	1.03	1.00	1.00	24591	10509
	3	C	1.25	244	5.05	1.00	0.90	1.00	1.02	1.00	1.00	29161	12462
	4	C	1.25	244	4.52	1.00	0.90	1.00	1.04	1.00	1.00	20863	8916
Shin & LaFave	SL 1	D	1.25	329	4.91	1.00	0.91	1.00	1.00	1.08	1.00	25975	11100
	SL 2	D	1.25	227	5.07	1.00	0.88	1.00	1.00	1.15	1.00	28541	12197
	SL 3	D	1.25	362	5.45	1.00	1.00	1.00	1.00	1.06	1.00	32704	13976
	SL 4	D	1.25	279	5.12	1.05	1.00	0.87	1.00	1.12	1.00	26508	11328
Teng & Zhou	S1	C	1.25	275	4.94	1.00	1.00	1.00	1.11	1.00	1.00	27287	11661
	S2	C	1.25	275	4.96	1.00	0.94	1.00	1.11	1.00	1.00	27697	11836
	S3	C	1.25	245	4.99	1.00	0.89	1.00	1.11	1.00	1.00	28101	12009
	S5	C	1.25	250	5.08	1.13	0.94	1.00	1.11	1.00	1.00	29664	12677
	S6	C	1.25	230	5.06	1.13	0.89	1.00	1.11	1.00	1.00	29281	12513

Table 4.7 shows the predicted values of shear strength for all specimens at three critical points. The experimental values are also provided in this table in order to make a comparison. The percent errors in the table show the accuracy of the prediction. The error percentages are computed by using **Equation (4.15)**.

In **Table 4.8**, the predicted joint shear strain values are compared with the experimental values. The accuracy is also shown with the percent error formula as it is done in the table for the prediction of joint shear strength behavior. In both tables, if the data for any points could not be obtained from the research reports, then the cell is filled with "NA".

Table 4.7: Prediction of Joint Shear Strength

Research Team	Specimen	$v_{j,u}$			$v_{j,i}$			$v_{j,cr}$		
		Predicted (MPa)	Exp. (MPa)	% error	Predicted (MPa)	Exp. (MPa)	% error	Predicted (MPa)	Exp. (MPa)	% error
Burak & Wight	1-S	7.174	8.512	-15.72	6.457	NA	NA	2.870	NA	NA
	2-S	6.698	7.877	-14.97	6.028	6.863	-12.17	2.679	3.407	-21.36
	3-S	6.518	7.557	-13.75	5.866	6.362	-7.80	2.607	2.949	-11.59
	2-N	5.454	4.885	11.66	4.909	4.489	9.35	2.182	1.366	59.71
	3-N	3.835	3.385	13.30	3.452	3.211	7.49	1.534	1.521	0.86
Chen & Chen	JC	4.772	3.630	31.48	4.295	3.434	25.06	1.909	1.517	25.85
	JE	4.355	3.767	15.61	3.920	3.466	13.11	1.742	1.695	2.76
Durrani & Wight	X1	6.313	6.170	2.32	5.682	NA	NA	2.525	NA	NA
	X2	7.099	6.829	3.95	6.389	NA	NA	2.840	NA	NA
	X3	6.198	6.094	1.71	5.578	NA	NA	2.479	NA	NA
Ehsani & Alameddine	LL8	6.200	7.257	-14.57	5.580	NA	NA	2.480	NA	NA
	LH8	8.201	7.069	16.01	7.381	NA	NA	3.281	NA	NA
	HL8	6.539	8.322	-21.42	5.886	NA	NA	2.616	NA	NA
	HH8	8.442	8.315	1.53	7.598	NA	NA	3.377	NA	NA
	LL11	6.619	6.488	2.03	5.957	NA	NA	2.648	NA	NA
	LH11	8.538	7.880	8.35	7.684	NA	NA	3.415	NA	NA
	HL11	6.822	8.161	-16.41	6.140	NA	NA	2.729	NA	NA
	HH11	8.823	8.611	2.45	7.940	NA	NA	3.529	NA	NA
	LL14	6.821	7.403	-7.86	6.139	NA	NA	2.728	NA	NA
	LH14	8.797	7.512	17.10	7.917	NA	NA	3.519	NA	NA
	HL14	6.960	NA	NA	6.264	NA	NA	2.784	NA	NA
	HH14	8.976	8.709	3.07	8.079	NA	NA	3.591	NA	NA
Ehsani & Wight	1B	6.018	7.329	-17.89	5.416	NA	NA	2.407	NA	NA
	2B	6.506	7.478	-13.00	5.856	NA	NA	2.602	NA	NA
	3B	7.191	7.290	-1.37	6.471	NA	NA	2.876	NA	NA
	4B	7.615	7.437	2.41	6.854	NA	NA	3.046	NA	NA
	5B	5.704	6.622	-13.86	5.134	NA	NA	2.282	NA	NA
	6B	5.664	4.901	15.56	5.098	NA	NA	2.266	NA	NA
Fujii & Morita	A1	6.427	9.857	-34.79	5.785	8.829	-34.48	2.571	4.905	-47.58
	A2	6.427	9.082	-29.23	5.785	7.848	-26.29	2.571	4.415	-41.76
	A3	7.330	9.857	-25.63	6.597	9.320	-29.21	2.932	4.905	-40.22
	A4	9.530	10.068	-5.35	8.577	9.418	-8.93	3.812	5.396	-29.35
	B1	4.861	5.891	-17.48	4.375	5.678	-22.96	1.944	3.441	-43.50
	B2	4.861	5.116	-4.99	4.375	4.732	-7.55	1.944	3.011	-35.43
	B3	5.629	6.524	-13.73	5.066	6.022	-15.88	2.251	3.441	-34.58
	B4	7.317	6.876	6.41	6.586	5.678	15.98	2.927	3.441	-14.95
Gentry & Wight	1	4.934	4.357	13.24	4.441	NA	NA	1.974	NA	NA
	2	4.671	4.493	3.98	4.204	NA	NA	1.869	NA	NA
	3	4.934	4.946	-0.23	4.441	NA	NA	1.974	NA	NA
	4	4.934	5.602	-11.92	4.441	NA	NA	1.974	NA	NA
Guimaraes, Kreger & Jirsa	J2	9.236	10.582	-12.72	8.312	NA	NA	3.694	NA	NA
	J4	9.531	9.727	-2.02	8.578	NA	NA	3.812	NA	NA
	J5	17.146	18.187	-5.72	15.432	NA	NA	6.858	NA	NA
	J6	17.544	16.582	5.80	15.790	NA	NA	7.018	NA	NA

Table 4.7 (Continued)

Research Team	Specimen	$v_{j,u}$			$v_{j,i}$			$v_{j,cr}$		
		Predicted (MPa)	Exp. (MPa)	% error	Predicted (MPa)	Exp. (MPa)	% error	Predicted (MPa)	Exp. (MPa)	% error
Kaku & Asakusa	Specimen 1	5.214	6.200	-15.91	4.692	6.000	-21.79	2.086	4.000	-47.86
	Specimen 2	5.135	6.200	-17.18	4.621	6.100	-24.24	2.054	4.000	-48.65
	Specimen 3	4.674	5.300	-11.81	4.207	5.000	-15.87	1.870	2.500	-25.22
	Specimen 4	5.624	6.000	-6.27	5.061	5.400	-6.27	2.249	3.000	-25.02
	Specimen 5	5.086	5.200	-2.20	4.577	4.800	-4.64	2.034	3.000	-32.19
	Specimen 6	4.741	5.100	-7.04	4.267	5.000	-14.67	1.896	2.700	-29.77
	Specimen 7	5.034	6.300	-20.09	4.531	5.800	-21.89	2.014	4.000	-49.66
	Specimen 8	5.039	6.100	-17.40	4.535	5.800	-21.81	2.016	4.000	-49.61
	Specimen 9	4.653	6.000	-22.45	4.188	5.300	-20.98	1.861	2.500	-25.55
	Specimen 10	5.623	6.050	-7.06	5.060	5.900	-14.23	2.249	4.000	-43.77
	Specimen 11	5.146	6.000	-14.23	4.631	5.200	-10.94	2.058	3.000	-31.39
	Specimen 12	4.631	5.000	-7.38	4.168	4.500	-7.38	1.852	3.000	-38.25
	Specimen 13	4.546	5.300	-14.23	4.091	4.500	-9.08	1.818	3.500	-48.05
	Specimen 14	5.136	5.900	-12.96	4.622	5.200	-11.11	2.054	3.000	-31.53
	Specimen 15	5.121	6.000	-14.66	4.609	5.000	-7.83	2.048	3.000	-31.73
	Specimen 16	4.590	6.100	-24.76	4.131	5.000	-17.38	1.836	4.000	-54.10
	Specimen 17	4.636	4.400	5.36	4.172	4.000	4.30	1.854	2.000	-7.28
	Specimen 18	4.655	3.000	55.17	4.190	2.500	67.58	1.862	2.000	-6.90
Kitayama, Otani & Aoyama	A1	6.172	9.182	-32.79	5.554	NA	NA	2.469	NA	NA
	A2	8.229	11.019	-25.32	7.406	NA	NA	3.292	NA	NA
	A3	8.964	12.243	-26.79	8.067	NA	NA	3.585	NA	NA
	A4	6.723	9.488	-29.15	6.050	NA	NA	2.689	NA	NA
LaFave & Wight	EWB 1	5.157	5.344	-3.50	4.641	4.004	15.92	2.063	1.214	69.92
	EWB 2	5.164	4.937	4.60	4.648	4.130	12.54	2.066	2.225	-7.16
	EWB 3	4.486	4.748	-5.50	4.038	4.049	-0.27	1.795	1.612	11.33
	ENB 1	5.110	2.960	72.65	4.599	1.875	145.23	2.044	1.012	101.89
Lee & Ko	S0	4.435	3.943	12.49	3.992	NA	NA	1.774	NA	NA
	S50	4.199	3.757	11.76	3.779	NA	NA	1.680	NA	NA
	W0	5.728	4.844	18.26	5.155	NA	NA	2.291	NA	NA
	W75	5.422	4.875	11.22	4.880	NA	NA	2.169	NA	NA
	W150	5.126	4.931	3.97	4.614	NA	NA	2.050	NA	NA
Oka & Shiohara	J-1	9.663	NA	NA	8.696	NA	NA	3.865	NA	NA
	J-2	9.663	NA	NA	8.696	NA	NA	3.865	NA	NA
	J-4	9.601	NA	NA	8.641	NA	NA	3.840	NA	NA
	J-5	9.648	NA	NA	8.683	NA	NA	3.859	NA	NA
	J-6	8.769	NA	NA	7.892	NA	NA	3.508	NA	NA
	J-7	8.918	10.494	-15.02	8.026	10.037	-20.04	3.567	4.691	-23.97
	J-8	8.769	NA	NA	7.892	NA	NA	3.508	NA	NA
	J-10	8.268	12.346	-33.03	7.441	11.728	-36.55	3.307	5.679	-41.76
	J-11	7.735	NA	NA	6.962	NA	NA	3.094	NA	NA
Quintero-Febres & Wight	IWB1	7.114	5.391	31.96	6.403	NA	NA	2.846	NA	NA
	IWB2	6.486	6.823	-4.95	5.837	NA	NA	2.594	NA	NA
	IWB3	5.501	5.354	2.75	4.951	NA	NA	2.200	NA	NA

Table 4.7 (Continued)

Research Team	Specimen	$v_{j,u}$			$v_{j,i}$			$v_{j,cr}$		
		Predicted (MPa)	Exp. (MPa)	% error	Predicted (MPa)	Exp. (MPa)	% error	Predicted (MPa)	Exp. (MPa)	% error
Raffaelle & Wight	1	5.780	6.004	-3.74	5.202	5.335	-2.50	2.312	1.847	25.18
	2	5.545	5.117	8.37	4.991	4.330	15.27	2.218	1.894	17.10
	3	5.795	5.417	6.97	5.215	4.617	12.96	2.318	2.052	12.96
	4	5.273	4.756	10.89	4.746	3.899	21.73	2.109	1.283	64.47
Shin & LaFave	SL 1	6.065	5.938	2.13	5.458	5.324	2.52	2.426	2.048	18.47
	SL 2	6.401	8.652	-26.01	5.761	7.704	-25.21	2.561	2.370	8.03
	SL 3	7.246	5.583	29.79	6.521	5.211	25.15	2.898	1.861	55.74
	SL 4	6.565	7.565	-13.22	5.908	6.916	-14.58	2.626	2.594	1.24
Teng & Zhou	S1	6.862	8.600	-20.21	6.175	7.970	-22.52	2.745	NA	NA
	S2	6.482	8.600	-24.62	5.834	7.970	-26.80	2.593	NA	NA
	S3	6.162	8.300	-25.76	5.546	7.960	-30.33	2.465	NA	NA
	S5	7.537	7.500	0.49	6.783	6.520	4.03	3.015	NA	NA
	S6	7.137	7.300	-2.23	6.424	6.520	-1.48	2.855	NA	NA

Table 4.8: Prediction of Joint Shear Strain

Research Team	Specimen	γ_{max}			γ_i			γ_{cr}		
		Predicted (rad)	Exp. (rad)	% error	Predicted (rad)	Exp. (rad)	% error	Predicted (rad)	Exp. (rad)	% error
Burak & Wight	1-S	0.01643	NA	NA	0.00657	NA	NA	0.00099	NA	NA
	2-S	0.01177	0.01049	12.21	0.00471	0.00400	17.71	0.00071	0.00050	41.25
	3-S	0.01281	0.01270	0.87	0.00512	0.00355	44.35	0.00077	0.00050	53.73
	2-N	0.01778	0.01150	54.60	0.00711	0.00769	-7.52	0.00107	0.00154	-30.73
	3-N	0.01113	0.00846	31.61	0.00445	0.00538	-17.22	0.00067	0.00077	-13.13
Chen & Chen	JC	0.01585	0.01710	-7.32	0.00634	0.00514	23.33	0.00095	0.00143	-33.51
	JE	0.01586	0.02290	-30.72	0.00635	0.00657	-3.41	0.00095	0.00086	11.07
Durrani & Wight	X1	0.01151	NA	NA	0.00460	NA	NA	0.00069	NA	NA
	X2	0.01259	NA	NA	0.00503	NA	NA	0.00076	NA	NA
	X3	0.01177	NA	NA	0.00471	NA	NA	0.00071	NA	NA
Ehsani & Alameddine	LL8	0.01137	NA	NA	0.00455	NA	NA	0.00068	NA	NA
	LH8	0.01384	NA	NA	0.00553	NA	NA	0.00083	NA	NA
	HL8	0.01181	NA	NA	0.00472	NA	NA	0.00071	NA	NA
	HH8	0.01412	NA	NA	0.00565	NA	NA	0.00085	NA	NA
	LL11	0.01065	NA	NA	0.00426	NA	NA	0.00064	NA	NA
	LH11	0.01273	NA	NA	0.00509	NA	NA	0.00076	NA	NA
	HL11	0.01088	NA	NA	0.00435	NA	NA	0.00065	NA	NA
	HH11	0.01303	NA	NA	0.00521	NA	NA	0.00078	NA	NA
	LL14	0.01000	NA	NA	0.00400	NA	NA	0.00060	NA	NA
	LH14	0.01195	NA	NA	0.00478	NA	NA	0.00072	NA	NA
	HL14	0.01014	NA	NA	0.00406	NA	NA	0.00061	NA	NA
	HH14	0.01212	NA	NA	0.00485	NA	NA	0.00073	NA	NA

Table 4.8 (Continued)

Research Team	Specimen	γ_{max}			γ_i			γ_{cr}		
		Predicted (rad)	Exp. (rad)	% error	Predicted (rad)	Exp. (rad)	% error	Predicted (rad)	Exp. (rad)	% error
Ehsani & Wight	1B	0.01333	NA	NA	0.00533	NA	NA	0.00080	NA	NA
	2B	0.01388	NA	NA	0.00555	NA	NA	0.00083	NA	NA
	3B	0.01409	NA	NA	0.00564	NA	NA	0.00085	NA	NA
	4B	0.01423	NA	NA	0.00569	NA	NA	0.00085	NA	NA
	5B	0.01425	NA	NA	0.00570	NA	NA	0.00085	NA	NA
	6B	0.01194	NA	NA	0.00477	NA	NA	0.00072	NA	NA
Fujii & Morita	A1	0.01131	0.02930	-61.39	0.00453	0.00933	-51.49	0.00068	0.00133	-48.96
	A2	0.01131	0.04800	-76.43	0.00453	0.01330	-65.97	0.00068	0.00133	-48.96
	A3	0.01240	0.02930	-57.66	0.00496	0.00670	-25.94	0.00074	0.00107	-30.44
	A4	0.01491	0.02930	-49.13	0.00596	0.00800	-25.47	0.00089	0.00053	67.79
	B1	0.01288	0.02670	-51.74	0.00515	0.01200	-57.05	0.00077	0.00213	-63.70
	B2	0.01288	0.03200	-59.74	0.00515	0.00533	-3.30	0.00077	0.00133	-41.87
	B3	0.01428	0.02400	-40.51	0.00571	0.00667	-14.37	0.00086	0.00107	-19.94
	B4	0.01716	0.02400	-28.51	0.00686	0.01070	-35.86	0.00103	0.00160	-35.66
Gentry & Wight	1	0.00683	NA	NA	0.00273	NA	NA	0.00041	NA	NA
	2	0.00694	NA	NA	0.00277	NA	NA	0.00042	NA	NA
	3	0.00683	NA	NA	0.00273	NA	NA	0.00041	NA	NA
	4	0.00683	NA	NA	0.00273	NA	NA	0.00041	NA	NA
Guimaraes, Kreger & Jirsa	J2	0.01197	0.01350	-11.36	0.00479	0.00432	10.80	0.00072	0.00054	32.96
	J4	0.01167	0.01140	2.35	0.00467	0.00405	15.24	0.00070	0.00054	29.65
	J5	0.01284	0.00700	83.43	0.00514	0.00324	58.52	0.00077	0.00079	-2.35
	J6	0.01231	0.00486	153.20	0.00492	0.00162	203.84	0.00074	0.00053	40.37
Kaku & Asakusa	Specimen 1	0.01336	0.00600	122.72	0.00535	0.00220	142.97	0.00080	0.00022	264.46
	Specimen 2	0.01193	0.01158	3.03	0.00477	0.00526	-9.27	0.00072	0.00042	70.45
	Specimen 3	0.01117	0.01470	-24.00	0.00447	0.00211	111.78	0.00067	0.00042	59.59
	Specimen 4	0.01241	0.01158	7.17	0.00496	0.00316	57.09	0.00074	0.00063	17.82
	Specimen 5	0.01239	0.01050	18.03	0.00496	0.00210	136.06	0.00074	0.00021	254.10
	Specimen 6	0.01141	0.01710	-33.28	0.00456	0.00526	-13.24	0.00068	0.00050	36.90
	Specimen 7	0.01288	0.00600	114.69	0.00515	0.00200	157.63	0.00077	0.00050	54.58
	Specimen 8	0.01182	0.00650	81.92	0.00473	0.00232	103.87	0.00071	0.00021	237.85
	Specimen 9	0.01124	0.02000	-43.79	0.00450	0.00421	6.80	0.00067	0.00063	6.72
	Specimen 10	0.01244	0.00842	47.72	0.00498	0.00211	135.79	0.00075	0.00021	255.37
	Specimen 11	0.01193	0.01050	13.62	0.00477	0.00211	126.15	0.00072	0.00042	70.02
	Specimen 12	0.01179	0.01470	-19.80	0.00472	0.00316	49.23	0.00071	0.00063	11.92
	Specimen 13	0.01055	0.02080	-49.26	0.00422	0.01160	-63.61	0.00063	0.00126	-49.74
	Specimen 14	0.01200	0.01050	14.32	0.00480	0.00200	140.07	0.00072	0.00042	71.07
	Specimen 15	0.01211	0.01470	-17.59	0.00485	0.00200	142.30	0.00073	0.00021	244.50
	Specimen 16	0.01146	0.00631	81.59	0.00458	0.00250	83.34	0.00069	0.00042	63.31
	Specimen 17	0.01130	0.01370	-17.52	0.00452	0.00273	65.57	0.00068	0.00063	7.28
	Specimen 18	0.01123	0.01050	7.00	0.00449	0.00210	113.99	0.00067	0.00042	60.11
Kitayama, Otani & Aoyama	A1	0.01254	NA	NA	0.00502	NA	NA	0.00075	NA	NA
	A2	0.01150	NA	NA	0.00460	NA	NA	0.00069	NA	NA
	A3	0.01221	NA	NA	0.00488	NA	NA	0.00073	NA	NA
	A4	0.01331	NA	NA	0.00532	NA	NA	0.00080	NA	NA

Table 4.8 (Continued)

Research Team	Specimen	γ_{max}			γ_i			γ_{cr}		
		Predicted (rad)	Exp. (rad)	% error	Predicted (rad)	Exp. (rad)	% error	Predicted (rad)	Exp. (rad)	% error
LaFave & Wight	EWB 1	0.00692	NA	NA	0.00277	NA	NA	0.00042	NA	NA
	EWB 2	0.00682	NA	NA	0.00273	NA	NA	0.00041	NA	NA
	EWB 3	0.00879	NA	NA	0.00352	NA	NA	0.00053	NA	NA
	ENB 1	0.01642	NA	NA	0.00657	NA	NA	0.00099	NA	NA
Lee & Ko	S0	0.01738	NA	NA	0.00695	NA	NA	0.00104	NA	NA
	S50	0.01645	NA	NA	0.00658	NA	NA	0.00099	NA	NA
	W0	0.01265	NA	NA	0.00506	NA	NA	0.00076	NA	NA
	W75	0.01196	NA	NA	0.00478	NA	NA	0.00072	NA	NA
	W150	0.01297	NA	NA	0.00519	NA	NA	0.00078	NA	NA
Oka & Shiohara	J-1	0.01129	NA	NA	0.00452	NA	NA	0.00068	NA	NA
	J-2	0.01129	NA	NA	0.00452	NA	NA	0.00068	NA	NA
	J-4	0.01168	NA	NA	0.00467	NA	NA	0.00070	NA	NA
	J-5	0.01138	NA	NA	0.00455	NA	NA	0.00068	NA	NA
	J-6	0.01064	NA	NA	0.00426	NA	NA	0.00064	NA	NA
	J-7	0.01077	NA	NA	0.00431	NA	NA	0.00065	NA	NA
	J-8	0.01064	NA	NA	0.00426	NA	NA	0.00064	NA	NA
	J-10	0.01306	NA	NA	0.00523	NA	NA	0.00078	NA	NA
	J-11	0.01247	NA	NA	0.00499	NA	NA	0.00075	NA	NA
Quintero-Febres & Wight	IWB1	0.00653	NA	NA	0.00261	NA	NA	0.00039	NA	NA
	IWB2	0.00693	NA	NA	0.00277	NA	NA	0.00042	NA	NA
	IWB3	0.00833	NA	NA	0.00333	NA	NA	0.00050	NA	NA
Raffaelle & Wight	1	0.01192	0.01090	9.39	0.00477	0.00273	74.70	0.00072	0.00090	-20.51
	2	0.01562	0.01320	18.36	0.00625	0.00500	24.98	0.00094	0.00136	-31.08
	3	0.01356	0.00960	41.20	0.00542	0.00545	-0.51	0.00081	0.00045	80.74
	4	0.01604	0.01820	-11.86	0.00642	0.00500	28.33	0.00096	0.00090	6.94
Shin & LaFave	SL 1	0.01045	0.02210	-52.73	0.00418	0.00958	-56.38	0.00063	0.00125	-49.86
	SL 2	0.01470	0.01750	-16.03	0.00588	0.00583	0.82	0.00088	0.00083	5.85
	SL 3	0.00915	0.00600	52.51	0.00366	0.00370	-1.08	0.00055	0.00050	9.81
	SL 4	0.01429	0.02250	-36.47	0.00572	0.00850	-32.74	0.00086	0.00100	-14.24
Teng & Zhou	S1	0.01196	0.01000	19.56	0.00478	0.00430	11.22	0.00072	0.00083	-13.88
	S2	0.01137	0.01300	-12.54	0.00455	0.00400	13.70	0.00068	0.00083	-18.10
	S3	0.01219	0.02000	-39.03	0.00488	0.00540	-9.67	0.00073	0.00150	-51.22
	S5	0.00883	0.00800	10.39	0.00353	0.00300	17.75	0.00053	0.00063	-15.22
	S6	0.00933	0.01800	-48.19	0.00373	0.00340	9.71	0.00056	0.00125	-55.24

CHAPTER 5

ANALYTICAL VERIFICATION OF THE JOINT MODEL

5.1 PROCEDURE

After the parametric joint model which accurately predicts the experimental behavior is generated and calibrated, the specimens are analyzed using PERFORM 3D v 4.0 [8] which is a non-linear dynamic analysis program. The specimens used in the testing of connection regions are composed of beams, columns and joint. Individual models are defined for each element and cyclic loading that was applied in the experiment is imposed to the models by creating a ground acceleration record. Finally, the analytical results and the experimental results are compared. In order to obtain the most accurate results; beam, column or joint model definitions were calibrated. In this chapter; the details of the specimen modeling and the procedure to impose cyclic deformations as dynamic earthquake loading are explained and the analytical results are presented and compared with the experimental results to verify the proposed joint model.

5.2 SPECIMEN MODELING

The specimens are modeled by using Perform-3D. The model for interior connection regions consists of two columns, two beams and a joint panel zone element; whereas for the exterior connections two columns, one beam and a joint panel zone element are used (**Figure 5.1**). For most of the selected experiments, the test set-up is as shown in **Figure 5.1** and the lateral loading was applied to the top of the column. However, for some experiments on exterior connections, the beams were aligned vertically as in **Figure 5.2**

and the loading was applied at the beam end. The details of each individual element model are given below:

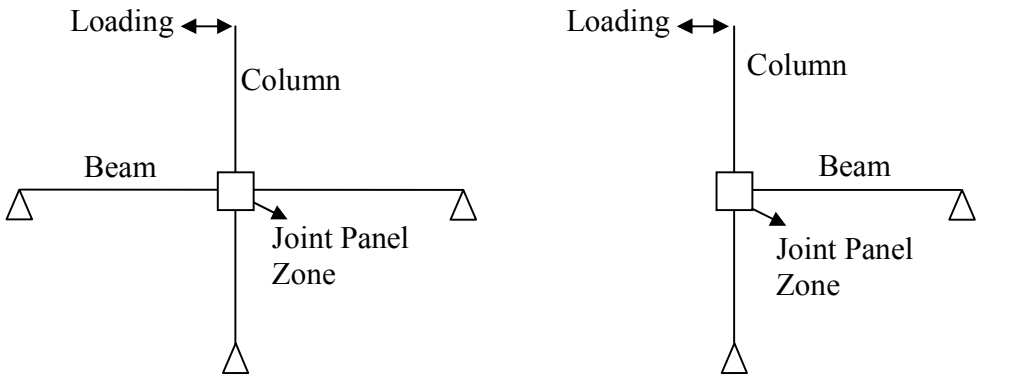

a) Interior Connections b) Exterior Connections

Figure 5.1: Specimen Models when the Loading is Applied at the Top of the Column

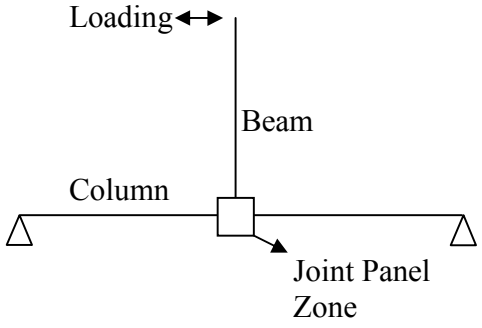

Figure 5.2: Specimen Model when the Loading is Applied at the Beam End

5.2.1 Beam Element

The beam element is defined as a frame compound component including three basic components which are rigid end zones at the beam end near the joint, semi-rigid moment

connection hinge next to the rigid end zone and a uniform elastic cross-section for which cracked stiffness is considered **(Figure 5.3)** The rigid end zone length is selected as one half of the column width, and the stiffness of this zone is 10 times larger than the stiffness of the elastic beam cross-section component

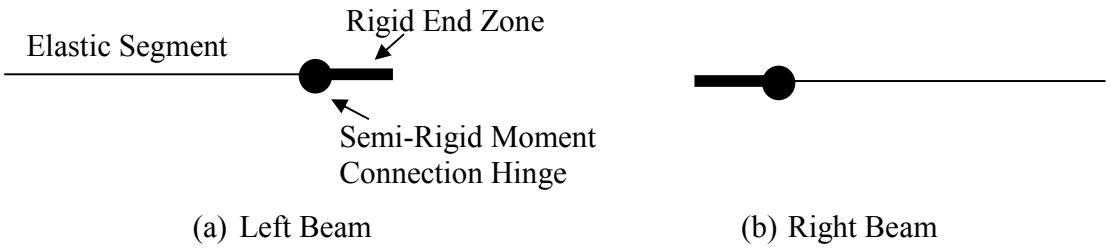

(a) Left Beam (b) Right Beam

Figure 5.3: Beam Compound Component

Semi-rigid moment connection hinges are the main components that represent the inelastic activity taking place throughout the beams. This is similar to rotation hinges and moment vs. rotation behavior of the beam is modeled using this component. In order to get this inelastic relationship, moment-curvature behavior of the beams is obtained by Response 2000. While computing the moment capacity of the beams, strain hardening of reinforcing steel is taken as 1.1, which is believed to give the best results after different strain hardening values in between 1.0 and 1.25 are compared analytically. Afterwards, the rotation values are obtained by multiplying the curvature values by the plastic hinge length that is taken as the half of the effective beam depth (L_p= 0.5d). As a result, the model shown in **Figure 5.4** is used in defining semi-rigid moment connection hinges. A 20 percent strength decrease was assumed to occur at higher rotation values based on the experimental values.

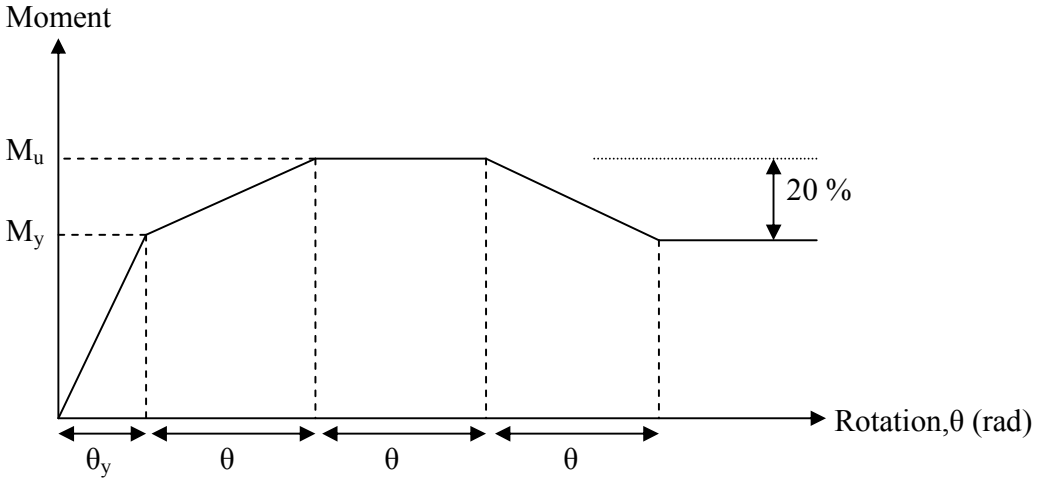

Figure 5.4: Beam Model

Elastic Segment of the beam element is defined based on the main parameters that are section dimensions, moment of inertia (I), modulus of elasticity (E), and Poisson's Ratio (ν). The moment of inertia is computed by taking into account the gross area which includes the effective slab width. The cracked moment of inertia is obtained by taking 35 % of the gross moment of inertia and used in the analysis. The modulus of elasticity was computed by using **Equation (5.1)** and Poisson ratio was taken as 0.17.

$$E=4750\cdot\sqrt{f_c} \qquad \textbf{(5.1)}$$

The inelastic hysteresis loops enclose smaller areas when compared to elasto-plastic behavior due to friction, bar slip and pinching. Therefore, PERFORM 3D requires energy dissipation coefficients at critical rotation points. Energy dissipation coefficient is taken as the ratio of the area under the hysteresis curve to the area under the elasto-plastic counterpart of that curve. These coefficients were set equal to 0.3 up to ultimate moment, and 0.2 after the beam started to lose its strength.

5.2.2 Column Element

Similar to the beam element, the column element was modeled as a frame compound component consisting of a rigid end zone near the end of the column side, an inelastic P-

M-M hinge and an elastic column cross-section at the free end. **Figure 5.5** shows an illustration of a column compound element. The rigid end zone length was taken as the half of the beam depth and had a stiffness that was 10 times larger than that of the elastic column cross-section.

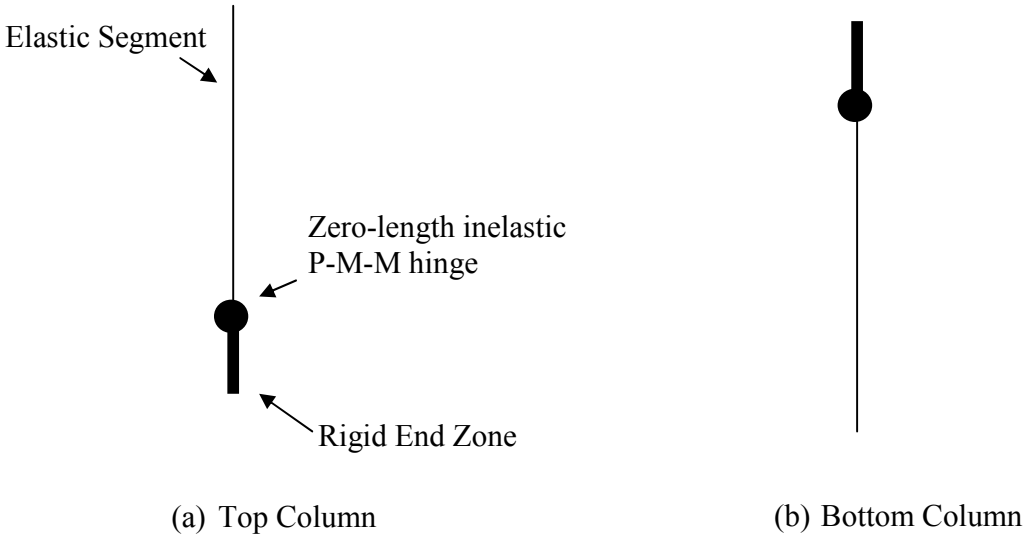

Figure 5.5: Column Element

The reason why zero-length P-M-M hinges were used is that these hinges are rigid-plastic hinges and remain elastic up to a moderate load level. Since the inelastic activity in the columns was not as significant as in the beams and they remain mostly in the elastic range due to strong column-weak beam approach, using P-M-M hinges was an appropriate modeling type for columns. For defining the hinges, moment versus axial load yield (interaction) surface were plotted and utilized in the component as shown in **Figure 5.6**. In this figure, P_C, P_B and P_T represent the column axial capacity under compression, at balanced state and under tension respectively and the balanced moment capacity is shown as M_B.

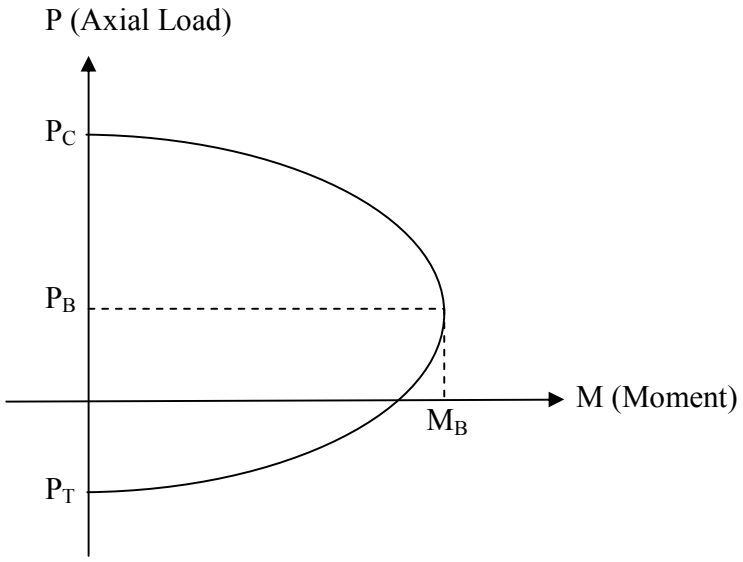

Figure 5. 6: Column Interaction Diagram

As in the beam; section dimensions, moment of inertia (I), modulus of elasticity (E), and Poisson's Ratio (ν) are the main parameters used to define the elastic segment of the column element. The cracked moment of inertia was taken as 70 % of the moment of inertia computed with gross cross-sectional dimensions. The energy dissipation coefficients were taken as 0.3 for all critical rotation points.

5.2.3 Joint Element

In order to represent the inelastic activity in the joint region, connection panel zone element in PERFORM 3D is used. This element has only one node, therefore the intersection of beam and column axes was specified as the node of the connection panel zone. The rigid end zones of beams and column elements are connected to rigid links of the panel zone. A rotational spring attached to the panel zone has a nonlinear moment-rotation relationship that enables the definition of the inelastic behavior. The panel zone model is shown in **Figure 5.7**.

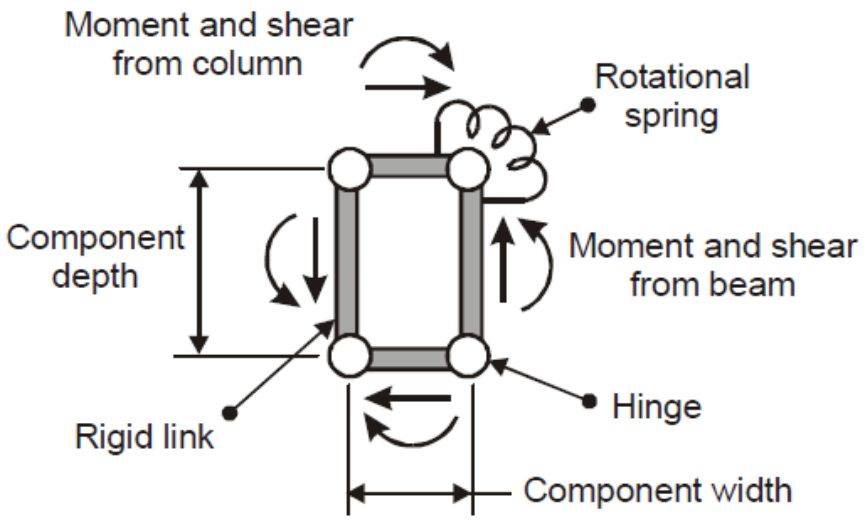

Figure 5.7: Panel Zone Model (Perform-3D User Manual [8])

As described in Chapter 4, the inelastic behavior of joint region can be established by parametric equations. Using these equations, inelastic joint shear strength versus shear strain relationship is generated for connection regions. However, since the connection element models the joint moment versus joint shear strain relationship of the joint region in Perform 3D, shear stress values are converted to moment values by multiplying them with the effective joint width (b_j) and the column depth (h_c) to obtain the joint shear force and the depth of the beam between the top and the bottom reinforcement layers (d´´) to obtain the moment through the connection (**Equation 5.2**). The effective joint width was computed by following the ACI 352R-02 formula given in **Equation 2.4** except for wide beams where Equation 2.10 is used.

$$M_j = v_j \cdot b_j \cdot h_c \cdot d'' \qquad \textbf{(5.2)}$$

The above-mentioned procedure was carried out for all critical shear strain points and eventually joint moment versus shear strain relationship was obtained. It was observed form the test results that the connection moment capacity decreases to about 20 % of the maximum moment capacity. Therefore, a 20 % reduction was made after the ultimate moment value. The whole relationship is illustrated in **Figure 5.8**.

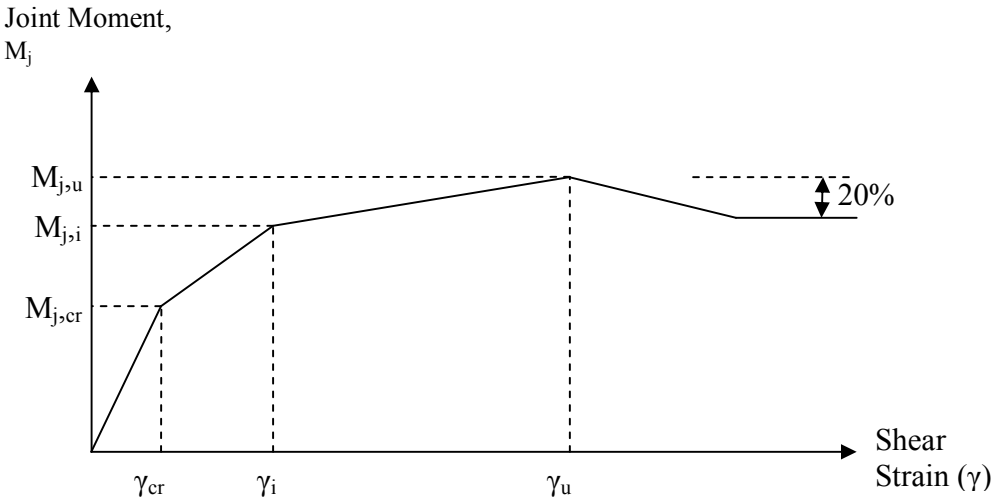

Figure 5.8: Joint Model

5.3 IMPOSING GROUND ACCELERATION RECORDS

The experimental studies utilized in the database all had quasi static cyclic loading. In other words, a specified cyclic deformation or drift pattern was applied to the subassembly. In this loading sequence, the displacement or drift was increased by a certain amount in each cycle. An example cyclic loading pattern was shown in **Figure 5.9** which belongs to the experimental investigation of Burak and Wight [3]. In this displacement history graph, each cycle of a new drift level were applied twice in order to assess the strength and stiffness degradation during the repeated cycles. Moreover, drift cycles with lower amplitudes were added occasionally in order to evaluate the loss of stiffness at low drift levels.

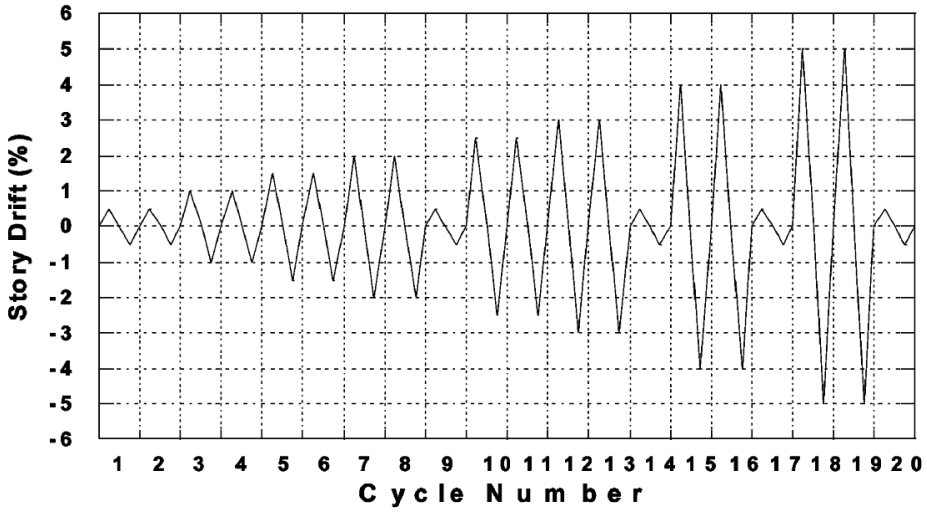

Figure 5. 9: Displacement History (Burak & Wight [3])

Performing a static push-over analysis on the specimens may be sufficient in order to analyze the specimens. However, this procedure is difficult to be established since consequential push-over loading should be defined for each cycle. Therefore, it is time-consuming to follow this procedure for the analytical study which involves loading patterns of numerous cycles. One other option to define the same loading sequence as of the experimental study is to simulate it using a dynamic earthquake analysis.

In order to simulate the cyclic deformations, the procedure, the steps of which are explained below, is followed:

1) The node on which the displacement is imposed and the direction of loading is chosen.
2) A considerable large mass (in the range of 10^{10} kN) is assigned to this node. Thus, a structure with a high natural period is obtained.
3) The actual displacement history having a typical form shown in **Figure 5.10** is selected.
4) The ground acceleration records that provide the selected displacement history are set up. To obtain the displacement record as in **Figure 5.10**, a velocity record is required. This velocity record (Figure 5.11) can be obtained by defining sharply

peaked acceleration pulses as illustrated in **Figure 5.12**. The procedure for defining required acceleration pulses are described as follows:

a) Peak acceleration of the first pulse is selected as a_1

b) The change in the velocity is $a_1.\Delta t$, where Δt is the time step. The displacement in the second pulse is $N.a_1.\Delta t^2$, where N is the number of time steps until the next pulse and it must be high enough to make the pulses sharply peaked. Therefore, it is generally taken about 100. Pulses extend over two time steps and the area of a pulse gives the required velocity change.

c) In order to obtain a unit displacement, the a_1 value is computed as:

$$a_1 = \frac{1}{N \cdot \Delta t^2} \qquad \textbf{(5.3)}$$

d) In the second pulse, displacement should be changed by 2 units. Therefore, the acceleration of the second pulse must be the minus 2 times that of first pulse.

e) This process is carried out until all loading pattern was obtained. N value is adjusted based on the amplitude changes in order to obtain the required displacement pattern.

5) With the generated synthetic earthquake record, a dynamic earthquake load case is set up and the structure is analyzed.

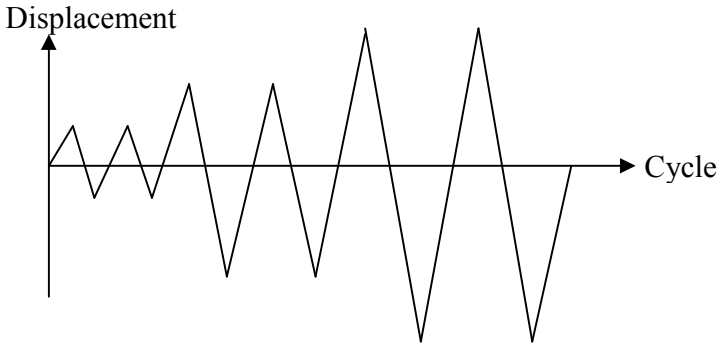

Figure 5. 10: Typical Displacement History

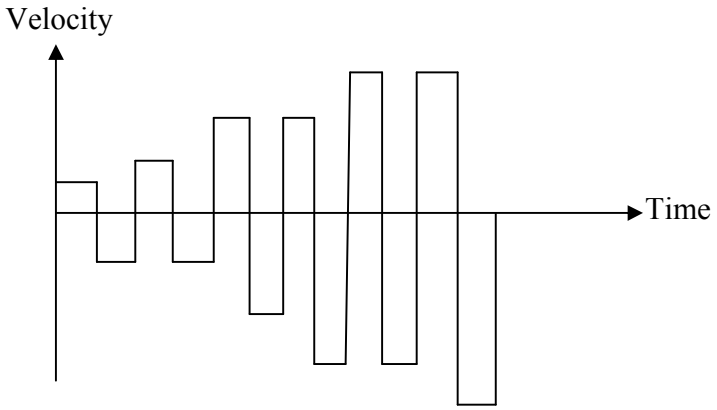

Figure 5.11: Required Velocity Record

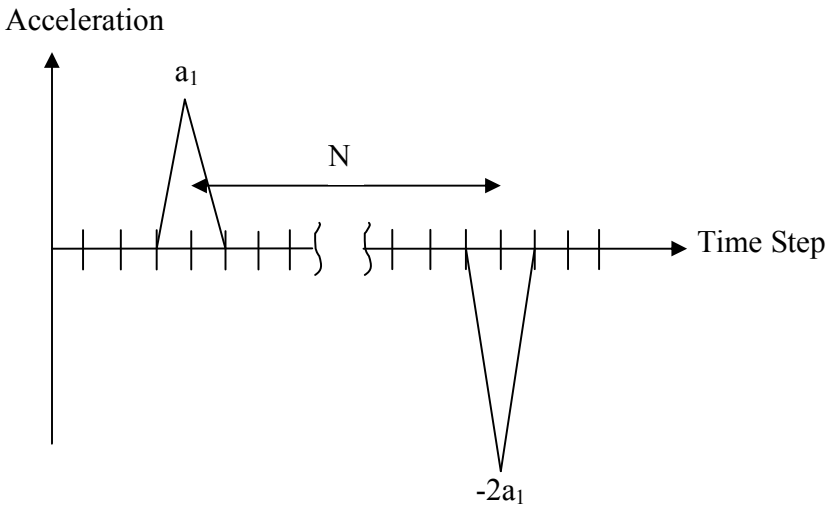

Figure 5.12: Defining Acceleration Pulses

5.4 RESULTS OF ANALYTICAL VERIFICATION

The proposed joint model is verified through the dynamic earthquake analysis in PERFORM–3D. As it is described in the above sections, the subassemblies are modeled in this computer software and the displacement history applied to the subassemblies in the test is imposed as ground acceleration records and the results are presented in this section. The specimens included in the database whose displacement records were available could be modeled and analyzed. The analytical results are presented below and compared with the experimental results in order to test the validity and accuracy of the model.

5.4.1 Specimens of Burak and Wight

Specimen 2-S, 3-S, 2-N and 3-N of this experimental study, which had the same displacement history applied during the experiment, were analyzed by applying dynamic earthquake loading. The main variables considered in this experimental study are eccentricity, beam width to column width ratio, column aspect ratio and the presence of slab. The experimental test setup and the loading pattern is given in **Appendix A1**. Lateral load vs. story drift response is shown in **Figure 5.13**. In this figure, the curve that belongs to the experimental response is also provided in order to check the accuracy of the model. As it is seen from the figure, analytical lateral load response represents the experimental response realistically. Specimen 2-S and 3-S showed a better correlation in predicting the maximum story shear. The cyclic degradation in higher drift levels closely matched with the experimental ones. This accuracy showed that the connection modeling is suitable for eccentric interior connections that contains floor slab. Specimen 2-N and 3-N also have an acceptable accuracy, however, the prediction in one direction is not adequate for specimen 3-N. This may be due to the fact that the effect of wide beams may not be characterized accurately because of the limited data that can be obtained for specimens that includes wide beams.

In all analytical predictions, pinching cannot be reproduced since there is not an option to define the pinching behavior in PERFORM-3D. As a result of this limitation of the

software, wider loops are observed in the hysteresis curves. Nevertheless, this does not affect the main objective of this study which is to estimate the envelope behavior of the connection region and the maximum values for lateral load, story drift, joint shear stress and deformation.

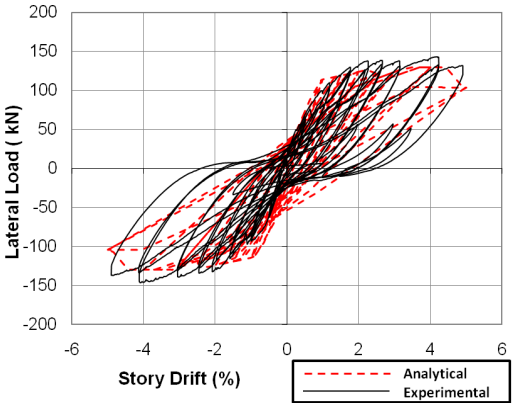

a) Specimen 2-S

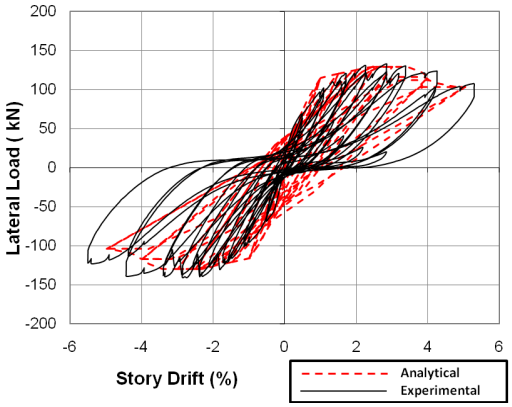

b) Specimen 3-S

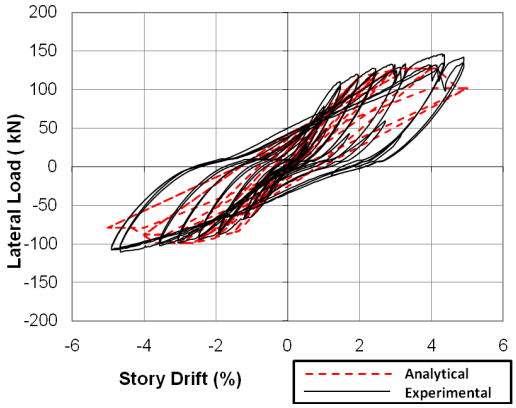

c) Specimen 2-N

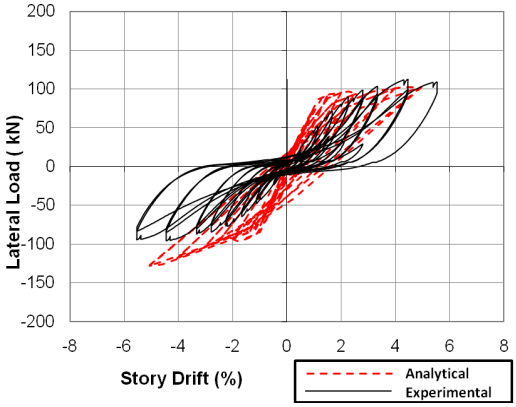

d) Specimen 3-N

Figure 5.13: Lateral Load vs. Story Drift Response (Specimens of Burak and Wight [3])

The comparison of the analytical and experimental response of joint shear strength vs. deformation is presented in **Figure 5.14**. The maximum joint shear strength of the analytical model has good accuracy. After the maximum shear strength has been reached, the analytical behavior diverged from the experimental behavior since slip is not considered in defining the maximum joint shear strain. When loading is in the normal beam direction; beam failure is the governing case in specimen 2-N, therefore, the joint did not experience shear distortions as high as the experimental values. However, the model captures the difference of joint behavior in two directions due to the difference in the positive and negative bending capacities of the beam in the loading direction. For specimen 3-N, although the strength capacity of the joints is very close to the actual response, the effect of wide beam has a negative effect on the analytical prediction and a widening of the hysteresis loops are observed. In the joint shear stress vs. strain diagram of specimens 2-S and 3-N, an unrealistic ascending portion is observed at the end of the strength degradation. This problem results from the limitations of the program and could not be eliminated. Since the trilinear behavior is imposed to the panel zone by the means of an added parallel stiffness as shown in **Figure 5.15**, there is not an option to reduce it after a certain deformation. Although this affected the overall load-displacement comparison, the maximum strength and strain capacity was not influenced. To make a realistic comparison, the specimens faced with this problem can be assumed to have a uniform reduction in strength starting from the point of unwanted increase and the strength values corresponding to the deformation values obtained from the model can be modified as shown in the envelope curve given in **Figure 5.16**.

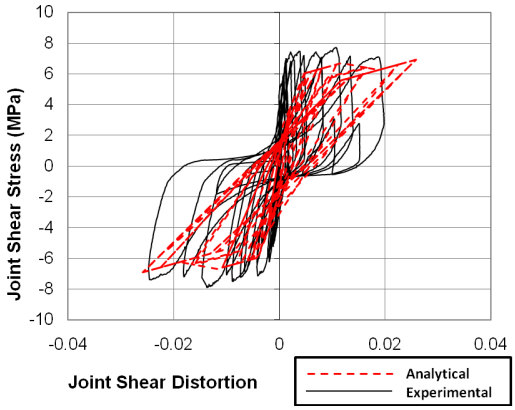

a) Specimen 2-S

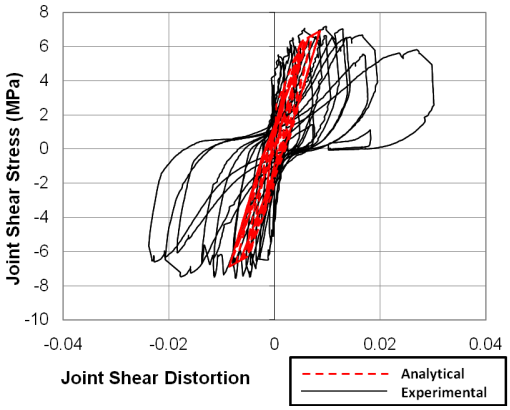

b) Specimen 3-S

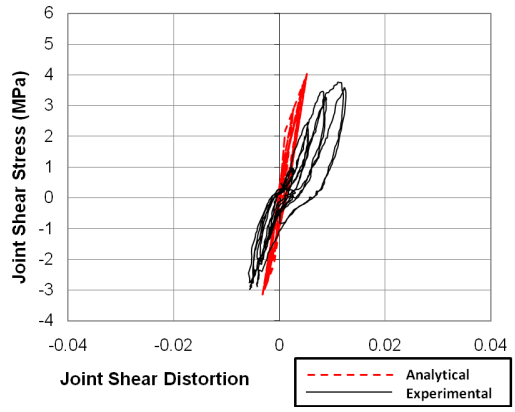

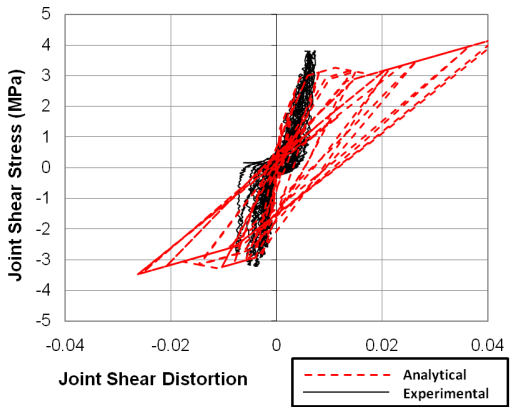

Figure 5.14: Joint Shear Stress vs. Joint Shear Distortion Responses (Specimens of Burak and Wight [3])

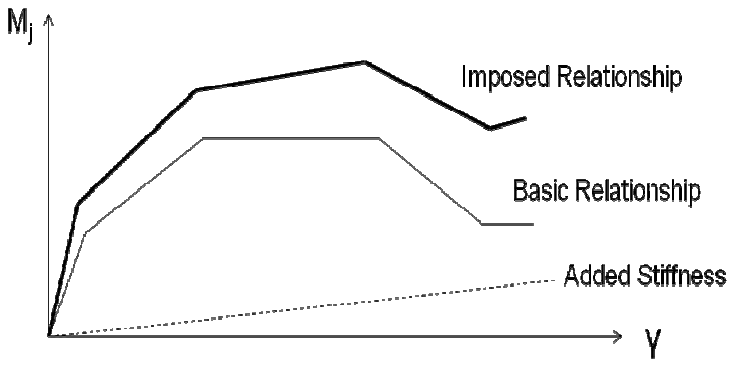

Figure 5.15: Defining the Joint Moment vs. Deformation Trilinear Relationship by Imposing an Additional Stiffness

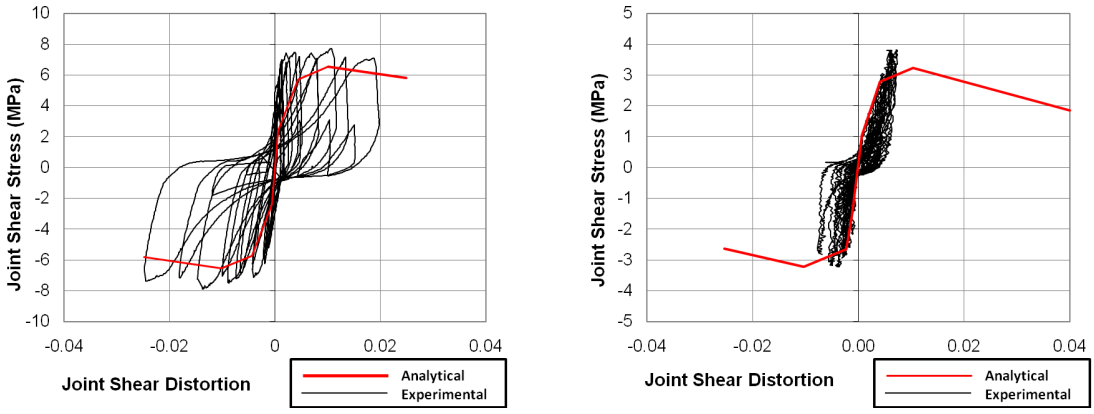

a) Specimen 2-N **b) Specimen 3-N**

Figure 5.16: Envelope Curve for the Analytical Joint Shear Stress vs. Shear Strain Response (Specimens of Burak and Wight [3])

Finally, the beam end moment vs. plastic hinge rotation curves are compared in **Figure 5.17**. As the load-deforamation response, the analytical modeling showed good correlation with the experimental results in terms of beam plastic hinge response. Since Specimens 2-S and 3-S hold the best acccuracy, it can be concluded that the analytical

model works better in interior eccentric connections having floor system, when compared to exterior ones especially with wide beams.

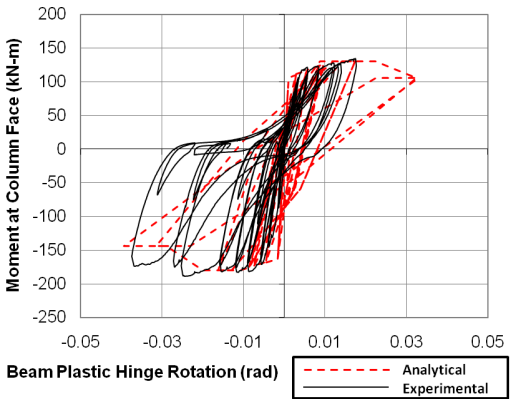

a) Specimen 2-S

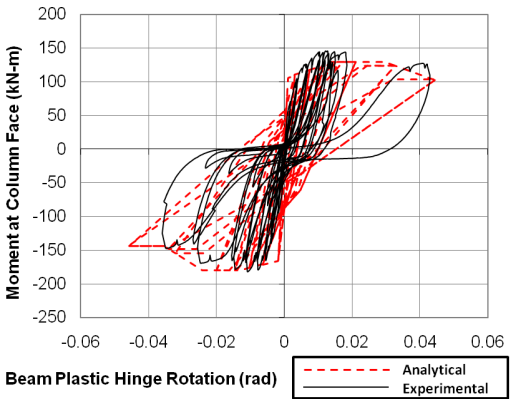

b) Specimen 3-S

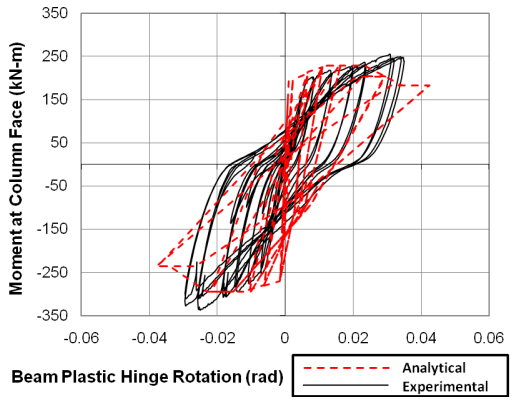

c) Specimen 2-N

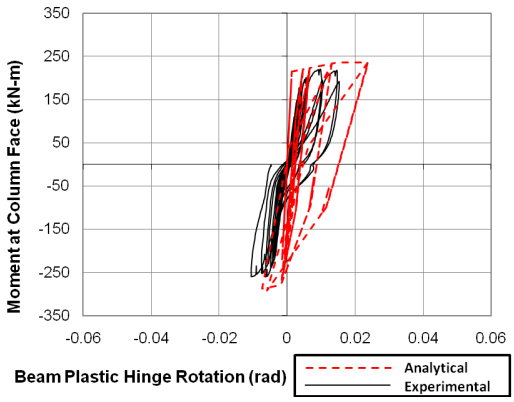

d) Specimen 3-N

Figure 5. 17: Beam moment vs. Beam Plastic Hinge Rotation Responses (Specimens of Burak and Wight [3])

5.4.2 Specimens of Kaku and Asakusa

18 specimens of Kaku and Asakusa are included in the database. The main variables of the specimens in this experimental study are joint reinforcement ratio, column axial load and compressive strength of concrete. Specimens 1, 2, 3, 6, 9 and 12 were modeled and analyzed in Perform-3D. Specimens 1, 2 and 3 were selected in order to compare the axial load effect which ranges from 0 to 0.17 $N/A_g.f_c'$ and specimens 6, 9 and 12 were selected to compare the effect resulting from the variation of the lateral reinforcement ratio. Although the volumetric reinforcement ratio parameter for all specimens are equal to 1.0 since $\rho_{onelayer}$ is smaller than 1.0, the comparison was made to prove that when volumetric reinforcement ratio is not extremely small, it does not proportionally reduce the joint capacity, however, when too small it increases the joint deformations. The loading sequence applied to the specimens are given in Appendix A.1. As it can be seen from the test-setup, beams of these specimens were vertically aligned and the loading was applied at the beam end horizontally. The same orientation was used in the analytical modeling and the mass was introduced at the beam end. The results for displacement versus beam end deflection response for the selected specimens are presented in **Figure 5.18**. For all specimens the load vs. displacement response is accurately predicted by analytical modeling when compared to the experimental results. In all cases, it was observed that the beam hinging governs the behavior rather than joint shear failure. Therefore, strength degradation was observed in all specimens. Specimen 1 and Specimen 2 give good results up to high drifts and the strength degradation response of other specimens is acceptable in addition to the ascending portion of the relationship. It should be noted that the complete diagram of modeling response of Specimen 3 and Specimen 6 cannot be given since higher beam end displacement values of the actual response was not included in the original publication.

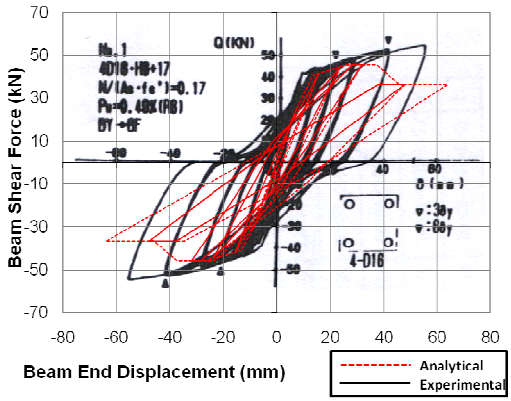

a) Specimen 1

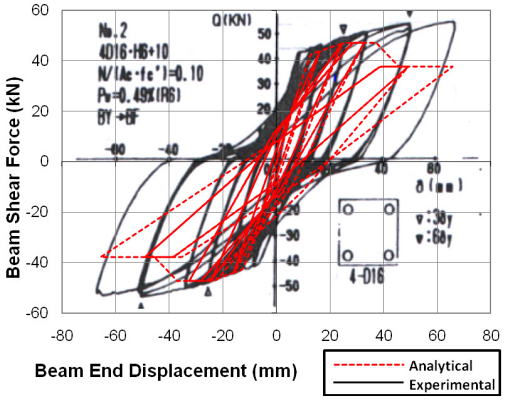

b) Specimen 2

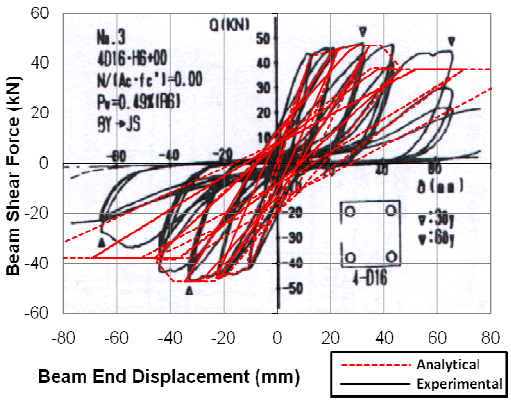

c) Specimen 3

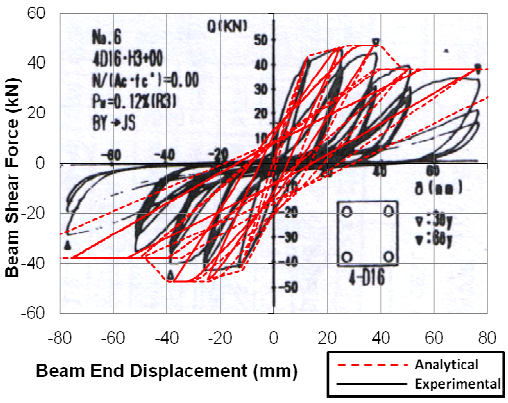

d) Specimen 6

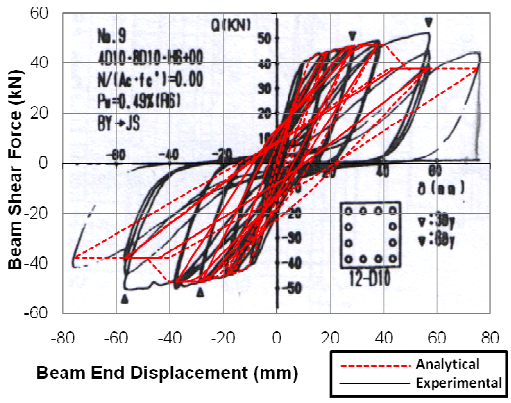

e) Specimen 9

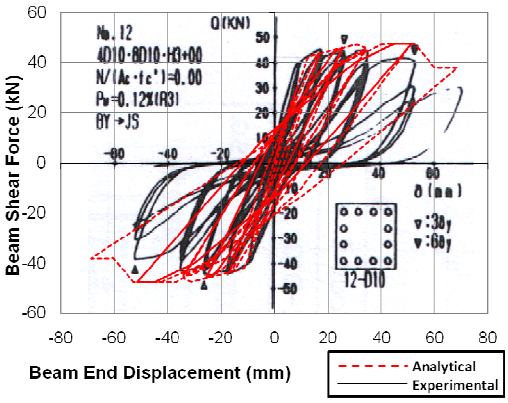

f) Specimen 12

Figure 5.18: Beam Shear Force vs. Beam End Displacement Responses (Specimens of Kaku and Asakusa [19])

The joint shear stress vs. strain responses are presented in **Figure 5.19**. As mentioned before, specimens 1, 2 and 3 are analyzed in order to see the effect of axial load since the axial load varies in these specimens (0.17 $N/A_g.f_c'$ for Specimen 1; 0.10 $N/A_g.f_c'$ for Specimen 2 and no axial load for Specimen 3). As the experimental response, the analytical response for these specimens showed an increase in the deformation capacity with the increase in the axial load. The maximum strength predictions are successful since the analytical predictions underestimate the strength only at a rate of about 20%. Specimens 6 and 12 have the same joint reinforcement ratio and same beam properties and no axial load was applied to both of these specimens. The difference is that the compressive strength of Specimen 12 is 20 % smaller than that of Specimen 9. From the joint behavior response, it can be inferred that the concrete compressive strength (f_c') is an influential parameter on seismic behavior of RC beam-to-column connections and may be overvalued in the earlier studies and as a result in this analytical study. In order to represent the effect of joint transverse reinforcement ratio effect, parameter $\rho_{onelayer}$, is defined and the parameter is 1.0 for all specimens of Kaku and Asakusa. The analytical verification of specimens 6, 9 and 12 showed that the variation of volumetric reinforcement ratio did not affect the joint strength significantly. However, it affects the maximum shear deformation values, therefore, the model underestimates these deformations. This information indicates that $\rho_{onelayer}$ parameter should be modified for specimens with extremely low amounts of joint transverse reinforcement.

Beam moment vs. plastic hinge rotations were also obtained for all specimens. However, they are not included herein, since the experimental responses are not available and without making a comparison verification of the model can not be performed.

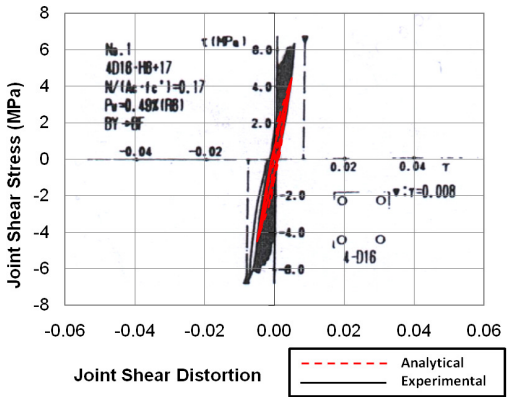

a) Specimen 1

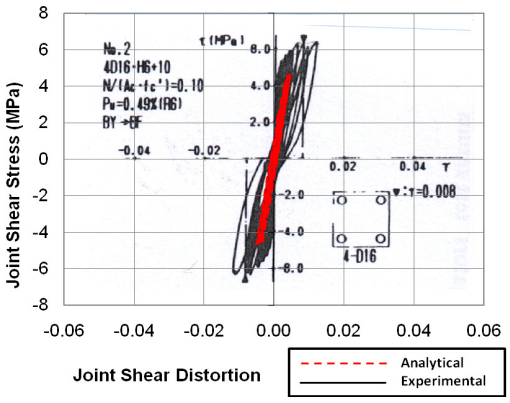

b) Specimen 2

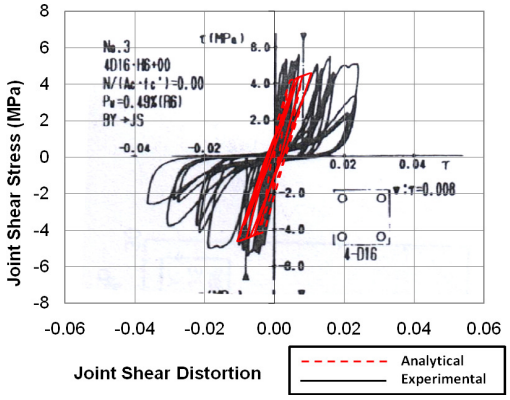

c) Specimen 3

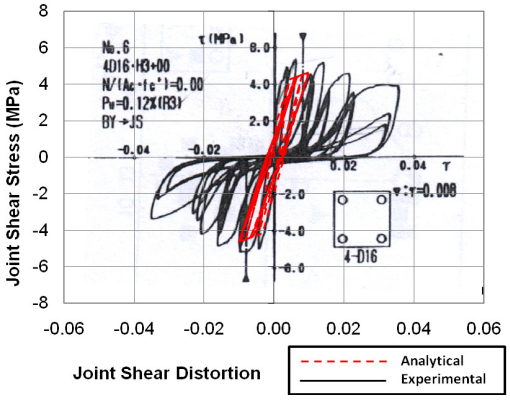

d) Specimen 6

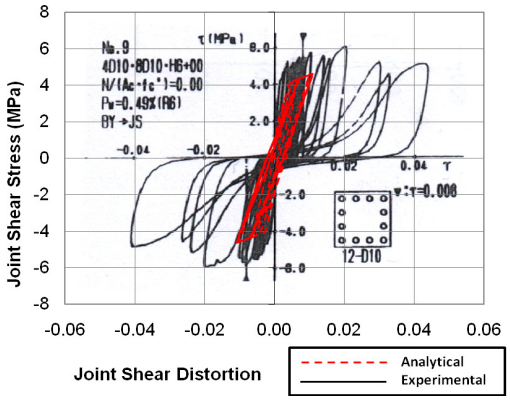

e) Specimen 9

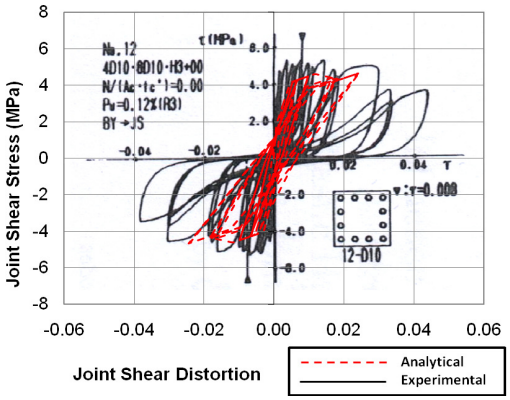

f) Specimen 12

Figure 5.19: Joint Shear Stress vs. Joint Shear Distortion Responses (Specimens of Kaku and Asakusa [19])

5.4.3 Specimens of LaFave and Wight

The specimens of this experimental study are used to define a parameter that represents the influence of the wide beams on the joint shear strength since three of the specimens (EWB1, EWB2 and EWB3) have wide beams in the loading direction whereas one specimen has a conventional beam (ENB1). The load vs. displacement diagrams in **Figure 5.20** shows the overestimation in the strength capacity and the initial stiffness. As in Specimen 3-N of Burak and Wight [3] mentioned before, there is a need for an improvement of the parameter that defines wide beam effect. Nonetheless, the overall trend is acceptable since the drift values corresponding to the strength increase and degradation points are quite accurate. Specimen EWB1 had anchorage failure at 4 % drift; therefore, the model can not predict the behavior after that point, as can be seen in **Figure 5.20**. For Specimen ENB1 the maximum strength attained is predicted with only 15 % deviation, but the initial stiffness is higher than the experimental results.

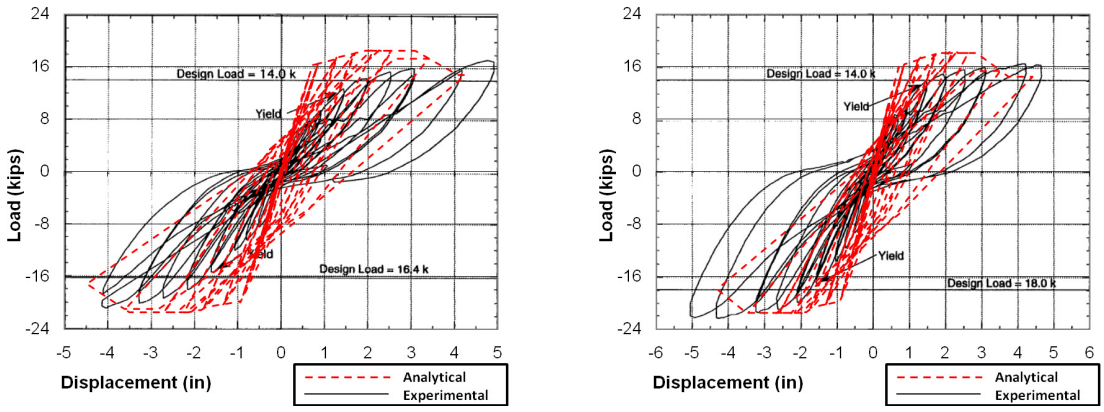

a) Specimen EWB1 **b) Specimen EWB2**

Figure 5.20: Load vs. Displacement Response (LaFave and Wight [24])

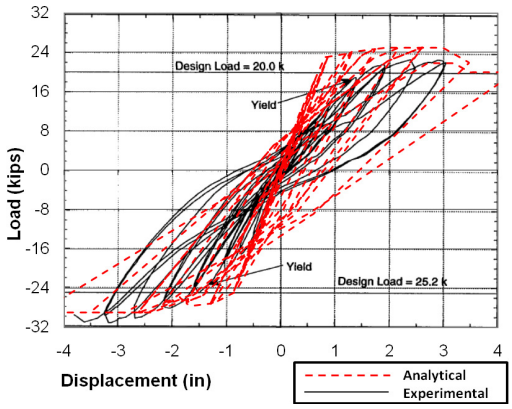

c) Specimen EWB3

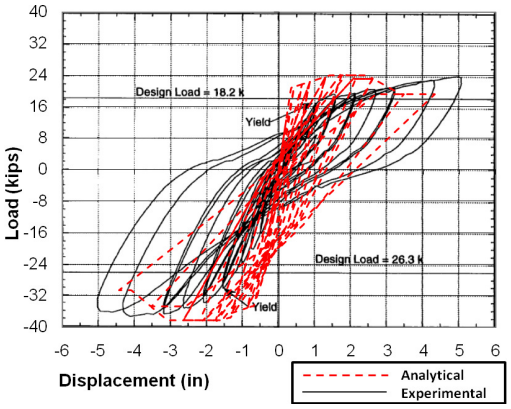

d) Specimen ENB1

Figure 5.20: Load vs. Displacement Response (LaFave and Wight [24])

Although the joint shear stress vs. strain relationship is not available; to obtain the joint shear force, beam end moment values can be divided by the distance between the top and bottom layers of beam reinforcement. The comparison of the analytical and experimental results for beam end moment vs. beam end rotation is given in **Figure 5.21**. These results are quite accurate as well, especially, first yielding of the beam plastic hinging region is predicted successfully. However, the beam end rotations are overestimated which is believed to be partly due to the change of the spandrel beam width, which was chosen to be a variable in this experimental program.

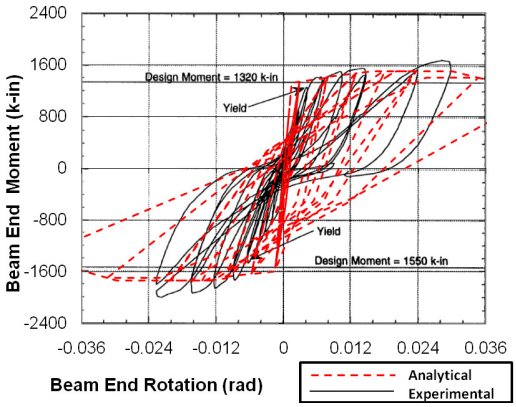

a) Specimen EWB1

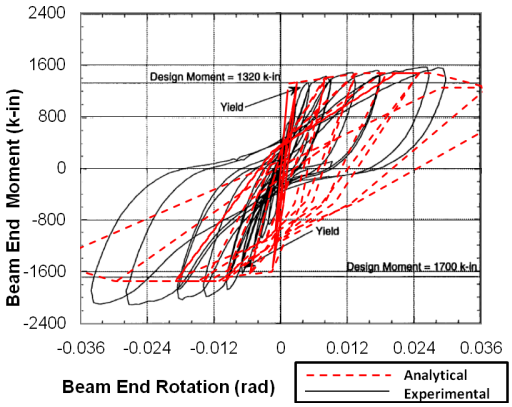

b) Specimen EWB2

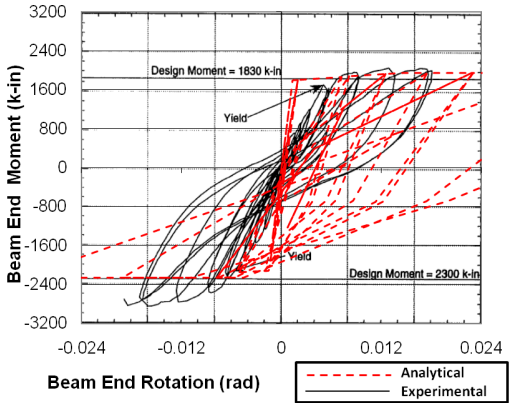

c) Specimen EWB3

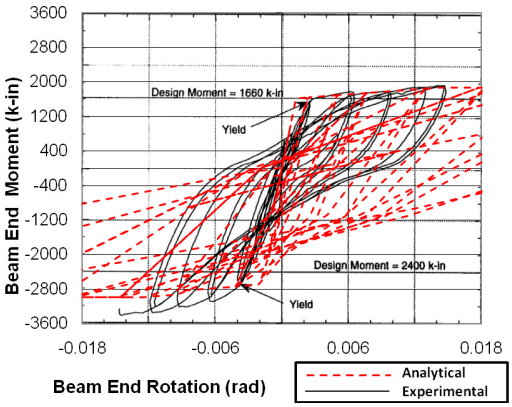

d) Specimen ENB1

Figure 5.21: Beam End Moment vs. Rotation Response (LaFave and Wight [24])

5.4.4 Specimens of Raffaelle and Wight

The main variable of the experimental study by Raffaelle and Wight is eccentricity. Four eccentric specimens of Rafaelle were tested and the analytical model is verified by comparing the test results with the analytical ones. Besides the eccentricity, member dimensions and the reinforcement detailing of beams vary in different specimens. Although the column dimensions are the same in all specimens, the effective joint width changes due to differences in eccentricity and the beam depth. The story shear vs. story

drift curves are given in **Figure 5.22**. The analytical results match with the experimental results with high accuracy, therefore the analytical joint model is verified one more time for the eccentric interior connections. It is observed that as the eccentricity increases, the ultimate story shear force decreases. Moreover, Specimen 4 attains the highest strength since it has the deepest beam and thus the highest flexural capacity. Up to 3% story drift, the ductility characteristics of the four specimens are similar. After that point, the beam width and the eccentricity amount influenced the energy dissipation capacity. For instance the beam width of Specimen 2 is smaller; therefore it has smoother stiffness degradation as captured by the model.

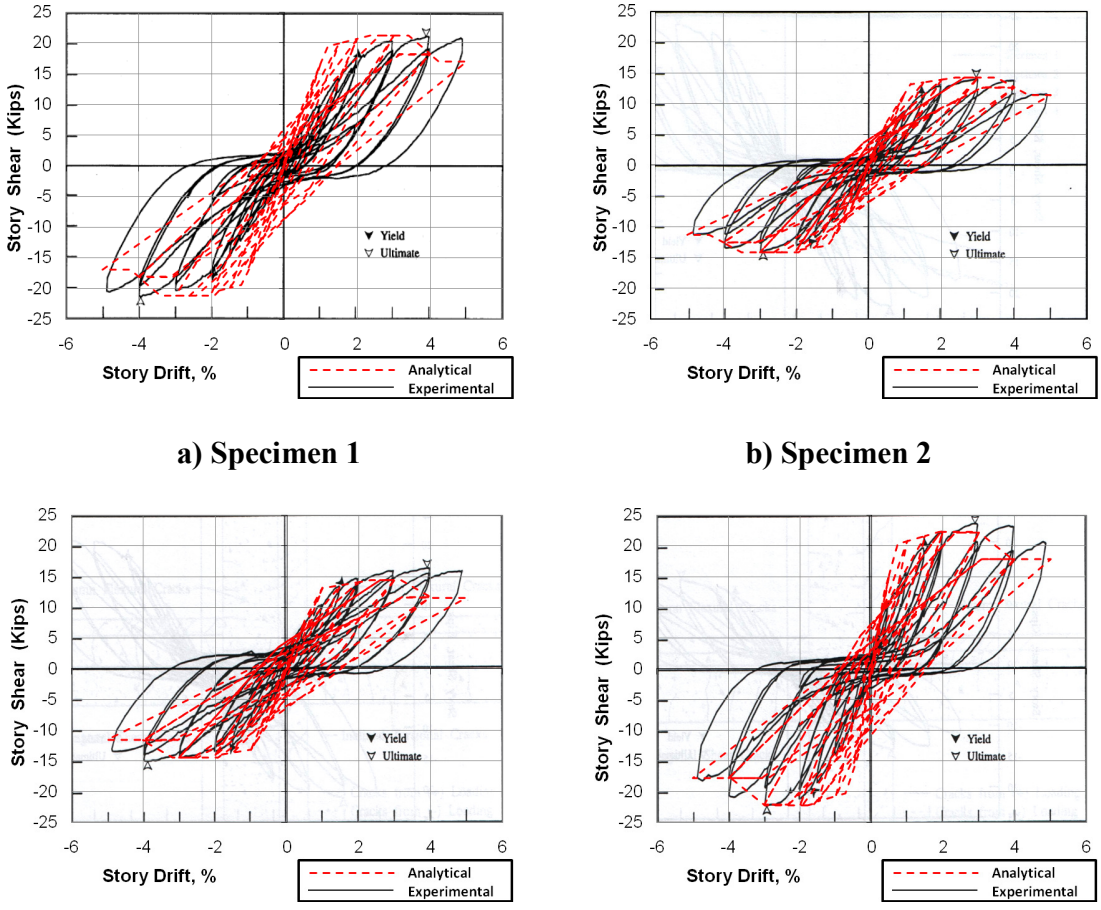

a) Specimen 1 **b) Specimen 2**

c) Specimen 3 **d) Specimen 4**

Figure 5.22: Story Shear vs. Story Drift Responses (Specimens of Rafaelle and Wight [32])

The experimental response of beam plastic hinge was not available. However, the joint shear vs. joint deformation behavior comparison is presented in **Figure 5.23**. In this figure, the joint shear stress vs. strain relationship of the connection panel element was compared with the experimental joint response measured both at the flush (outer) and offset (inner) joint faces. In order to make a comparison, the average of both figures can be taken into account since the panel zone gives an average response. When the specimens are considered individually, it is observed that the maximum joint capacity is predicted successfully in the analytical modeling. Besides, the maximum joint strain values also closely match with the average shear deformation response obtained in the experiments.

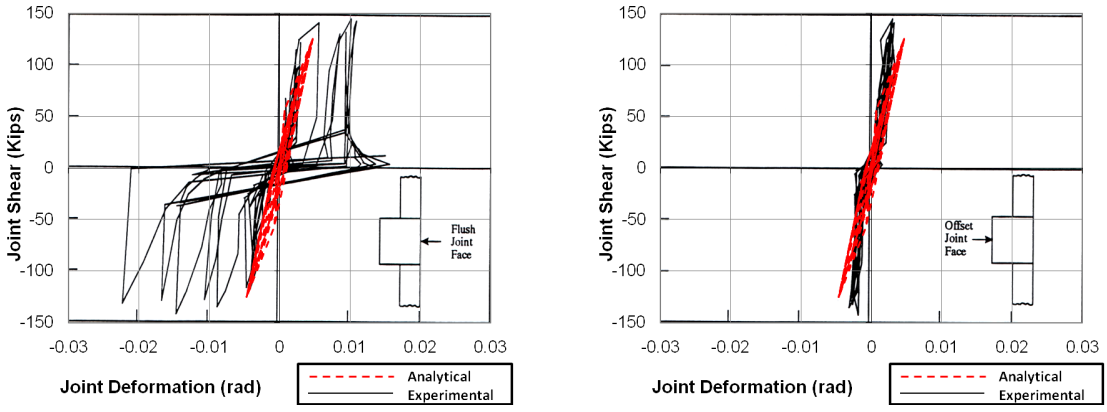

a) Specimen 1

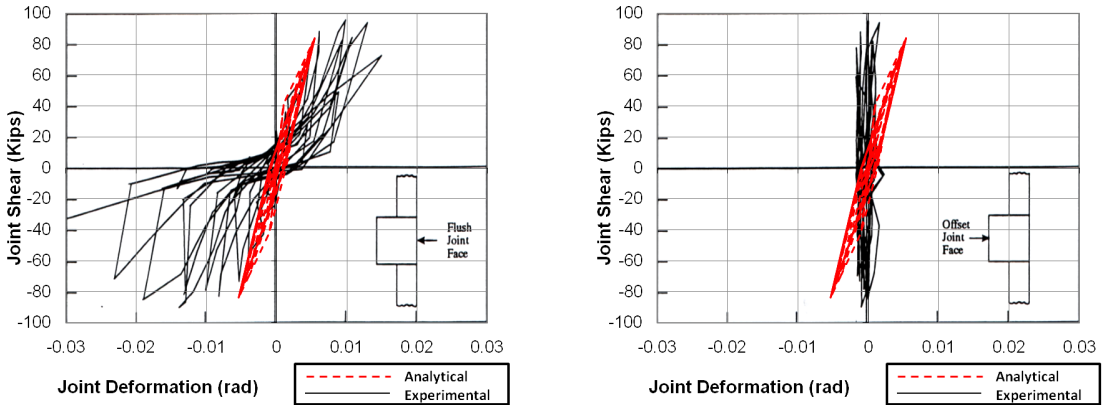

b) Specimen 2

Figure 5.23: Joint Shear vs. Joint Deformation Responses (Specimens of Raffaelle and Wight [32])

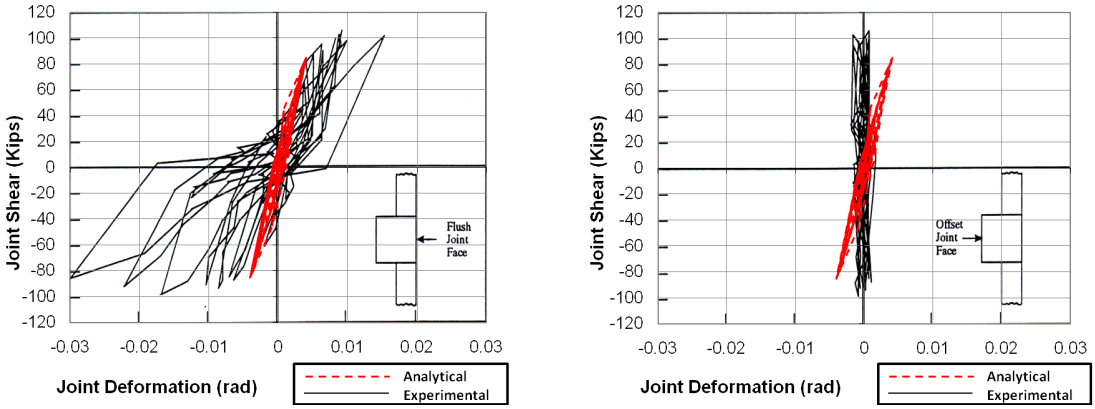

c) Specimen 3

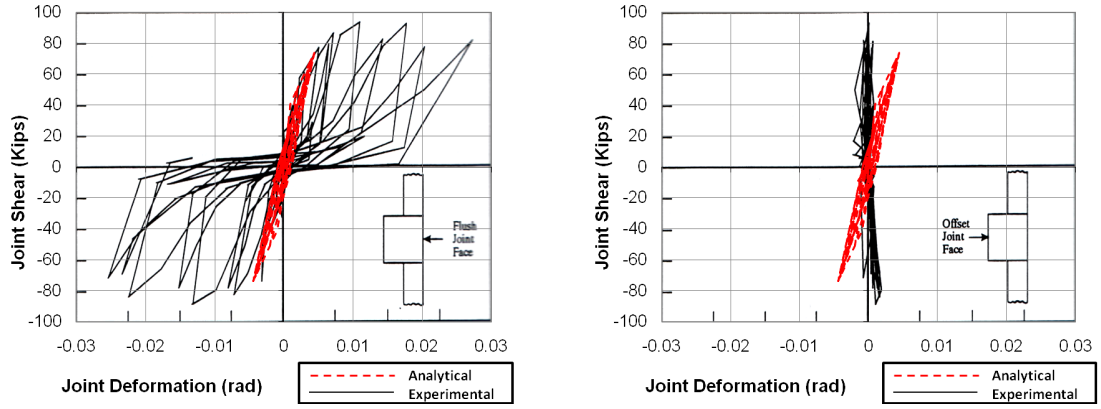

d) Specimen 4

Figure 5.23: Joint Shear vs. Joint Deformation Responses (Specimens of Raffaelle and Wight [32])

5.4.5 Specimens of Shin and LaFave

Four interior specimens of Shin and LaFave (SL1, SL2, SL3, and SL4) are utilized in the analytical verification of the joint model. SL1 and SL2 are eccentric specimens whereas SL3 and SL4 are concentric and all specimens have slab. Specimens vary in terms of joint hoop reinforcement and concrete compressive strength. As for the member dimensions; Specimen SL2 has a smaller beam width than others and the column dimension of SL4 differs so that the column aspect ratio in the strong direction is larger

than 1.0. The story shear vs. story drift diagrams are shown in **Figure 5.24**. Shear strength capacity prediction is acceptable in these specimens. Beam yielding governs in specimen SL3 due to the effect of high concrete compressive strength and absence of eccentricity. The initial stiffness of this specimen is higher than others for these reasons. SL4 has the highest amount of slab reinforcement; therefore, has a high slab index which led to attaining the highest story shear response.

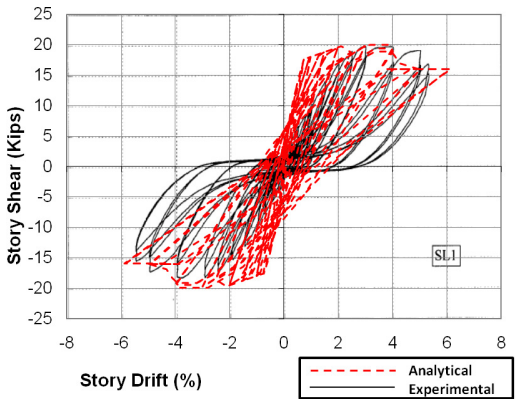

a) Specimen SL1

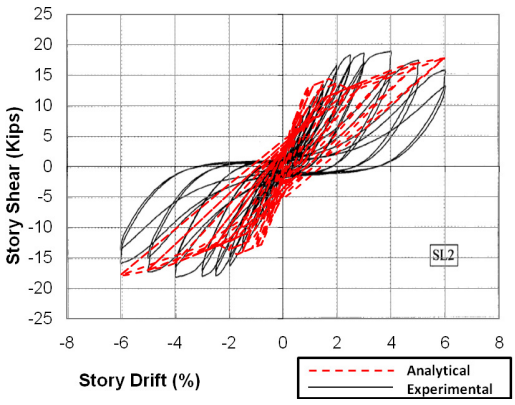

b) Specimen SL2

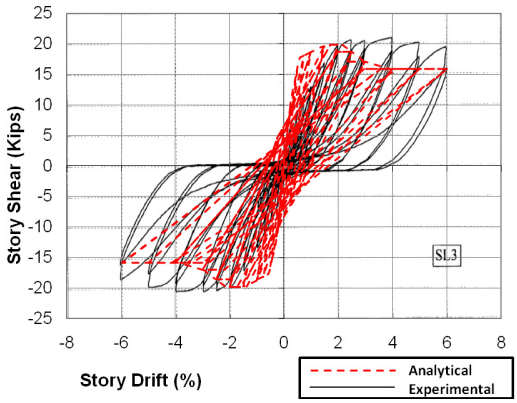

c) Specimen SL3

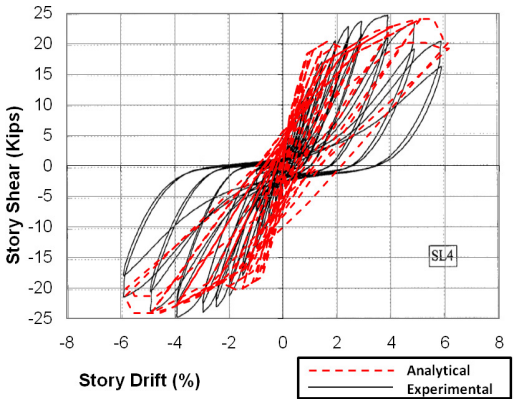

d) Specimen SL4

Figure 5.24: Story Shear vs. Story Drift Relationship (Specimens of Shin and LaFave [30])

Joint shear force vs. joint shear deformation is presented in **Figure 5.25**. The overall behavior is accurate and the maximum joint capacity is predicted sufficiently. Since beam yielding is the governing failure type in SL3 as mentioned before, the joint region was not affected much and therefore has narrower loops. The joint behavior up to strain values of about 0.01 showed good correlation with the experimental ones. However, after that point an unrealistic ascending portion was observed in this specimen similar to the problem faced with in Specimens 2-S and 3-N of Burak and Wight. This problem results from the limitations of the program and could not be eliminated as mentioned before. Although this unrealistic case affected the overall load-displacement comparison, the maximum strength and the strain capacity is not influenced. To make a realistic comparison the model is modified for the specimens facing this problem as shown in the envelope curve given in **Figure 5.26**.

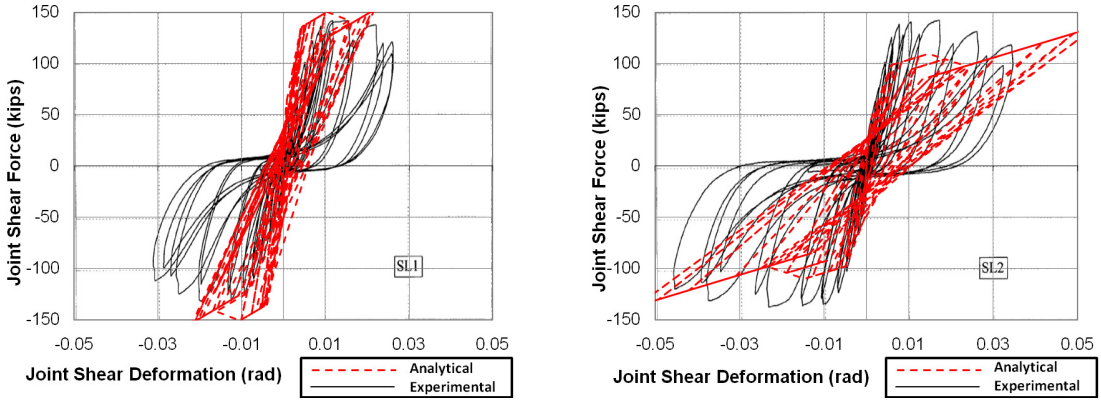

a) Specimen SL1 **b) Specimen SL2**

Figure 5.25: Joint Shear Force vs. Joint Shear Deformation Response (Specimens of Shin and LaFave [30])

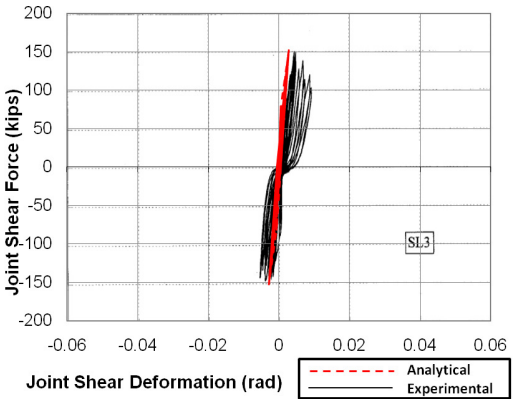

c) Specimen SL3

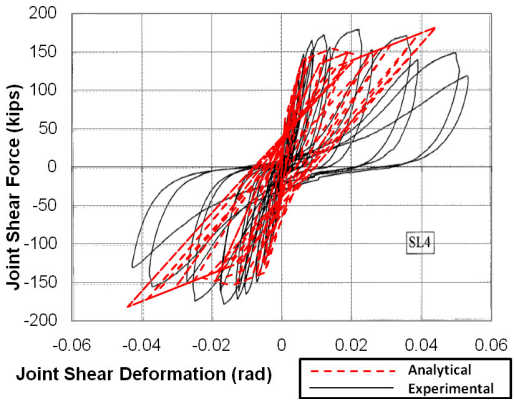

d) Specimen SL4

Figure 5.25: Joint Shear Force vs. Joint Shear Deformation Response (Specimens of Shin and LaFave [30])

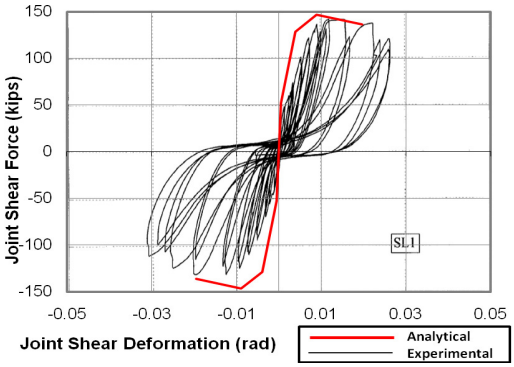

a) Specimen SL1

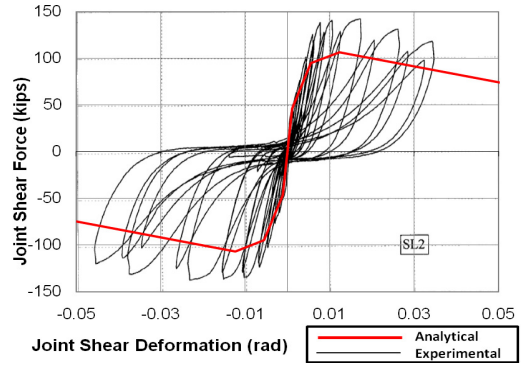

b) Specimen SL2

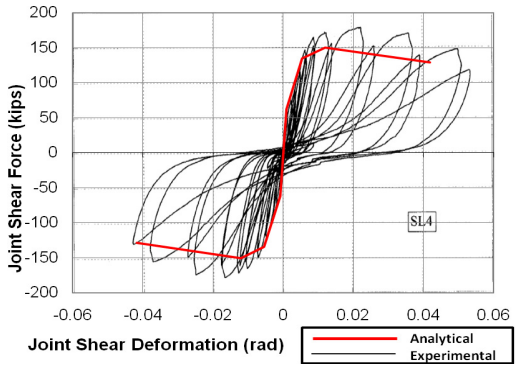

c) Specimen SL4

Figure 5.26: Envelope Curves for the Analytical Joint Shear Stress vs. Shear Strain Response (Specimens of Shin and LaFave [30])

5.4.6 Summary of the Model Verification Results

In order to see the effect of including joint model in RC beam-to-column connections, all specimens are also modeled by assuming the connection regions as rigid zones. In other words, the specimens are analyzed once again by removing the joint model. The result for 2-S specimen is shown in **Figure 5.27**. It can be seen from this figure that the story drifts are underestimated when the joint model is not considered in the analysis. Moreover, the beam rotations are significantly overestimated, which could lead to unrealistic failure of these members when the Turkish Earthquake Code (2007) limitations on strain values are checked. The maximum joint shear strength is attained at higher story drift levels in the experimental data, however, when the connection region is modeled as a rigid zone, the strain capacity is predicted lower than actual one and the connection behavior cannot be studied. On the other hand, modeling the connection region by the proposed analytical joint model also underestimates the experimental behavior in some cases leading to conservative strength estimations, but for some cases lower shear distortions.

Table 5.1 summarizes the differences in drift values between the analytical and experimental response. It can be concluded that the analytical model represents the actual response with acceptable tolerance. Comparisons of drift with and without the connection model for all specimens selected for this study are presented in **Table 5.2**. From this table, the need for using an analytical model for the connection region emerges, since the ultimate drift values using a rigid joint is underestimated when compared to the model with joint panel zone and with the experimental values.

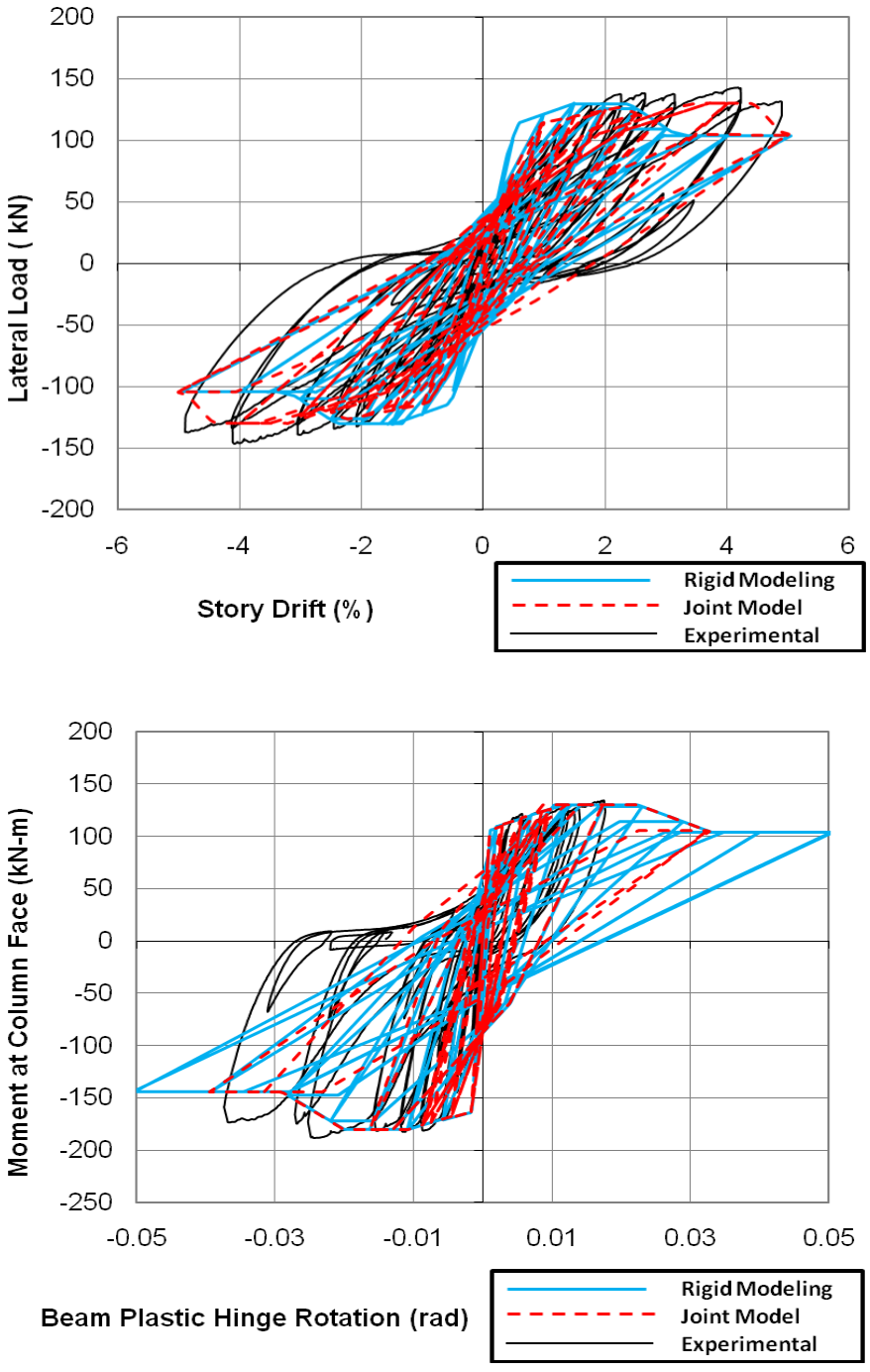

Figure 5.27: Analysis Results of Specimen 2-S (Burak and Wight [3])

Table 5.1: Comparison of Experimental and Analytical Story Drifts

Specimen	Experimental			Connection with joint model			Deviation (%)		
	Drift,cr	Drift,i	Drift,u	Drift,cr	Drift,i	Drift,u	Drift,cr	Drift,i	Drift,u
2-S	0.54	1.77	4.25	0.35	0.91	4.23	-35.19	-48.59	-0.47
3-S	0.288	1.35	3.39	0.3	0.928	3.19	4.17	-31.26	-5.90
2-N	0.58	1.28	4.18	0.61	1.83	3.93	5.17	42.97	-5.98
3-N	0.97	2.16	5.32	0.376	1.11	4.68	-61.24	-48.61	-12.03
Specimen 1	0.3	1.05	5.5	0.48	1.29	3.54	60.00	22.86	-35.64
Specimen 2	0.43	0.91	4.8	0.5	1.24	3.55	16.28	36.26	-26.04
Specimen 3	0.27	1.17	3.99	0.47	1.29	3.75	74.07	10.26	-6.02
Specimen 6	0.25	1.21	3.8	0.38	1.21	3.81	52.00	0.00	0.26
Specimen 9	0.32	1.05	5.5	0.47	1.14	3.9	46.88	8.57	-29.09
Specimen 12	0.34	0.87	3.53	0.51	1.29	4.91	50.00	48.28	39.09
1	0.77	2.12	3.88	0.43	1.16	3.26	-44.16	-45.28	-15.98
2	0.50	1.50	3.02	0.45	1.07	3.36	-10.00	-28.67	11.26
3	0.46	1.62	3.81	0.42	0.94	3.01	-8.70	-41.98	-21.00
4	0.44	1.63	2.90	0.26	0.68	2.85	-40.91	-58.28	-1.72
SL1	0.64	2.48	3.99	0.21	0.70	3.65	-67.19	-71.77	-8.52
SL2	0.58	1.77	4.17	0.25	0.85	1.61	-56.90	-51.98	-61.39
SL3	0.27	1.33	3.83	0.21	0.55	2.05	-22.22	-58.65	-46.48
SL4	0.51	1.81	3.65	0.23	0.82	2.01	-54.90	-54.70	-44.93
EWB1	0.52	1.56	5.21	0.79	2.04	3.35	51.92	30.77	-35.70
EWB2	0.44	1.67	4.51	0.79	1.84	3.05	79.55	10.18	-32.37
EWB3	0.82	1.73	3.3	0.89	2.2	3.29	8.54	27.17	-0.30
ENB1	0.47	1.81	5.32	0.38	1.4	2.76	-19.15	-22.65	-48.12

Table 5.2: Comparison of Story Drifts for Specimens Analyzed with and without the Joint Model

Specimen	Connection with rigid joint			Connection with joint model			Deviation (%)		
	Drift,cr	Drift,i	Drift,u	Drift,cr	Drift,i	Drift,u	Drift,cr	Drift,i	Drift,u
2-S	0.25	0.63	2.41	0.35	0.91	4.23	40.00	44.44	75.52
3-S	0.28	0.68	2.84	0.3	0.928	3.19	7.14	36.47	12.32
2-N	0.47	1.23	3.46	0.61	1.83	3.93	29.79	48.78	13.58
3-N	0.6	1.15	3.08	0.376	1.11	4.68	-37.33	-3.48	51.95
Specimen 1	0.49	1.13	3.38	0.48	1.29	3.54	-2.04	14.16	4.73
Specimen 2	0.42	1.07	3.39	0.5	1.24	3.55	19.05	15.89	4.72
Specimen 3	0.35	0.94	3.05	0.47	1.29	3.75	34.29	37.23	22.95
Specimen 6	0.25	0.89	3.31	0.38	1.21	3.81	52.00	35.96	15.11
Specimen 9	0.38	0.95	3.23	0.47	1.14	3.9	23.68	20.00	20.74
Specimen 12	0.51	0.95	3.28	0.51	1.29	4.91	0.00	35.79	49.70
1	0.48	0.90	3.06	0.43	1.16	3.26	-10.42	28.89	6.54
2	0.41	0.79	3.12	0.45	1.07	3.36	9.76	35.44	7.69
3	0.38	0.76	2.92	0.42	0.94	3.01	10.53	23.68	3.08
4	0.29	0.53	2.73	0.26	0.68	2.85	-10.34	28.30	4.40
SL1	0.22	0.46	2.14	0.21	0.70	3.65	-4.55	52.17	70.56
SL2	0.23	0.69	1.90	0.25	0.85	1.61	8.70	23.19	-15.26
SL3	0.18	0.46	2.03	0.21	0.55	2.05	16.67	19.57	0.99
SL4	0.22	0.62	2.08	0.23	0.82	2.01	4.55	32.26	-3.37
EWB1	0.79	1.96	3.31	0.79	2.04	3.35	0.00	4.08	1.21
EWB2	0.78	1.75	3.3	0.79	1.84	3.05	1.28	5.14	-7.58
EWB3	0.76	2.2	3.3	0.89	2.2	3.29	17.11	0.00	-0.30
ENB1	0.36	1.3	2.5	0.38	1.4	2.76	5.56	7.69	10.40

Table 5.3: Comparison of Story Drifts for Specimens Analyzed with Rigid Joint and Experimental Story Drifts

Specimen	Experimental			Connection with rigid joint			Deviation (%)		
	Drift,cr	Drift,i	Drift,u	Drift,cr	Drift,i	Drift,u	Drift,cr	Drift,i	Drift,u
2-S	0.54	1.77	4.25	0.25	0.63	2.41	-53.70	-64.41	-43.29
3-S	0.288	1.35	3.39	0.28	0.68	2.84	-2.78	-49.63	-16.22
2-N	0.58	1.28	4.18	0.47	1.23	3.46	-18.97	-3.91	-17.22
3-N	0.97	2.16	5.32	0.6	1.15	3.08	-38.14	-46.76	-42.11
Specimen 1	0.3	1.05	5.5	0.49	1.13	3.38	63.33	7.62	-38.55
Specimen 2	0.43	0.91	4.8	0.42	1.07	3.39	-2.33	17.58	-29.38
Specimen 3	0.27	1.17	3.99	0.35	0.94	3.05	29.63	-19.66	-23.56
Specimen 6	0.25	1.21	3.8	0.25	0.89	3.31	0.00	-26.45	-12.89
Specimen 9	0.32	1.05	5.5	0.38	0.95	3.23	18.75	-9.52	-41.27
Specimen 12	0.34	0.87	3.53	0.51	0.95	3.28	50.00	9.20	-7.08
1	0.77	2.12	3.88	0.48	0.90	3.06	-37.66	-57.55	-21.13
2	0.50	1.50	3.02	0.41	0.79	3.12	-18.00	-47.33	3.31
3	0.46	1.62	3.81	0.38	0.76	2.92	-17.39	-53.09	-23.36
4	0.44	1.63	2.90	0.29	0.53	2.73	-34.09	-67.48	-5.86
SL1	0.64	2.48	3.99	0.22	0.46	2.14	-65.63	-81.45	-46.37
SL2	0.58	1.77	4.17	0.23	0.69	1.90	-60.34	-61.02	-54.44
SL3	0.27	1.33	3.83	0.18	0.46	2.03	-33.33	-65.41	-47.00
SL4	0.51	1.81	3.65	0.22	0.62	2.08	-56.86	-65.75	-43.01
EWB1	0.52	1.56	5.21	0.79	1.96	3.31	51.92	25.64	-36.47
EWB2	0.44	1.67	4.51	0.78	1.75	3.3	77.27	4.79	-26.83
EWB3	0.82	1.73	3.3	0.76	2.2	3.3	-7.32	27.17	0.00
ENB1	0.47	1.81	5.32	0.36	1.3	2.5	-23.40	-28.18	-53.01

The contribution of joint shear distortion to story drift can be estimated from the geometry by assuming beams and columns remained rigid and the joint faces remained vertical to the framing members. Typical specimen geometry used in story drift calculations are illustrated in **Figure 5.28**. The solid lines in this figure represent exterior subassemblies with one beam framing into the joint, and the dashed lines represent the interior specimens.

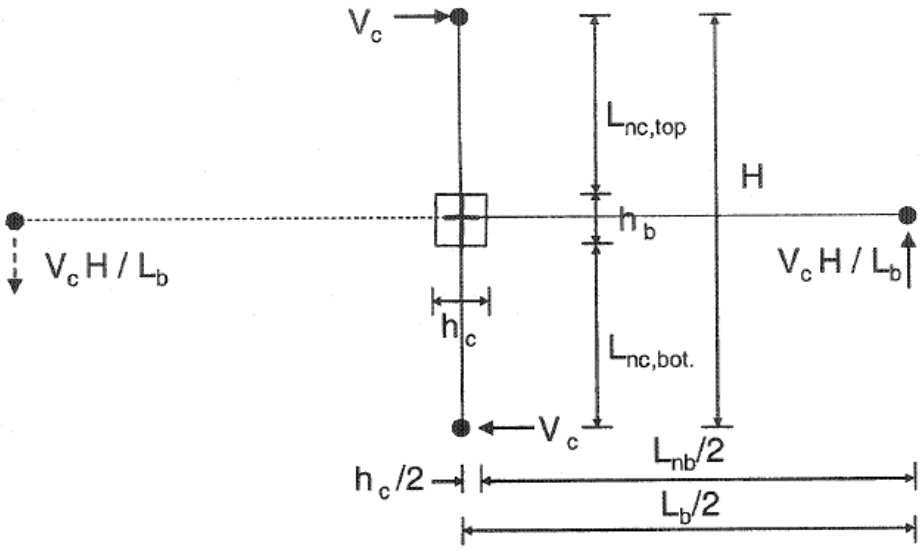

Figure 5.28: Specimen Geometry used in Story Drift Computations (Burak and Wight [3])

The equation derived to compute the contribution of joint shear distortions on story drifts is given in **Equation (5.4).** This equation is valid for both interior and exterior specimens.

$$\Delta_j = H \cdot \gamma \cdot (1 - \frac{h_b}{H} - \frac{h_c}{L_b}) \qquad \textbf{(5.4)}$$

where, H is the full height of the specimen,

γ is the joint shear distortion,

h_b and h_c are the beam and column depths, respectively,

L_b is the span length of the beam.

Beam and column elastic rotations, beam plastic hinge rotations and beam end rotations are the other components that contribute to the total story drift. The contribution of beam rotations to the story drift are computed by using moment-area theorem and the following equations are obtained (Burak and Wight [3])

The story displacement resulting from the beam elastic rotations:

$$\Delta b_e = \frac{V_c \cdot H \cdot L_{nb}^{\,3}}{12E_b \cdot I_b \cdot L_b} \quad \textbf{(5.5)}$$

The story displacement resulting from the beam plastic hinge rotations:

$$\Delta b_{ph} = \frac{H \cdot \theta_{ph} \cdot (L_{nb} - L_{ph})}{L_b} \quad \textbf{(5.6)}$$

The story displacement resulting from the beam end rotations:

$$\Delta b_{end} = \frac{H \cdot \theta_{b,end} \cdot L_{nb}}{L_b} \quad \textbf{(5.7)}$$

In these equations, V_c is the column shear applied in positive or negative loading direction, E_b is the modulus of elasticity of concrete in the beam, I_b is the effective moment of inertia of the beam, which is taken as 35 % of the gross moment of inertia, H is the total height of the subassembly, L_b, L_{nb}, L_{ph} are the span length, net length and plastic hinge length of beam, θ_{ph} is the plastic hinge rotation, and $\theta_{b,end}$ is the concentrated rotation at the beam end.

The column elastic rotations, although very small due to the strong column-weak beam design philosophy, have contribution to the story drift. The following equation is derived for the displacement resulting from the column elastic rotations by considering the beams and connection regions infinitely rigid and using moment-area theorem:

$$\Delta c_e = \frac{V_c}{3E_c \cdot I_c}(L_{nc,top}^{\,3} - L_{nc,bot.}^{\,3}) \quad \textbf{(5.8)}$$

where, V_c is the column shear applied in positive or negative loading directions,

E_c is the modulus of elasticity of concrete in column,

I_c is the effective moment of inertia of the column, which is equal to 70 % of the

gross moment of inertia,

$L_{nc,top}$ and $L_{nc,bot.}$ are the net lengths of top and bottom column respectively.

The story drift contributions resulting from beam, column and joint components are computed for Specimen 2-S at each 0.5 % story drift increments and shown in **Figure 5.29** as a percentage of the total story drift. As it can be seen from the figure, joint shear distortion constitutes between 20 and 50 % of total story drift. The rest of the story drift is caused by column elastic rotation, beam elastic rotation and beam plastic hinge rotation.

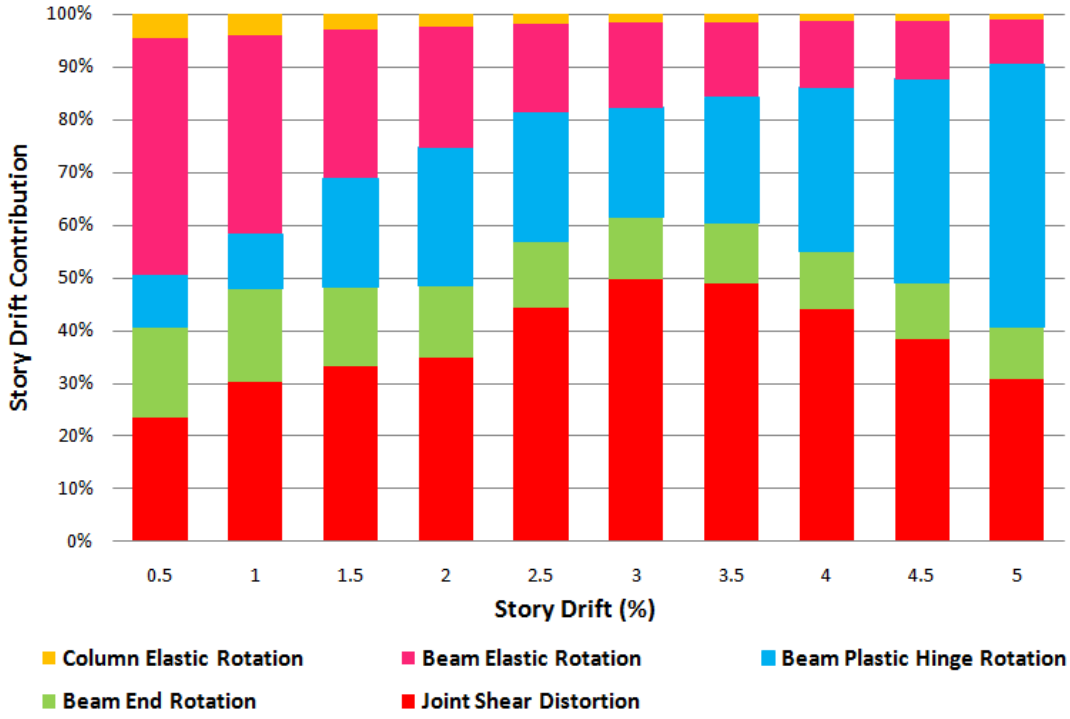

Figure 5.29: Average Story Drift Components of Specimen 2-S, Burak and Wight [3]

The influence of joint shear distortion on total story drift is also computed for other specimens, whose joint distortion response are available from the analysis, at 2 % drift level and presented in **Table 5.4**. It can be observed from this table that joint shear distortions contribute to the story drifts up to 70 % in some cases and about 40 % as an

average.This clearly indicates the need for considering a joint model in nonlinear analysis.

Table 5.4: Displacement Resulting from Joint Shear Distortions and its Contribution to Total Story Drift at 2 % Drift Level

Specimen	Displacement due to Joint Shear Distortion (mm)	Total Displacement (mm)	Contribution of Joint Shear Distortion (%)
2-S	20.84	51.80	40.24
3-S	14.07	51.80	27.17
2-N	6.12	51.80	11.82
3-N	21.83	51.80	42.13
Specimen 1	3.94	30.80	12.80
Specimen 2	2.93	30.80	9.52
Specimen 3	5.70	30.80	18.52
Specimen 6	6.29	30.80	20.42
Specimen 9	6.10	30.80	19.81
Specimen 12	6.43	30.80	20.88
1	7.49	44.72	16.75
2	8.62	44.72	19.28
3	6.46	44.72	14.44
4	6.56	44.72	14.66
SL1	22.95	58.94	38.94
SL2	42.85	58.94	72.70
SL3	6.58	58.94	11.16
SL4	43.02	58.94	72.98
EWB1	2.65	44.72	5.92
EWB2	2.48	44.72	5.55
EWB3	5.45	44.72	12.18
ENB1	1.48	44.72	3.31

CHAPTER 6

SUMMARY AND CONCLUSIONS

6.1 SUMMARY

The main objective of this study is to develop an analytical joint model to accurately predict the inelastic behavior of reinforced concrete beam-to-column connections subjected to earthquake loading. For this purpose, first, an experimental database of reinforced concrete connections is generated which includes geometric characteristics and material properties of the specimens and the test results under cyclic loading. Then, the statistical correlations of key parameters that influence the seismic behavior of beam-to-column connections with the experimental joint shear strength and shear strain are investigated. After this evaluation, the parameters that are found to have a significant influence on the nonlinear joint response are incorporated into the model. In the equations, the parameters are defined in terms of ratios and powers of some of the key individual parameters to accurately represent their effect on the strength and strain capacity and obtain the minimum average error and the highest correlation with the experimental values. While carrying out these steps, the guidelines given in ACI Committee 318 (2008), Building Code Requirements for Structural Concrete, and ACI-ASCE Committee 352 (2002), Recommendations for Design of Beam-Column Connections in Monolithic Reinforced Concrete Structures, are followed in obtaining the parameters used in design. Finally, the connection subassemblies are modeled and the cyclic loading was applied analytically using Perform 3D. The loading patterns are taken same as the experimental loading history in order to be able to compare the analytical results with the experimental ones.

6.2 CONCLUSIONS

Based on the results of this analytical investigation, the following conclusions are drawn:

1. Statistical correlation method indicates that the most influential factors on shear strength of reinforced concrete beam-to-column connections are compressive strength of concrete, volumetric joint transverse reinforcement ratio and effective joint width. The effect of eccentricity between the longitudinal beam and column centerlines, axial load applied to the column and presence of wide beams and slab should not be neglected to accurately predict the behavior of connections subjected to cyclic loading.

2. A statistical combination of the key parameters is used to predict the joint shear strength and the average error turned out to be -4 % whereas the absolute average error is 14 %. The correlation between experimental and predicted joint shear strengths is 88 %. The best predictions with this model are obtained for eccentric exterior and concentric interior connections which have slab in the floor system but no wide beams.

3. Although a low number of the maximum shear strength predictions are higher than the experimental values, the proposed formula is generally conservative. Furthermore, since the guidelines of ACI 352 Recommendations (2002) are followed, it can be used for design applications.

4. The predicted formula gives closer results to the experimental data for well-detailed connection regions that are designed following the ACI 318R-08 and ACI 352R-02 design codes. Additional experimental results are required to predict the behavior of beam-to-column connections that has low amount of transverse reinforcement.

5. The proposed formula for joint shear strength prediction gives more conservative results with less scatter when compared to the equation recommended by ACI 352 R-02.

6. It is observed that limitations on joint shear strength given in Turkish Earthquake Code (TEC 2007) are mostly unconservative when compared to the joint shear strength by the proposed formula and the nominal joint shear strength equation given in ACI 352R-02. The deviations are generally large which indicates that the guidelines of TEC 2007 on the seismic behavior of beam-to-column connections should be revised.

7. Since joint shear deformation behavior involves high amount of uncertainty resulting from the data reading errors, the prediction of shear strain is difficult. Nevertheless, the most affective parameters on joint shear strain capacity can be determined evaluating the prior experiments. The joint shear strength, confinement provided by transverse beams, effective joint width and the column depth are observed to be the most influential parameters on joint shear strain behavior. Therefore, these parameters are included in the joint shear strain prediction.

8. The envelope of the nonlinear hysteretic behavior of joint region that is incorporated into the model can be predicted by considering three critical points at which significant slope change is observed. Therefore, a trilinear joint model that represents this nonlinear behavior is developed. While developing the model, special attention was given to keep the model simple and conservative to be used in design applications.

9. The proposed joint model is introduced to the subassembly model as a panel zone element. The beams and columns are modeled by considering their moment vs. rotation relationships. When a dynamic time history analysis is carried out, it is observed that proposed analytical joint model, in general, gives reasonably close results to the experimental ones.

10. The model is verified by comparing the experimental results with the analytical response in terms of overall load-displacement relationship, joint element response, and beam plastic hinge response. It was observed that, in general, the seismic behavior of connection regions is reasonably predicted.

11. The significance of concrete compressive strength, axial load and volumetric joint transverse reinforcement ratio on the joint shear response is also verified by this analysis series.

12. The developed analytical model is least accurate for connections with wide beams in the loading direction. The limited number of available experimental data may lead to a wrong interpretation of the wide beam effect. This parameter can be improved in a future research project by adding new wide beam-to-column connection subassemblies to the database as their experimental data becomes available.

13. When the results of the analysis with and without joint model are compared, it is concluded that assuming a rigid joint region in modeling results in underestimation of the story drift. Moreover, even the maximum drifts obtained with joint model are up to 60% lower than the experimental drifts for some specimens.

14. The contribution of beam and column rotations and joint shear distortions to the total story drift are calculated and it is observed that joint shear deformations causes in average 20 - 25 % of the story drift. The rest of the story drift results from column and beam elastic rotations, beam plastic hinge rotations and beam end rotations.

6.3 FUTURE RESEARCH

Although the developed model gives reasonable results for most of the subassemblies, further enhancement may be accomplished to obtain more accurate results. As

mentioned before, the effect of wide beams can not be sufficiently represented in the model due to the limited number of specimens including wide beams. Therefore, this effect should be investigated in more detail by including new wide beam-to-column specimens in the database.

Slip of the reinforcing bars is one of the parameters that is considered to be influential on the seismic behavior of the joint. Since experimental information is not available for slip in most of the specimens, this parameter could not be investigated in detail.

Pinching of the hysteresis curves could not be modeled in this analytical study due to the limitations of the selected software. Currently, there is no commercially available software that includes pinching in element modeling; however, a software with more sophisticated element models, such as OpenSees (http://opensees.berkeley.edu), could be used in the future, if energy dissipation capacity is selected as one of the parameters to be evaluated.

Finally, the analytical modeling of more connection types such as roof (knee) connections and spread-ended connections can be carried out. In order to propose an analytical model for these types of connections, more experimental studies should be carried out to obtain more data and evaluate their behavior in detail.

REFERENCES

[1] ACI Committee 318, 2008, Building Code Requirements for Structural Concrete , 318-08, *American Concrete Institute*, Farmington Hills, Michigan.

[2] ACI-ASCE Committee 352, 2002, "Recommendations for Design of Beam-Column Connections in Monolithic Reinforced Concrete Structures", *ACI 352R-02*, *American Concrete Institute*, Farmington Hills, Michigan.

[3] Burak, B. and Wight, J.K., 2005, "Seismic Behavior of Eccentric Reinforced Concrete Beam-Column-Slab Connections", *Ph.D. Thesis*, The University of Michigan, Ann Arbor.

[4] Canbolat, B. B, 2008, "Structural Applications of A Reinforced Concrete Beam-Column-Slab Connection Model For Earthquake Loading", *The 14th World Conference on Earthquake Engineering,* October 12-17, 2008, Beijing,China.

[5] Canbolat, B. B. and Wight, J.K., 2008, "Experimental Investigation on Seismic Behavior of Eccentric Reinforced Concrete Beam-Column-Slab Connections", *ACI Structural Journal,* Title no. 105-S16., pp. 154-162.

[6] Chen, C.C. and Chen, G., 1999, "Cyclic Behavior of Reinforced Concrete Eccentric Beam-Column Corner Joints Connecting Spread-Ended Beams", Technical Paper, *ACI Structural Journal*, Title no. 96-S50, pp. 443-450.

[7] Climent, A.B., 2005, "Shaking table tests of reinforced concrete wide beam-column connections", *Earthquake Engineering and Structural Dynamics*, 2005;34, pp. 1833-1839

[8] Clyde, C., Pantelides, C. P., and Reaveley, L. D.,2000, Performance-based Evaluation of Exterior Reinforced Concrete Building Joints for Seismic Excitation, *Pacific Earthquake Engineering Research Center, PEER Report 2000/05*, University of California, Berkeley, CA.

[9] Computers and Structures Inc. (CSI), 2006, *User Manual for PERFORM-3D v4.0*, Berkeley, California, USA, August 2006.

[10] Durrani, A. J. and Wight, J. K., 1985, "Behavior of Interior Beam-to-Column Connections Under Earthquake-Type Loading", *ACI Structural Journal*, Title no. 82-30., pp. 343-349.

[11] Ehsani, M.R. and Wight J.K., 1985, "Exterior Reinforced Concrete Beam-to-Column Connections Subjected to Earthquake-Type Loading", Technical Paper, *ACI Structural Journal*, Title no. 82-43, pp. 492-499.

[12] Ehsani, M.R. and Alameddine, F., 1991, "Design recommendations for Type 2 High-Strength Reinforced Concrete Connections", Technical Paper, *ACI Structural Journal*, Title no. 88-S30, pp. 277-290.

[13] French, C.W., and Moehle, J.P., 1991, "Effect of Floor Slab on Behavior of Slab-Beam-Column Connections", *Design of Beam-Column Joints for Seismic Resistance – ACI SP-123*, pp. 225-258.

[14] Fujii, S. and Morita, S., 1991, "Comparison between Interior and Exterior RC Beam-Column Joint Behavior", *Design of Beam-Column Joints for Seismic Resistance – ACI SP-123*, pp. 145-165.

[15] Gentry, T.R. and Wight, J. K., 1994, "Wide beam-Column Connections under Earthquake-Type Loading", *Earthquake Spectra*, Vol. 10, No.4, pp. 675-702.

[16] Guimaraes, G.N; Kreger, M.E. and Jirsa, J.O, 1992, "Evaluation of Joint-Shear Provisions for Interior Beam-Column-Slab Connections Using High-Strength Materials", Technical Paper, *ACI Structural Journal*, Title no. 89-S10, pp. 89-98.

[17] Joh, O.; Goto, J. and Shibata, T., 1991, "Influence of Transverse Joint and Beam Reinforcement and Relocation of Plastic Hinge Region on Beam-Column Joint Stiffness Deterioration" *Design of Beam-Column Joints for Seismic Resistance – ACI SP-123*, pp. 187-223.

[18] Kaku, T. and Asakusa, H., 1991, "Bond and Anchorage of Bars in Reinforced Concrete Beam-Column Joints", *Design of Beam-Column Joints for Seismic Resistance – ACI SP-123*, pp. 401-424.

[19] Kaku, T. and Asakusa, H.,1991, "Ductility Estimation of Exterior Beam-Column Subassemblages in Reinforced Concrete Frames", *Design of Beam-Column Joints for Seismic Resistance – ACI SP-123*, pp. 167-185.

[20] Kim, J. and LaFave, J.M., 2008, "Key Influence Parameters for the Joint Shear Behavior of Reinforced Concrete (RC) Beam-column Connections", Engineering Structures, doi: 10.1016/j.engstruct.2006.12.012.

[21] Kim, J. and LaFave, J.M., 2008, "Probabilistic Joint Shear Strength Models for Design of RC Beam-Column Connections", *ACI Structural Journal*, Title no. 105-S71, pp. 770-780.

[22] Kim, J., LaFave, J.M. and Song, J., 2009, "Joint Shear Behavior of Reinforced Concrete Beam-Column Connections", *Magazine of Concrete Research*, 61-No.2, pp. 119-132.

[23] Kitayama, K. ; Otani, S. and Aoyama, H. 1991, " Development of Design Criteria For RC Interior beam-Column Joints", *ACI SP-12*3 Design of Beam-Column Joints for Seismic Resistance, American Concrete Institute, Michigan, pp. 97-123.

[24] LaFave, J.M. and Wight, J.K., 1999, "Reinforced Concrete Exterior Wide Beam-Column-Slab Connections Subjected to Lateral Earthquake Loading", *ACI Structural Journal*, Title no. 96-S64, pp. 577-586.

[25] LaFave, J.M.; Bonacci, J.F.; Burak, B.; and Myoungsu, S., 2005, "Eccentric Beam-Column Connections-Performance and Design of Joints Subjected to Seismic Lateral Load Reversals," *Concrete International*, V. 27, No.9, Sept. 2005, pp. 58-62

[26] Lee, H.J., and Ko, J., 2007, "Eccentric Reinforced Concrete Beam-Column Connections Subjected to Cyclic Loading in Principal Directions", *ACI Structural Journal*, Title no. 104-S44, pp. 459-467.

[27] Lowes, N.L., and Altoontash, A., 2003, "Modeling of Reinforced-Concrete Beam-Column Joints Subjected to Cyclic Loading", *Journal of Structural Engineering*, American Society of Civil Engineers, New York, Vol. 129, No.12. , pp. 1686-1697.

[28] Mitra, N., and Lowes, N. L., 2007, "Evaluation, Calibration, and Verification of a Reinforced Concrete beam-Column Joint Model", *Journal of Structural Engineering*, American Society of Civil Engineers, New York, Vol. 133, No.1. , pp. 105-120.

[29] Parra-Montesinos, G.J. and Wight J.K., 2002, "Prediction of Shear Strength and Shear Distortion in R/C Beam-Column Joints", SP197-10.

[30] Shin, M. , 2004, "Performance of Reinforced Concrete Edge Beam-Column-Slab Connections Subjected to Earthquake Loading", *Ph.D. Thesis*, University of Illinois at Urbana-Champaign, Urbana – Illinois.

[31] Shin, M., and LaFave, J.M., 2004, "Modeling of cyclic joint shear deformation contributions in RC beam-column connections to overall frame behavior", *Structural Engineering and Mechanics,* Vol. 18, No. 5, pp.645-669.

[32] Rafaelle, S. G., Wight, J.K., 1995, "Reinforced Concrete Eccentric Beam-Column Connections Subjected to Earthquake-Type Loading", *ACI Structural Journal*, Title no. 92-S6, pp. 45-55.

[33] Shiohara, H. 2001, "New Model for Shear Failure of RC Interior Beam-Column Connections"*, Journal of Structural Engineering*, American Society of Civil Engineers, New York, Vol. 127, No.2. , pp. 152-160.

[34] Teng, S. and Zhou, H., 2008, "Eccentric Reinforced Concrete Beam-Column joints Subjected to Cyclic Loading", *ACI Structural Journal*, Title no. 100-S15, pp. 139-148.

[35] Turkish Earthquake Code: Specifications for the Buildings to be Constructed in Disaster Areas, 2007, *Ministry of Public Works and Settlement*, Ankara, Turkey.

[36] Quintero-Febres, C.G. and Wight, J.K., 2001, "Experimental Study of Reinforced Concrete Interior Wide Beam-Column Connections Subjected to Lateral Loading*", ACI Structural Journal*, Title no. 98-S55, pp. 572-581.

[37] Zhou, H., 2009, "Reconsideration of Seismic Performance and Design of Beam-Column Joints of Earthquake-Resistant Reinforced Concrete Frames", *Journal of Structural Engineering*, American Society of Civil Engineers, New York, Vol. 135, No.7. , pp. 762-773.

[38] OpenSees, "*Open System for Earthquake Engineering Simulation - Home Page*. Web", last visited on 30/06/2010, http://opensees.berkeley.edu.

APPENDIX A

SELECTED EXPERIMENTS

A.1. TEST SETUP AND SPECIMEN DETAILING

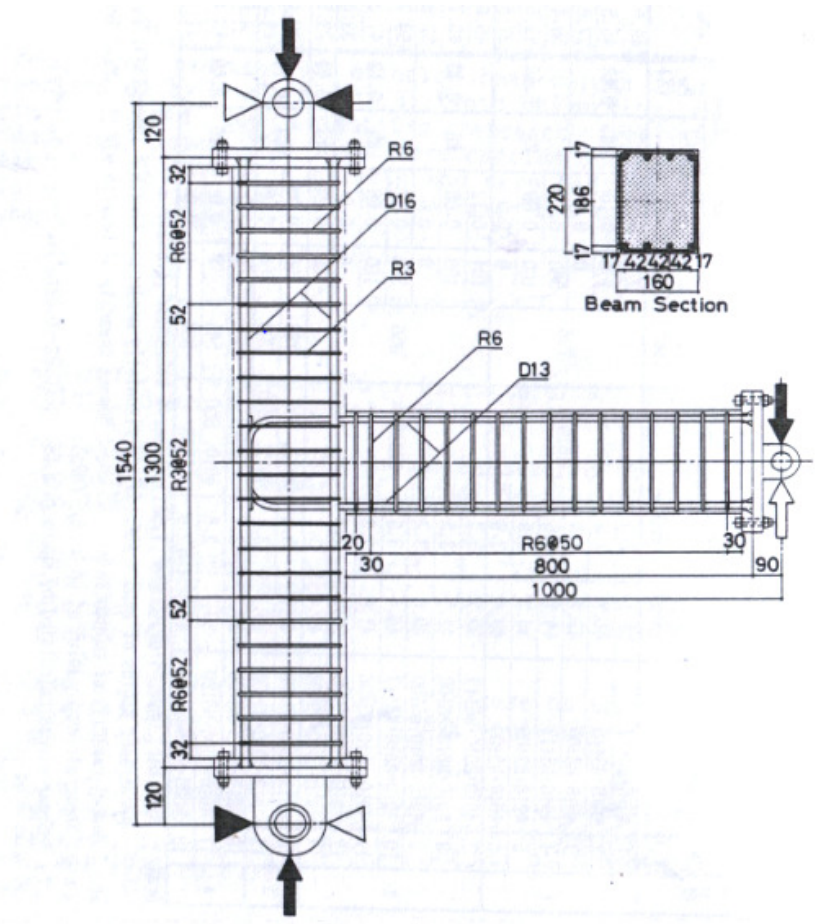

Figure A.1.1: Test Setup - Specimens of Kaku and Asakusa

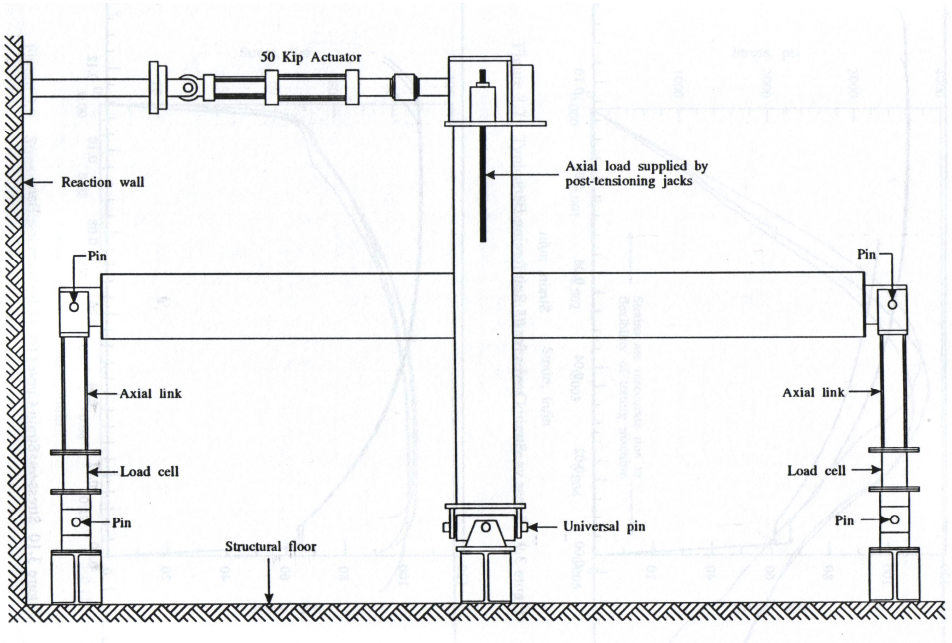

Figure A.1.2: Test Setup - Specimens of Rafaelle and Wight

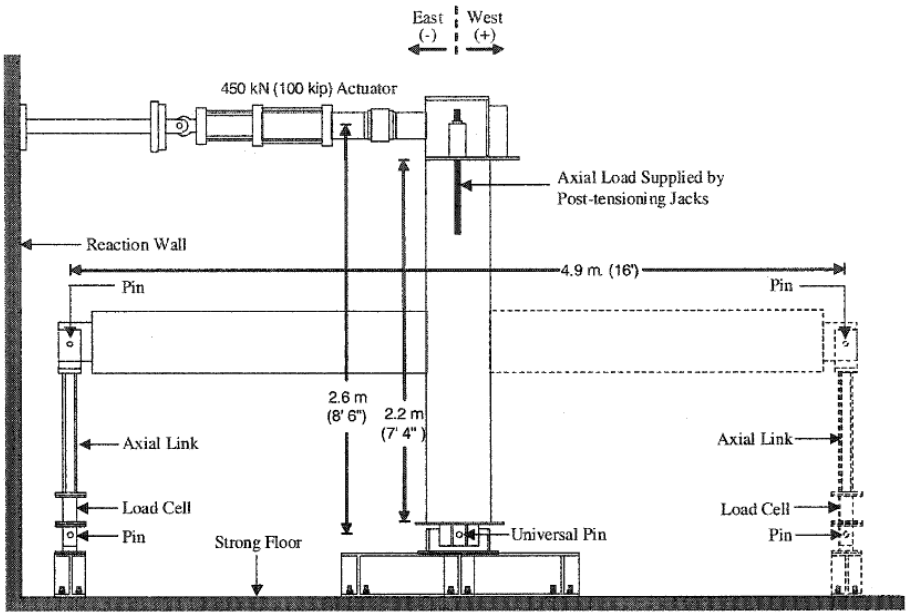

Figure A.1.3: Test Setup - Specimens of Burak and Wight

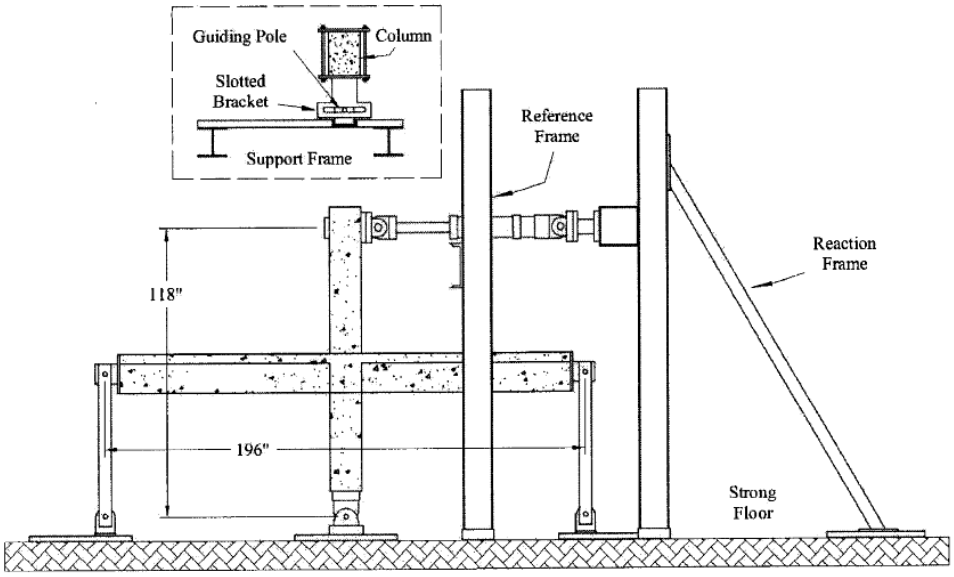

Figure A.1.4: Test Setup - Specimens of Shin and LaFave

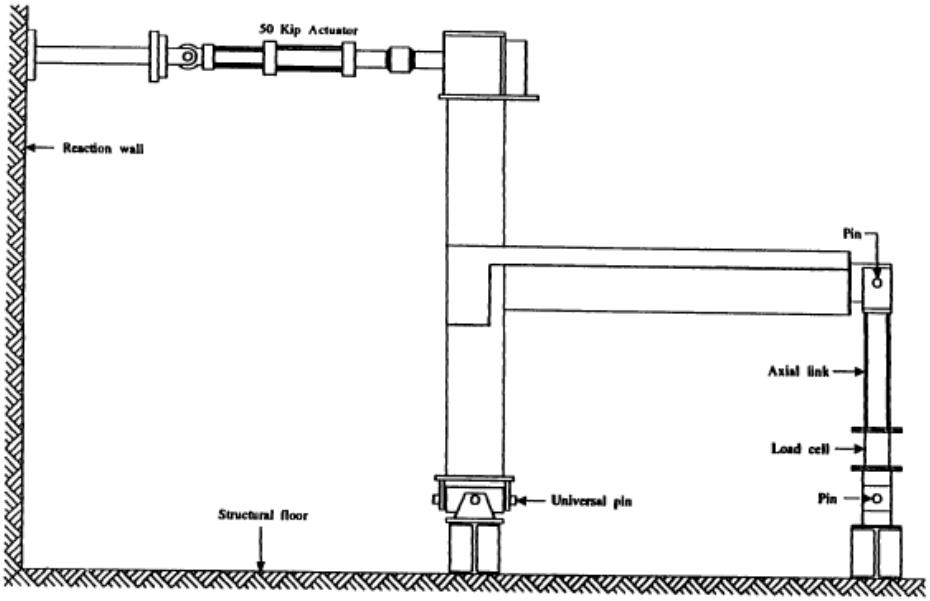

Figure A.1.5: Test Setup - Specimens of LaFave and Wight

A.2. LOADING HISTORIES

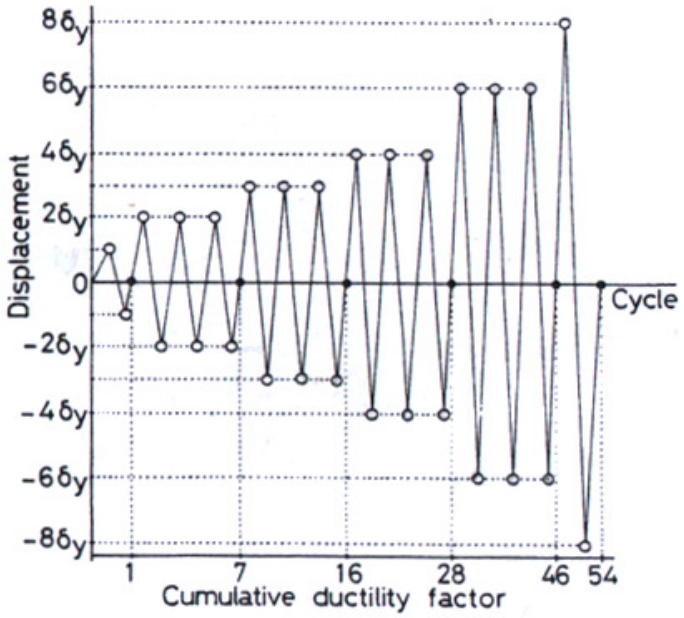

Figure A.2.1: Imposed Loading - Specimens of Kaku and Asakusa

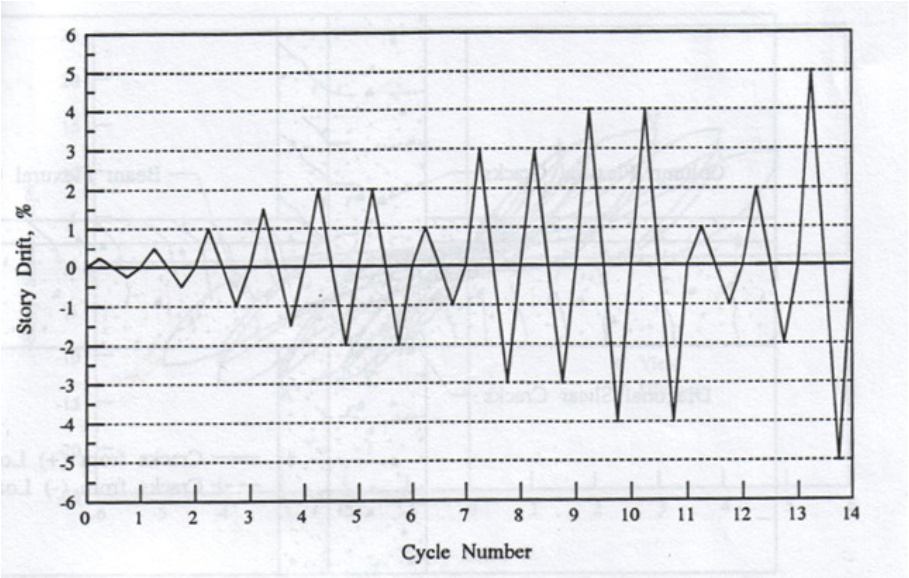

Figure A.2.2: Imposed Loading - Specimens of Rafaelle and Wight

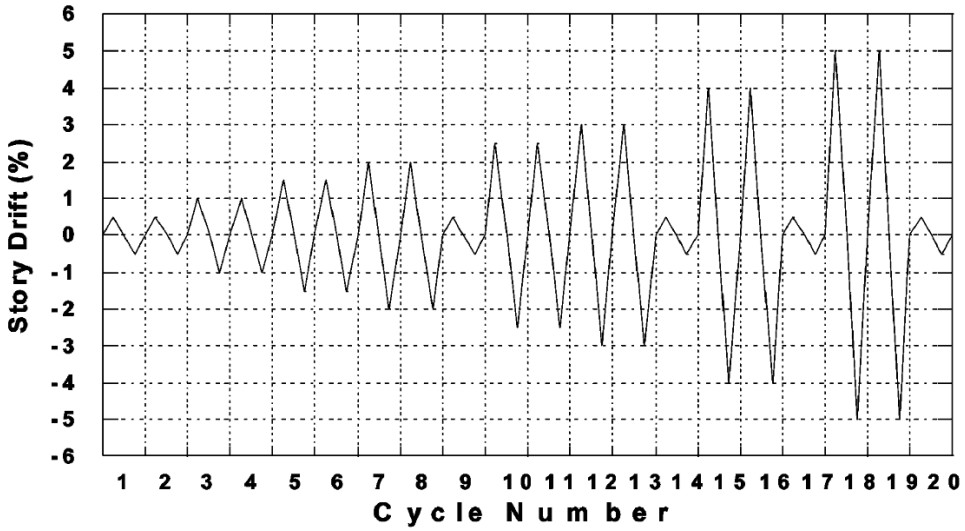

Figure A.2.3: Imposed Loading - Specimens of Burak and Wight

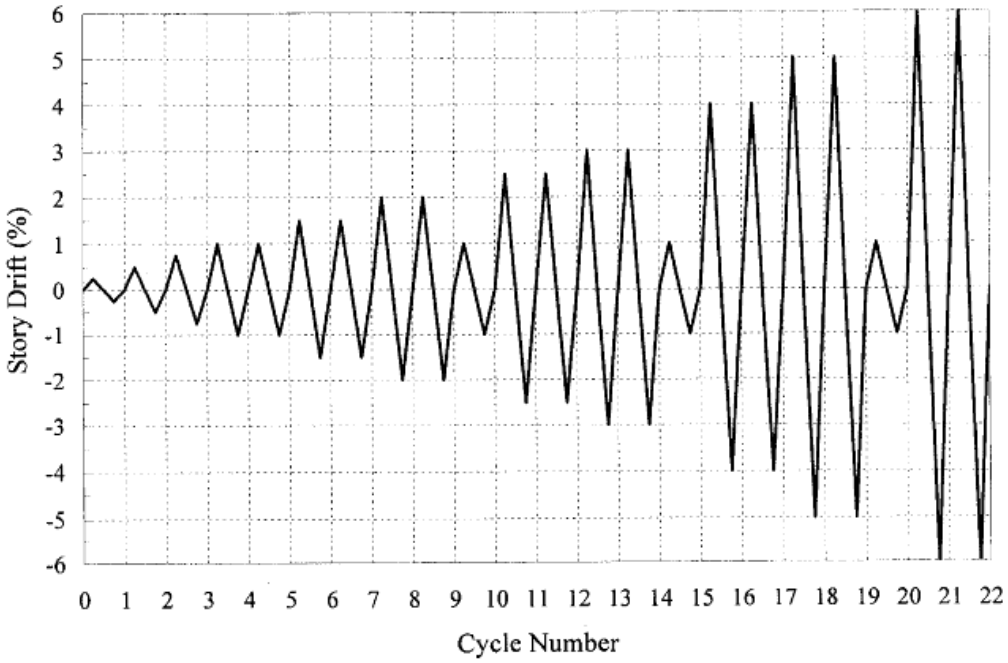

Figure A.2.4: Imposed Loading - Specimens of Shin and LaFave

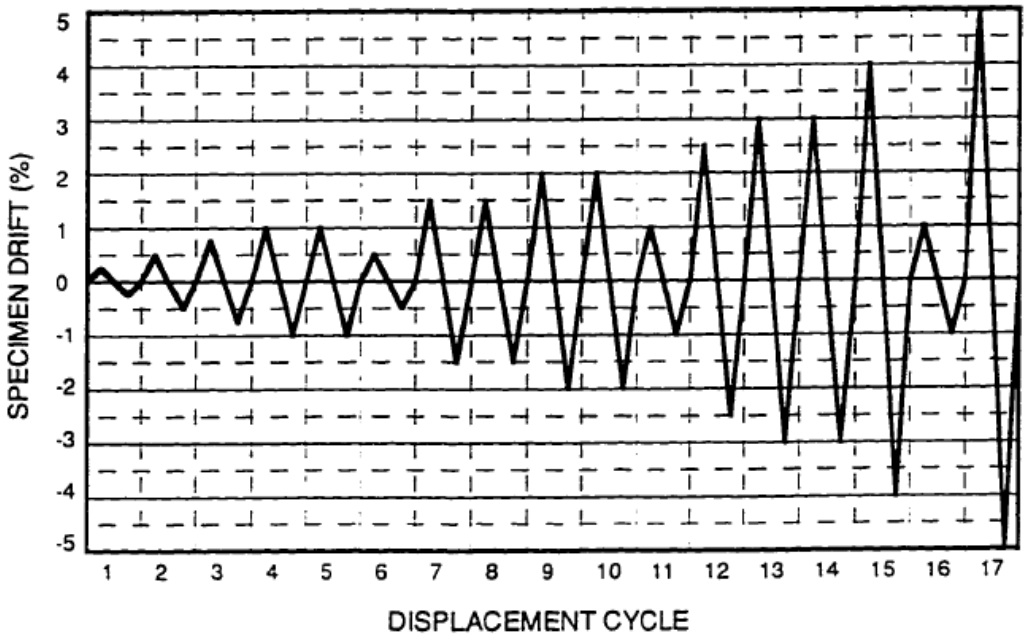

Figure A.2.5: Imposed Loading - Specimens of LaFave and Wight